Catalytic materials based on silica and alumina: structural features and generation of surface acidity.

Guido Busca [a]

[a] Dipartimento di Ingegneria Civile, Chimica e Ambientale (DICCA), Università degli Studi di Genova, via all'Opera Pia 15, I-16145 Genova, Italy

Abstract. The structural, surface chemical and catalytic properties of the materials belonging to the SiO_2-Al_2O_3 system are reviewed critically. In particular, amorphous silicas, transitional aluminas, different silica-aluminas (silica-rich and alumina-rich) and protonic zeolites are taken into considerations. The nature of the acid sites, of the Lewis and of the Brønsted type, over these surfaces is discussed and rationalized, based on the fundamental chemistry and structural chemistry of silicon and aluminum compounds.

1. Introduction.

The history of catalysts based on mixed oxides of silicon and aluminum is strictly bound to the history of hydrocarbon chemistry and, in particular, of the Catalytic Cracking refinery process [1]. This process was first developed by the french Eugene Houdry in the twenties of the 20th century, and then realized at the industrial level in USA in the thirties [2,3]. Since that times, this process is a key for the full exploitation of heavy oils and the production of high-octane gasoline. In particular, it had a relevant role in allowing in the USA the preparation of high octane aviation gasoline, thus determining the better performances of allied aircrafts than the German ones during second world war.

Acid-activated bentonite clay catalysts were originally used for this process, starting from 1937, when it was configured as a fixed-bed process, with several reactors and cyclic regeneration of one of them. At the beginning of the forties, moving bed catalytic cracking (MBCC) processes, and the first Fluid Catalytic Cracking processes were put into operation [4]. Starting from 1942, synthetic "low-alumina" amorphous silica-alumina catalysts were applied, with ca 13% Al_2O_3 wt/wt [5]. "High-alumina" silica-alumina catalysts containing up to 30 % Al_2O_3 wt/wt [6] were introduced starting from 1955. Synthetic protonic faujasite zeolites were developed at Union Carbide and Mobil, and applied to FCC at Mobil in the early sixties [7,8,9]. This was the beginning of the large use of acid zeolites as heterogeneous catalysts in refinery and petrochemistry [10,11,12]. Also aluminas [10,13] and silica-aluminas [10,14,15] find a number of applications in industrial chemistry as acid

catalysts. On the other hand, silica, alumina, amorphous silica-aluminas and zeolites have also a large number of application as supports for sulphide [16], metal [17], halide [18] or other oxide catalysts [19].

The interest for these materials is not strictly related to the era of fossil fuels, but will be further improved in the incoming era of renewable raw materials. In fact, solid acids have a very relevant potential role, as catalysts and catalyst supports, e.g.,in the conversion of ligneocellulosic biomass [20,21] and wastes [20,22] to useful products, in several steps of the new green organic chemistry based on renewables and for a number of environmental applications [23].

In this review the main characteristics and, in particular, the origin of the acid properties of materials arising from silica and alumina and their mixtures will be discussed on a fundamental chemical ground.

2. Silicas

2.1 Basic chemistry of silicas and silicic acids.

As everybody knows, silicon is a semimetallic element. Tetravalent silicon is soluble in strongly basic water solutions as orthosilicate anion, $[SiO_4]^{4-}$. By decreasing pH, the different polyhydrogen orthosilicate anions $[H_nSiO_4]^{(4-n)-}$ form progressively up to forming orthosilicic acid H_4SiO_4 which is a weak polyprotic acid with $pK_{a1} \sim 9.5$ and $pK_{a4} \sim 19$ [24]. At slightly basic, neutral and acidic pH, depending also on its concentration, orthosilicic acid tends to polymerize to metasilicic acids $(H_2SiO_3)_m$, finally giving rise to precipitation [25] and/or gelation [26] producing amorphous silica, SiO_2 (precipitated silica and silica gel, respectively). Actually, some crystalline silicic acids have been prepared and characterized [27,28,29,30].

Correspondingly, both crystalline and amorphous silicas start to be dissolved at pH $\geq$ 8.5 and are dissolved rapidly and completely in basic solutions (pH $\geq$ 10), while they are substantially stable at acidic pH, in equilibrium with $2\ 10^{-3}$ M of H_4SiO_4 [31].

The weak acidic nature of silicic acids is associated to the very low size of the Si^{4+} formal cation (0.26 Å radius [32]), its moderately high charge and the intermediate electronegativity of the element, that make the Si-O bond highly covalent, but do not allow to produce formal double bonds with oxygen. According to this, delocalization of the negative charge of the deprotonated species, like trihydrogen-silicate anions $[H_3SiO_4]^-$, is not possible, and this is a main reason why orthosilicic acid is not a strong acid.

Interestingly, it has been reported that acidity of silanols increases with the size of the silicate-polymeric species, being polysilicic acids ($pK_{a1} \sim 6.5$) definitely stronger than

pyrosilic (or disilicic) acid (pK_{a1} ~ 9.0) and orthosilicic acid (pK_{a1} ~ 9.5) [33,34]. This can be explained by the delocalization of the negative charge of the dissociated species over Si-O-Si siloxane bonds. In fact, siloxane groups, whose bond angle Si-O-Si is very flexible in contrast to the O-Si-O bond angle that is not, have some character of “double bond” which is associated to an hyper-conjugation effect, i.e. the $n_O \rightarrow \sigma^*_{Si\text{-}O}$(vicinal) interaction, a bonding interaction between an oxygen lone pair and the antibonding orbital of the vicinal Si-O bond [35,36,37]. These interactions can allow the delocalization of the terminal anionic charge of a silicate species ($Si\text{-}O^-$) over the siloxane bridges, the more the larger is the polysilicate entity.

Thus, in practice the orthosilicate anion is a quite strong base, whose strength decreases by protonation ($SiO_4^{4-} > HSiO_4^{3-} > H_2SiO_4^{2-} > H_3SiO_4^- >> H_4SiO_4$) and by oligomerization to polysilicate ions ($SiO_4^{4-} > Si_2O_7^{6-} > Si_3O_{10}^{8-} >\ldots$). Conversely, silicic acids are weak polyprotic acid whose acidity increases upon oligomerization.

2.2 Preparations of amorphous silicas.

Most industrial preparations of amorphous silicas use sodium silicate as a precursor. This material is relatively cheap but may be somehow contaminated by aluminium and iron. More expensive but purer alkoxy-silanes represent alternative precursors. Rice husk ash (RHA) can also be a cheap raw material for silicas production [38,39]. The preparation of silicas from solutions of silicate species is obtained around neutral conditions or in acidic conditions, as said above.

Precipitated silicas. Although many different recipes have been proposed, precipitated silicas are commonly produced [40] by partial neutralization of sodium or potassium silicate solutions. Sulphuric acid is mostly used, mixed with sodium silicate in water still retaining alkaline pH. Reaction is performed under stirring at 50-90 °C. The precipitate is then washed, filtered and dried. During precipitation, progressive particle growth occurs up to 4-5 nm clusters, that successively agglomerate to form sponge-like aggregates. Tuning preparation procedure parameters (choice of agitation, duration of precipitation, the addition rate of reactants, their temperature and concentration, and pH of precipitation, as well as drying conditions) allows tuning of final particle size and morphology, thus surface area and porosity. Precipitates typically have a broad meso/macroporous morphology. Very high surface areas may be obtained with these procedures (up to 750 m^2/g), with pore volume in the 0.4-1,7 cm^3/g range and average pore diameter in the 4-35 nm range. Typical impurities of these materials are sodium ions (< 0,8 %) with the likely presence of iron and aluminium

ions at the 500-1000 ppm level. Precipitated silica are commercially available such as the Sipernat family from Evonik and the Zeosil-Micropearl materials from Rhodia.

Silica gels. Silica gels are usually produced [41] by dissolving sodium or potassium silicate (10-20 % silica) into an acid, such as sulphuric acid (pH ~ 0.5-2). If the particles are smaller than 100 nm they form silica sols, stabile colloidal dispersions of amorphous silicon dioxide particles that can be used e.g. as polishing agent at production of silicon surfaces in the electronic industry. A gel is formed when the molecular weight of the micelles reaches approximately 6 million, thus the hydrosol viscosity reaches the no-pour point. In a second step the liquid is removed leaving a glass-like gel which is broken down into granules and then washed, aged, and dried, with 6 % volatiles and 22 Å average pore diameter.

Silica gels have pores with a wide range of diameters, typically between 5 Å and 3000 Å, and broad distributions. Silica gels synthesized with surface area as high as 800-900 m^2/g, an average pore size of about 20Å and effective pore volumes of 0,40 cm^3/g, are known as narrow pore silica gels, while wide pore silica gels are characterized by surface area ~ 400 m^2/g, average pore size of about 110Å and effective pore volumes of 1,20 cm^3/g [42].

Silica aerogels. Aerogels, first prepared in the late 1920s by Samuel Kistler, are highly transparent materials with very high surface area (>1000 m^2/g) and high void volume (85-98 %), prepared by supercritical drying of wet silica gels . Supercritical drying process can avoid capillary stress and associated drying shrinkage, which are usually prerequisite of obtaining aerogel structure. The conventional academic method of silica aerogel preparation is sol-gel process using organic silicon compounds, such as tetramethyl-orthosilicate (TMOS), tetraethyl-orthosilicate (TEOS) or polyethoxydisiloxane (PEDS) as precursors. Organo silanes are dissolved in a binary solution, typically water-methanol or water - ethanol, and hydrolysed in the presence of a catalyst, frequently an acid (hydrochloric, hydrofluoric, formic, nitric, sulphuric acid). Additives may be added to modify gel porosity during aging. Drying is performed after washing the gel with a solvent and then raising temperature and pressure to obtain supercritical conditions for the solvent (T > 239.5 °C, P > 79.783 atm for methanol, T > 241 °C, P > 60,567 atm for ethanol). In the case of low temperature supercritical drying, CO_2 is used as the solvent and this allows lower temperature for supercritical drying (T > 31.13 °C, P > 72.786 atm). Industrial preparations likely start from “water glass”, a much cheaper raw material, and may apply ambient pressure drying by solvent evaporation after previous silylation and hydrophobization of the surface. In fact, commercial aerogels may be hydrophobized, e.g. from aerogels from

CABOT, mainly used for insulation and daylighting, as intermetallic dielectric materials and acoustic applications.

Mesoporous silicas. After the work of Kresge et al. [43] at Mobil, and the even previous work of researchers of Toyota [44], mesoporous silicas containing somehow ordered structures of well-defined channels or interconnected cavities with size from few to several nm, have been developed. The preparation of these materials [45,46] commonly starts from silicon alkoxides hydrolysis performed in the presence of appropriate concentrations of detergent molecules acting as templates or Structure Directing Agents (SDA). With opportune reaction conditions, pores having different geometries can be obtained.

Many different materials, with different mostly mesoporous pore structure, but having sometimes also some microporosity, may be obtained by different preparation procedures and SDAs. Surface areas up to 1500 m^2/g are obtained, with well-defined mesoporosity. Such mesopores can be constituted by linear channels or interconnected cages, or even wormhole-like channels with hexagonal symmetry [47]. Although sometimes considered like very large pore zeolites, these materials are essentially amorphous materials with non-structural although sometimes ordered mesopores.

Stöber silica and spherical silica micro/nanomaterials with hierarchical structures. Monodisperse non porous spherical silica particles were prepared originally by W. Stöber et al. in 1968 [48] by hydrolysing TEOS in a mixed solution of ammonia, alcohol and water followed by condensation of silicic acid in basic conditions and calcination at 600 °C . Depending on reaction conditions, such non-porous spherical particles have diameters mostly between 50 and 600 nm resulting in surface areas between near 100 and few m^2/g [49]. In more recent years, silica spheres with multilevel pore structure have been obtained. Mesoporous hollow silica spheres may be prepared by different methods such as using hard templates (spherical particles of solids like polymers) and surfactants as pore structure SDAs, or using different fluids (including gas bubbles) as templating molecules [50]. The production of more complex materials such as core-in (hollow porous shell) spheres, multiple shell spheres and hierarchically porous spheres, with several levels of porosity present together, have also been obtained.

Fumed or pyrogenic silicas. Fumed silicas are produced by flame hydrolysis of silicon tetrachloride, a process invented in 1942 by H. Klöpfer a chemist at Degussa (now Evonik). This process consists in the reaction of $SiCl_4$ in a hydrogen-oxygen flame at high temperature, reported top be near 1100 °C (Degussa – Evonik) or 1800 °C (Cabot) [51], producing silica and hydrogen chloride. This procedure produces very small non-porous

amorphous primary particles, with a particle density of 2.20 g/cm^3, i.e. only slightly lower than that of crystalline silicas. These particles tend to agglomerate in linear and branched chain-like structures. The surface area of these materials is moderately high (100-400 m^2/g) and fully external, essentially depending from the particle size that ranges 5-16 nm. The weight loss by drying is quite low, 1-2,5 % depending roughly on the surface area, the morphology being stable nearly up to 800 °C, when sintering starts. From the point of view of the metal content these materials are very pure. In particular they do not contain alkali metal impurities. Typical impuritiy of these materials are residual chlorine, and, to a low extent, aluminium, titanium and iron. A typical practical characteristic of these materials is the very low apparent density (down to 30 g/l) and the volatility of the particles.

Amorphous silicas are mostly characterized by low bulk densities, sometimes as low as 1 g/cm^3, well lower than crystalline silicas. This is in part related to interparticle porosity as well as to defect structure.
These amorphous states are actually very stable, their sintering and crystallization, usually to cristobalite [52], being fast phenomena only at temperatures of the order of > 800 °C, giving rise to loss of surface area and porosity

2.3 Solid state chemistry of silica: amorphous versus crystalline phases.

As it is well-known, silica forms many different crystalline structures [53,54]. Except some high- pressure polymorphs like the rutile-type polymorph stishovite, which have octahedrally coordinated silicon, all crystalline silica structures present tetrahedrally coordinated silicon atom. This is a result of the valency four of silicon and the covalency of the Si-O bond [55]. At ambient pressure, SiO_2 has several major polymorphs. Those having thermodynamic stability ranges at ambient pressure are : low temperature trigonal α-quartz up to 570 °C, high temperature hexagonal β-quartz 570-870 °C, hexagonal β-tridymite 870- 1470 °C and high temperature cubic β-cristobalite 1470-1705 °C. Other tetrahedral-based crystalline phases, metastable at ambient pressure, exist like hexagonal α-tridymite and tetragonal α-cristobalite, and coesite, the last being thermodynamically stable at moderately high pressures. It seems interesting to remark that crystalline silica structures have relatively low density with respect e.g. crystalline aluminas as well as aluminum silicates (Table 1). This is largely due to the covalent tetrahedral coordination of silicon, corresponding to coordinaton 2 for oxygen, in contrast to the usually predominant coordination 6 of aluminum,

with oxygen in coordination 3 and 4. As a result of this, larger and more vacant interstices exist in the silica structures, as it will be discussed below.

Besides the previous structures, a number of silica metastable microporous crystalline phases have also been prepared, usually called silicalites [56]. They are fully siliceous zeolites, with a much lower density. They are prepared with the typical preparation techniques of zeolites (see below), using only a pure silicon source and organic structure directing agents (SDAs). Silicalite-1 is largely the better known and most used siliceous zeolite. Its crystalline framework is constituted by Si oxide tetrahedral structure, with the typical structural microporosity of the MFI structure zeolites. Two types of intersecting channels, both formed by 10-membered silicate rings, characterize this material. One channel type is straight and has a nearly circular opening (5.3 x 5.6 Å) along [010], while the other one is sinusoidal and has an elliptical opening (5.1 x 5.5 Å), along [100].

When prepared as a “perfect”, non defective form, its internal surface has an essentially covalent and hydrophobic character. Only the external surface presents hydrophilicity due to the presence of silanol groups. Alternatively, silicalite may be prepared in defective forms, where silanol nests substitute for vacant silicon atoms in the framework and in the internal cavities, thus generating more hydrophilicity. Several other fully siliceous zeolites have been synthesized in recent times.

Other purely siliceous zeolite-like materials have been prepared. Silicalite-2 [57] belongs to the framework denoted MEL, closely related to MFI, containing a two dimensional 10-ring pore structure. Both sets of pores are straight 5.3 x 5.4 Å wide. Purely siliceous zeolite BEA has also been prepared, both in the defective and in the non-defective forms [58]. BEA structure has a three-dimensional intersecting channel system, two mutually perpendicular straight channels each with a cross section of 6.6 - 6.7 Å, and a sinusoidal channel with a cross section of 5.6 - 5.6 Å.

Also other pure silica zeolites, such as ITQ-1, the siliceous form of zeolite MWW (MCM-22) [59], ITQ-3 [60], ITQ-29, the siliceous analog of zeolite A (LTA) [61], and fully siliceous FER [62] and SSZ73 (SAS topology) [63] have been prepared and characterized.

The tetrahedral-based structures of the silica polymorphs are associated to corner sharing tetrahedra producing a quite covalent Si-O-Si bond networks and differ for the relative arrangements of the tetrahedra.

2.4. The surface chemistry of silicas: terminal silanols and siloxane bridges.

As said, silica is a largely covalent oxide [55,64], in agreement with the high electronegativity of Si^{4+} [65]. Silicon atoms are revealed by the Si 2p binding energy XPS peak at ca. 103.5 eV [66,67] that can be deconvoluted into two peaks representing the Si 2p 3/2 and Si 2p 1/2 levels. The splitting between signals due to bulk silicon species and surface silicon atoms bonded to hydroxyl groups is also usually not detected [68].

^{29}Si MAS NMR spectra show a main peak denoted as Q4 signal, at 105-115 ppm [69,70], which is not influenced by ^{1}H-^{29}Si Cross Polarization experiments, due to bulk silicon atoms bonded to other four Si atoms through Si-O-Si bridges. Other signals, definitely weaker, denoted as Q3 qnd Q2 are evident, assigned to Si atoms located at the surface and bonded to three or two Si atoms through Si-O-Si bridges, as well as to terminal and germinal hydroxyl groups, respectively. Thus, the coordination of silicon atoms exposed at the surface is completed by hydroxyl groups, producing silanol species. Thus, Lewis acidity is absent in normal conditions. In fact, no coordination of basic probes is observed during adsorption, only H-bonding. It has been found that high temperature treatment, such as outgassing at > 1100 °C is needed to cause the formation of Lewis acid sites where pyridine and ammonia chemisorb by coordination [71]. Thus, the surface of silicas is, in usual conditions, essentially constituted by terminal silanols Si-OH (“isolated” or germinal, Fig. 1), as well as by Si-O-Si siloxane bridges.

2.4.1 The terminal silanol groups.

Indeed “terminal silanol” groups, Si-OH, essentially dominate the surface chemistry of silica in normal conditions [72], as discussed by Zhuravlev and coworkers [73,74] and reviewed more recently by Rimola et al. [75]. The presence of silanol sites is detected by using IR spectroscopy [76] being these groups responsible for a strong sharp O-H stretching band centered at ca 3745-8 cm^{-1}, with a tail or with some definite components at lower frequencies due to H-bonded silanol nest species. Isolated silanol groups are responsible for a very sharp IR band (O-H stretching) evident near 3740 cm^{-1} already after outgassing in mild conditions. This band sharpens by increasing outgassing temperature, the maximum being at the highest treatment temperature located near 3748 cm^{-1}. The band of free silanols is clearly asymmetric, having a pronounced tail towards lower frequency more evident in the cases of highly porous samples. In practice, it seems quite evident that the band of free silanols may actually be composed of different very sharp components, one of them being located more or less at 3744 cm^{-1}. This feature, according to [77,78], could be due to the geminal silanols, which are hardly distinguished from isolated silanols in the IR spectra,

whose presence is deduced from ^{29}Si MAS NMR data (see below). In the same range, maybe at 3741 cm^{-1}, would adsorb also couples of vicinal silanols [79].

On the other hand, probing the free surface silanols with adsorbed molecules of different sizes [80] indicates that part of the tail is due to silanol groups located in small nanopores having molecular size, thus not accessible to large molecules. The slightly lower OH frequency (ca 3700 cm^{-1}) show that these components are associated to internal but essentially free silanol groups, very slightly perturbed for some kind of weak interaction. Gallas et al. [81] showed on precipitated silicas OH groups partially unaccessible to D-exchange and to interaction with alcohols, whose accessibility depends inversely on alcohol size. Two other broad features are usually present in the IR spectra of silicas, recorded after outgassing at mild temperature, at 3530-3520 cm^{-1} and at 3660-3650 cm^{-1}. They have been assigned to clusters of vicinal H-bonded silanols [82] which at least in part condense at high temperature giving rise to siloxane bridges. In fact, their condensations does not contribute significantly to the increase of the band of free silanols [83]. In the case of microporous silica samples, these absorptions are stronger (relative to the band of the free silanols) than in the case of non-porous or less porous powders like fumed silica (Fig. 2 [83,84]).

Free silanol groups are also evident by ^{1}H MAS NMR spectroscopy, because they produce a sharp signal centered at 1,7 - 2 ppm [69,85,86,87]. A splitting of this signal may be due to external and internal silanol groups (1.8 and 2 ppm, respectively [85]). An additional broad signal located near 3 ppm is assigned to H-bonded silanols.

Terminal silanol groups are also evident being responsible for ^{1}H-^{29}Si Cross Polarization MAS NMR signals Q3 (due to Si atoms bonded through oxygen bridges to three other Si atoms and to a isolated OH group, at 98-102 ppm). A similar effect is also observed for the much weaker signal Q2 (due to Si atoms bonded through oxygen bridges to two other Si atoms and to two geminal OH groups, at 90-92.5 ppm) and this is the main evidence of the existence of a moderate fraction of germinal silanols Si(OH)$_2$.

IR and NMR techniques revealed the presence of silanol groups not only on high surface area silicas, but also on low surface area crystalline materials such as, e.g quartz dust [88,89]. Similarly, they are also present on the surface of silicalites [90,91,92,93], although in this case the main maximum is found at slightly lower frequencies, i.e. 3735 cm^{-1}. Additionally, the spectra of silicalite may show a broad absorption at lower frequency (3550–3500 cm^{-1}) which is very strong at 3500-3200 cm^{-1}, for “defective” silicalite samples. The shape and position of indicates that it is due to H-bonded silanols, providing evidence for silanol nests associated to defects in the crystal zeolitic lattice.

Silanol groups are very weakly Brønsted acidic, as shown by the adsorption of basic molecular probes [94], but represent the active sites in the adsorption [95] of both polar molecules such as water, giving rise to ΔH_{ads} ~ – 50 kJ/mol, and of non-polar molecules such as hydrocarbons, with which hydrogen bonding of moderate strength may occur (< 10 kJ/mol). This shows that the protonic activity of silanol groups is definitely weak but non-negligible. In fact, adsorption energy of ammonia on silicas may give rise to evolution of 150-230 kJ/mol [96]. The density of active silanols in amorphous silica is evaluated to be in the range 0.5-8 group /nm^2 depending on preparation and pretreatment [97,98,99].

Recent theoretical investigations [100] concerning the amorphous silica/water interface report the existence of two different types of silanols on silicas, with some hydroxyl groups (some convex geminals and some type of vicinals) which are more acidic (pK_a 2.1 – 2.9). Thus, part of the silica silanols are even more acidic than those of polysicic acids. Instead, concave geminals and the isolated groups would have quite a high pK_a (8.9 and 10.3, respectively), similar to the one of silicic acid in liquid water. This study provides evidence of the effect of the local stabilizing mechanisms of the anionic charge of the dissociated species in determining the acidity of the silanol groups. Similar values of pK_a have been calculated for different silanol species on the 100 and 101 faces of quartz [101]. These data agree with spectroscopic studies performed at the gas/solid interface showing that the silanol groups of silicas are indeed poorly acidic with respect to typical strong Brønsted acids (i.e. with $pK_a < 0$). However, most spectroscopic studies performed at the gas/solid interface do not provide evidence of different families of silanol groups interacting in strongly different ways with the basic probe molecules. Indeed, using very weak basic molecular probes such as CO, adsorbed at low temperature (140 K), two different interactions were observed. In fact, the adsorption of CO over silica outgassed at medium-high temperature causes the partial shift of the band of the free silanols (3745 cm^{-1}) to lower frequencies. The new component, assigned to silanols interacting with CO through the lone pair at the carbon atom, is centered at 3670 cm^{-1}, but a component at 3590 cm^{-1} is also evident in the subtraction spectrum. This confirms that in the case of pure silica, in spite of the sharpness of the band of the terminal silanols, some heterogeneity of these sites occurs, some of them being more acidic than others ($\Delta\nu$OH ~ 75 cm^{-1}; $\Delta\nu$OH ~ 155 cm^{-1}). The extent of these shifts are, in any case, in the range of weak Brønsted acidity [83]. In the CO stretching region a band at 2155 cm^{-1} is well shifted above the value of free CO, and this indicates that an electron withdrawing center interacts with the carbon atom. This band is due to CO H-bonded to the silanol groups.

The really moderate or weak protonic acidity of the silanol group is associated to three main reasons:

i) The silanol species is definitely stable

ii) The delocalization of the anionic charge, and consequently the stabilization of the dissociated from, after dissociation would be quite weak

iii) The stabilization of the protonated form of the base by the silica surface is alo weak, due to its covalency and the wek basicity of siloxane bridges (see below).

These factors make the proton jump associated to Brønsted equilibrium

$$\equiv O_3SiOH + NH_3(g) \leftrightarrows O_3SiOH\ldots NH_3 \leftarrow \equiv O_3SiO^- \ NH_4^+$$

(Fig. 3) unfavoured thermodynamically.

The value of the XPS O1s binding energy is near 532.8 eV [66,102] in both crystalline and amorphous silica. A splitting of this signal, not always observed, is associated to the presence of two different species, the siloxane oxygen (Si-O-Si) and the silanol oxygen (Si-OH), the latter being centered at slightly lower energy [68,103]. These high O1s binding energies are indication of weak basicity of surface oxygen species [104,105].

Indeed protonation of silanol group can occur [106] but only with very strong acids [101], due to its very weak basicity. The pKa of the $SiOH_2^+$ group was evaluated to be < -2 [101]. However, H- bonding interaction of silanol through its own proton with basic species strongly enhances the basicity of its own oxygen atom [107,108]. Conversely, increased Brønsted acidity of silanol groups was reported in the presence of coadsorbed acidic species such as SO_2 [109], possibly showing the reaction of the oxygen atom with such acidic compounds.

2.4.2 The surface siloxane bridges.

Siloxane bridges have been considered to be fully hydrophobic and unable to receive hydrogen bonding [72]. On the other hand, also siloxane bridges have some basicity [110] which is however very low [75]. Recent theoretical data indicate that siloxane bridge can be protonated too, its reactivity strongly depending on its strain: while vitreous silica has a main Si-O-Si angle of near 150°, bridges with 125-135 ° exist and they can undergo protonation [111]. Thus, the more strained the Si-O-Si angle, the more the oxygen basicityThe density of reactive strained siloxane sites is evaluated to be in the range 0.02-0.004 site/nm^2 [112].

The possible interaction of empty 3d orbitals of silicon with $2sp^3$ nonbonding orbitals of oxygen was considered to explain this poor basicity. More recently, the already cited hyper-conjugation effect, i.e. the $n_O \rightarrow \sigma^*_{Si\text{-}O}$(vicinal) interaction, a bonding interaction between an

oxygen lone pair and the antibonding orbital of the vicinal Si-O bond is considered [36,37]. It is likely that this hyper-conjugation increases by increasing the Si-O-Si angle.

Evidence for the non-basic nature of the oxygen species at the surface of silica is provided by the weak adsorption of CO_2, a largely used probe for surface basicity and nucleophilicity, which interacts in a molecular way on the hydroxyl groups of porous silicas [113] and fully siliceous zeolites [114] without any formation of carbonate or bicarbonate species. On the other hand, studies on the adsorption of strong Lewis acids as BF_3 reveal the reactivity of both siloxane and silanol oxygen species, the former before the latter, producing the opening of the siloxane bridge [115] producing $SiOBF_2$ species and, likely F-Si. On the other hand, Si-O-Si, appear to reveal some reactivity also with less aggressive polar molecules at least at high temperature [79,116,117,118].

In any case, the reactivity of siloxanes is very weak. However these sites can be involved in weak but not fully negligible interactions of the van der Waals type,for which experimental evidence was provided, the interaction with silanol groups being considered to be the main one, with maybe additional weaker van der Waals interactions involving mainly siloxane bonds [95,119,120].

2.4.3. Radical centers on silica.

It is well known that a number of radical defects can exist on the surface or in the bulk of amorphous and crystalline silicas, in particular when the sample is subjected to grinding or irradiation with heavy particles or ionizing radiation [121]. Among them, tri-bonded silicon radical (E' or silyl center) ≡Si• and oxygen vacancies (E" center) ≡Si• •Si≡ [122,123], siloxyl centers or non-bridging oxygen hole centers (NBOHC) ≡Si-O• [124], silico-peroxy radical ≡Si-O-O• [125], and, finally, silicon vacancies (≡Si-O•)$_4$ [126], etc. Some of these sites can also exist at the surface and influence the adsorptive and catalytic activity of silicas. Indeed, the existence of oxygen vacancy defect (OVD) sites, of the type ≡Si• •Si≡, was observed experimentally, whose number was shown to depend on pretreatment temperature, with an estimated density of approximately 10^{-3} sites/nm^2 for fused silica heated to 700 °C in vacuum [127]. Other chemically distinct defect sites may also be present on the silica surface, but with a sufficiently low density that their presence is not detectable using traditional methods. Indeed in most conditions, the existence and the role of these defects sites in adsorption is assumed to be negligible.

2.5.Silicas as a catalyst.

Amorphous silica, which has dozens of industrial applications as an adsorbent and a filler, does not seem to have real industrial application as a catalyst, but is very largely used as a support for catalysts and as a binder.

Even if silicas have been usually considered to be quite inert in catalysis, several studies report catalytic activity of silicas in oxidation reactions, in particular in the partial oxidation of methane(MPO) to formaldehyde [128,129].

$CH_4 + 2\ O_2 \rightarrow CH_2O + H_2O$

The activity of such silica catalysts was correlated with both the concentration of strained siloxane bridges and density of surface reduced sites stabilized in steady state conditions. Silica has also been reported to be active for the gas-phase ammoximation of cyclohexanone (by reaction with oxygen and ammonia) to the corresponding oxime [130,131], a key intermediate in the production of ε-caprolactam, and, finally, Nylon 6.

Silica gels have some acidity allowing catalysis of reactions such as the liquid-phase alkylation of phenols and some heterocyclic aromatic compounds with ter-butyl bromide [132], for the condensations of aromatic compounds with sulfenyl chlorides RSCl, chloromethyl sulfides $RSCH_2Cl$, sulfur chloride S_2Cl_2 and thionyl chloride $SOCl_2$ [133], and has been recently found to act as a good catalyst for the S → O acetyl migration to synthesize thiol compounds under mild conditions, showing the merits of high efficiency, high selectivity, long-life recyclability, low cost and scalable availability [134]. A very interesting potential new application of silica is in the hydrolysis of cellulose [135].
Generally silicas have almost no activity in several gas-phase acid catalyzed reactions such as e.g. ethanol dehydration [[136]].

Defective silicalite has an important industrial application as an acid catalyst in the vapour phase Beckmann rearrangment of cyclohexanone oxime to ε-caprolactam with the Sumitomo process [93,137], occurring near 300°C.

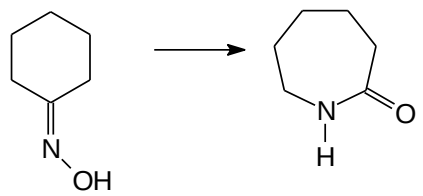

The active sites for this reaction, that is also catalyzed by siliceous beta zeolite [58] and, less efficiently, by amorphous silica are thought to be external and/or internal silanol nests.

2.6. Silicas as support for catalysts.

Silicas find a large industrial application as the support of catalysts [138,139]. This is due, among other reasons, to its good mechanical and thermal stabilities, and ease of scalability. Moreover, silicas are relatively surface-inert, thus allowing preserving the active phases and stabilizing moderately big metal particles, and providing surface area and porosity.

In Table 2 some relevant applications of silica as a catalyst support at the industrial level are reported.

Although the most common support of metals for hydrogenation of hydrocarbons is alumina, silica is used in several cases. Ni and copper catalysts supported on silica are largely used for hydrogenation. In most cases, indeed, the amount of silica is very small, being thus more a stabilizer than a support. Among the applications, the hydrogenation of nitro-compounds to anilines, benzene hydrogenation to cyclohexane, and nitriles hydrogenation to amines, hydrogenation of carbonyls and dehydrogenations of alcohols [145].

Amorphous silica, in particular when modified with alkoxy- or chlorosubstituted silyl compounds, can be used to weakly interact with molecular organic in contact with water solution, thus providing useful catalytic systems for reactions in water [149].

3. Aluminas: solid state chemistry and surface chemistry

3.1 Solution chemistry of Al^{3+} cation and the preparation of aluminum hydroxides.

As a typical metal element, aluminum is soluble in acidic solutions in its cationic form Al^{3+} forming the aquo $[Al(OH_2)_6]^{3+}$ cation. Al^{3+} displays a strong Lewis acidic behavior, not only coordinating six water molecules forming the hexa-aquo ion, but also coordinating a number of basic ligands including, e.g. complexes with several simple molecules such as ammonia [150] and pyridine [151,152], as well as with complex ligands [153] giving rise to coordination complexes mainly with coordination number four or six, but coordination five is also observed [154]. Coordination 3 is rarely observed, due to the excessive Lewis acidity of the metal ion [155]. In fact the d_0 electronic configuration of the Al^{3+} ion and its highly ionic bond with oxygen do not introduce any constraint to its coordination state.

In water solution the $[Al(OH_2)_6]^{3+}$ cation displays some acidity (pKa 4.85) thus producing by dissociation at higher pH the $[Al(OH_2)_5(OH)]^{2+}$ ion, reported to be predominant at 4.8 < pH

< 6 [156,157], likely with less tightly bound water molecules in the secondary hydration shell. Depending on the conditions, i.e. pH, concentration (hydrolysis ratio) and anions present, a number of polynuclear species can also be found in solution such as the dimers $[Al_2(OH)_4(H_2O)_4]^{4+}$, trimers $[Al_3(OH)_4(H_2O)_9]^{5+}$, the tridecameric (or Al13-mer) ion $[Al_{13}O_4(OH)_{24}(H_2O)_{12}]^{7+}$, and the Al30-mer $[Al_{30}O_8(OH)_{56}(H_2O)_{26}]^{18+}$ [158,159]. Aluminum hydroxides start to precipitate at pH 5-6. The minimum solubility of Al hydroxides in water is near neutrality, in the range pH = 6-7, because at pH > 8.5 the solubility increases again with the formation of $[Al(OH)_4]^-$ anion as well as a dimeric species, likely. $[(OH)_3Al–O–Al(OH)^3]^{2-}$ [160].

In conditions where the solubility is exceeded, “gelatinous” precipitates, XRD amorphous, usually first form. Depending primarily on temperature and pH, as well as on aging time, on the nature of anions present and on the copresence of organic components [161], different crystalline hydroxides or oxyhydroxides form (Table 3 and Fig. 4 [162]. At low temperature in excess water the hydroxides are preferentially formed, bayerite α-$Al(OH)_3$ if 5.8 < pH < 9 or gibbsite γ-$Al(OH)_3$ for pH < 5.8 and for pH > 9. At temperatures higher than about 80 °C, the oxyhydroxides become thermodynamically more stable than the trihydroxides and thus tend to form. Boehmite γ-AlOOH or a low crystallinity form pseudoboehmite are most easily formed at atmospheric pressure while the production of diaspore α-AlOOH usually needs higher pressures.

The preparation of (pseudo)boehmites is relevant because its decomposition product is γ-Al_2O_3, the most largely applied transitional alumina for adsorption and catalysis. Indeed, it is obtained, even commercially, by different ways, producing materials with different crystallinity, morphologies and impurities. Among them, we can cite the following:

a) acidification of sodium aluminate solutions (e.g. for the preparation of Versal alumina, from UOP).

b) reaction of sodium aluminate with aluminum sulphate (e.g. used by Grace)

c) neutralization of Al^{3+} acid solutions

d) hydrolysis of Al alkoxides produced by reaction of alcohols with Al metal (e.g. the modified ALFOL-like process used by Condea-Sasol)

e) rehydration of amorphous alumina.

The precipitation of Bayerite is used for the further preparation of η-Al_2O_3 and of θ-Al_2O_3, as done by Sasol starting again from alkolates using the modified ALFOL-like process.

The behavior of Al cations in solution points to the predominant ionicity of the Al^{3+}-O^{2-} bond, typical of metal species, in agreement with the moderate electronegativity of Al^{3+} [65], in

contrast to the definite covalency of the Si-O bond. In fact, this is justified by the larger ionic radius (0.39 Å for tetrahedral coordination, 0.53 Å for octahedral coordination) and lower charge of Al^{3+} with respect to Si^{4+}. However the amphotericity of aluminum hydroxides agrees with the borderline position of aluminum between metals and semimetals. In fact, the acidity of $Al(OH)_3$ appears to be comparable to that of the $Si(OH)_4$.

3.2 Preparation of catalytic aluminas.

γ-, η-, δ- and θ-Al_2O_3, are the most used transitional aluminas in the catalysis and adsorption fields. They are produced (Fig. 4) by calcination of precipitated hydroxides: γ-Al_2O_3 and δ-Al_2O_3 are mainly produced in sequence by calcination of boehmite γ-AlOOH (or its poorly crystallized form denoted as pseudoboehmite), while η- Al_2O_3 is produced by calcination of bayerite α-$Al(OH)_3$. θ-Al_2O_3 can be produced by calcination of both boehmite and bayerite at higher temperature, but usually the preparation for bayerite is preferred.

However, alternative processes to produce aluminas also exist and are used industrially. Degussa-Evonik prepares its Aluminium oxide C, now Aeroxide alumina, γ-Al_2O_3 or a mixture of γ- and δ-Al_2O_3, by flame hydrolysis of $AlCl_3$ [163]. Spherical γ-Al_2O_3 is produced by aluminum evaporation and oxidation [164].

Although the structure of γ-Al_2O_3, η-Al_2O_3 and δ-Al_2O_3 are still not fully established, it seems quite well supported today [10,165,166] that they are defective non stoichiometric spinels, with different distribution of cations and vacancies and maybe occupancy of non-spinel sites [167] as well as different distortion of the unit cell. ^{27}Al MAS NMR data [168,169] and Rietveld analyses of the XRD and neutron scattering patterns [170] confirm that Al ions are present both in octahedral and in tetrahedral coordination in the three structures. The presence of small amounts of pentacoordinated Al^{3+} is usually observed by ^{27}Al MAS NMR [168,169].

The structure of θ-Al_2O_3, instead, is well established. This phase is isostructural with beta-gallia (β-Ga_2O_3), also a spinel-derived structure, where half cations are octahedrally coordinated and half tetrahedrally coordinated.

All alumina and aluminum hydroxides convert at high temperature into α-Al_2O_3, corundum, whose structure is hexagonal with all Al ions in octahedral coordination. α-Al_2O_3, corundum, is the thermodynamically stable form as the bulk free energy is considered.

Amorphous alumina can also be prepared by vaopization of Al metal. Its structure is very rich in petacoordinated Al^{3+}, as evidenced by ^{27}Al MAS NMR spectra, with minor amounts of tetra- and hexa-coordinated aluminum [171]. Amorphous alumina is quite unstable. From

amorphous alumina, γ-Al_2O_3 is mostly formed by calcination, followed by θ-Al_2O_3 and α-Al_2O_3 [172].

3.3 Aluminum coordination in its oxides.

As already said, the s^0, p^0,d^0 Al^{3+} cations do not require particular coordination geometries. Octahedral coordination is the preferred in oxides and hydroxides, as seen for the stable oxide α-Al_2O_3 (corundum), all the four $Al(OH)_3$ polymorphs as well as the two AlOOH oxyhydroxide polymorphs, and also for the hydroxide silico-aluminate clays kaolinite and pyrophillite. Octahedral coordination also occurs in a number of aluminate mixed oxides such as in corundum-type solid solutions with Fe_2O_3 and Cr_2O_3, in perovskites when Al combines with very large trivalent cations (such as $LaAlO_3$ and $NdAlO_3$), in normal spinels when Al combines with small bivalent elements (e.g. $MgAl_2O_4$), in the kyanite Al silicate, etc. However, tetrahedral coordination is also very common, frequently together with octahedral coordination. This occurs in the metastable alumina phases θ-, δ-, η-, γ-Al_2O_3, in mullite and sillimanite Al silicates, in inverted spinels such as $ZnAl_2O_4$, etc… Tetrahedral coordination only also occurs in the form of isolated AlO_4 units such as in the $AlPO_4$ polymorphs, but also in the form of tridimensional frameworks: this essentially occurs in the cases of alkali- and alkali-earth aluminates. This is the case of the “crystobalite-like” structures of $NaAlO_2$ and $KAlO_2$, the “tridimite-like” structure of $CaAl_2O_4$ krotite, and in several other calcium and strontium aluminates [173,174]. Aluminates with a zeolite-like structure also exist such as the sodalite-like structures of $Ca_8[Al_{12}O_{24}](MO_4)_2$, with M = W, S and Cr [175,176].

Pentacoordinated aluminum species are definitely less frequent, but exist in a number of compounds: the Al silicate andalusite (see below), in the silico-aluminate grandidierite $Mg_{0.75}Fe^{2+}_{0.25}Al_3(BO_4)(SiO_4)O$ [177], in the aluminophosphates $AlPO_4$-21 [178], augelite $Al_2(PO_4)(OH)_3$ and senegalite $Al_2(PO_4)(OH)_3 \bullet (H_2O)$ [179], in aluminum borates [180], in the mixed oxides $Al_2Ge_2O_7$ and $LaAlGe_2O_7$ [181] and Lanthanum – Aluminum gallium borates [182], etc. Pentacoordinated Al ions is abundant in amorphous aluminas [171] and in liquid alumina where tetracoordinated Al are predominant but small amounts not only of 6-coordinated al but also of 3-coordinated Al are observed and in liquid alumina [183].

Coordination 3 is expected in gas-phase aluminum oxide clusters [184] but is not found in solid oxides usually. However, XRD and neutron diffraction studies of Zhou and Snyder [170] suggested that 3-coordinated Al^{3+} is present in small amount in the structure of η-Al_2O_3. On the other hand, Al K-edge XANES measurements indicated that 3-coordinated Al can exist in defective zeolites [185].

3.4 Lewis acidity and coordination of Al^{3+} centers.

According to its valence, Al species can produce compounds with coordination three when its bond can be assumed as essentially covalent. However, this is the case only of some gas-phase molecules, such as aluminum halides vapours at high temperatures [186]. The thermal chemistry of aluminum halides, in particular of aluminum chloride, may be relevant to the discussion of Al^{3+} as a Lewis acid. $AlCl_3$ is also an ionic solid with all Al ions in octahedral coordination [187]. However, it melts (or sublimates) at relatively low temperatures (192 °C or 182 °C, depending on the source) producing a liquid constituted by the dimeric form Al_2Cl_6, with tetrahedral coordination for Al^{3+}. The dimeric form predominates at low temperature also in the gas, with increasing content of the monomeric planar trigonal structure increasing in amount at higher temperatures (e.g. 70% at 673 K).

Interestingly, even if liquid $AlCl_3$ is dimeric (Al_2Cl_6), its direct reaction with basic molecules B gives easily "monomeric" tetrahedral complexes with the $BAlCl_3$ stoichiometry together with "monomeric" complexes bonding more than one basic molecule. In particular, the reaction of "dimeric" Al_2Cl_6 with pyridine is easy and gives rise to "monomeric" complexes $PyAlCl_3$, with tetrahedral Al ion, and Py_3AlCl_3 with octahedral Al ion [188,189]. Also with weaker bases, such as e.g. ethyl benzoate, Al_2Cl_6 reacts producing monomeric tetrahedral complexes, i.e. the colourless crystalline compound $AlCl_3(C_6H_5COOC_2H_5)$ [190]. The aluminum atom is tetrahedrally coordinated by three chlorine atoms and by the carbonyl oxygen atom of ethyl benzoate.

Al alkoxides have, most commonly, coordination four (tetrahedral) or six (mostly octahedral), although also coordination five is quite frequently observed (mostly planar-bipyramidal or square pyramidal [191]). On the other hand, it has been reported that, when the oxide-ligands are hindered, aluminum alkoxides can take monomolecular form with trigonal planar coordination for aluminum, with very strong Lewis acidity [192]. In general, the coordination of Al3+ in its complexes depends on the ligands present [193].

These data suggest that Al^{3+} can quite readily change its full coordination from three to six depending on the availability, strength and size of ligands, as well as from temperature.

3.5.The surface chemistry of catalytic aluminas.

3.5.1 Nature of the Lewis acid sites of aluminas.

The surface chemistry of aluminas has been the object of recent reviews [13,165]. The catalytic activity of γ-, η-, δ- and θ- aluminas is undoubtedly mostly related to the high ionicity

of the surface Al-O bond and, as a consequence, to the Lewis acidity of a small number of low coordination surface aluminum ions. The alumina's Lewis acid sites are well characterized by adsorption of basic probes such as pyridine, carbon monoxide, and several other bases followed by IR [13,165,194], ammonia and amines followed by calorimetry [195,196], triphenylphosphine followed by ^{31}P NMR [197], pyridine followed by advanced ^{15}N NMR techniques [198] and UV spectroscopy [199]. They are the strongest Lewis acids among binary metal oxides. Volumetric, TPD and calorimetric experiments allowed also to determine the amount of such very strong Lewis sites present on transitional alumina surfaces, which may however depend on the dehydroxylation degree (depending on the activation temperature) and on the peculiar phase and preparation. Several studies are performed with very weak bases (such as carbon monoxide) as molecular probes, performed after partial dehydroxylation of the surface by outgassing at high temperature [200]. However, it has been shown that removal even of adsorbed molecular water is not needed to reveal surface Lewis acidity if a base stronger than water (such as pyridine) is used as the probe [201]. Recent studies provided some evidence that also surface hydroxyl groups (formally formed by dissociative adsorption of water) can be displaced from Al^{3+} ions by molecules whose acidobasicity is similar to water such as alcohols [202]. Thus, in this case, also highly hydroxylated surfaces or even wet can act as Lewis acidic catalysts, dehydroxylation being not a prerequisite for the appearance of Lewis acidity [201,202]. On the other hand, as shown by Soled years ago [203], full dehydroxyltion of transitional alumina is actually not possible, needing outgassing at so high a temperature that phase transformation to corundum occurs.

Although it is clear that surface Lewis acid sites on alumina are due to coordinatively unsaturated Al^{3+} ions, some debate still concerns the coordination state of such surface ions. Several authors agree, mainly based on IR spectroscopy experiments, that at least three different types of Lewis acid sites (weak, medium, strong) exist on partly dehydroxylated transitional aluminas [198,200,204,205]. Lewis acid sites are certainly coordinatively unsaturated Al^{3+} ions at the surface, which, in principle, may be pentacoordinated (i.e., octahedral with one missing oxide ligand and hence a single free coordination site), tetracoordinated (octahedral with two free coordination sites or near-surface "bulk" tetrahedral sites) and trigonal or tricoordinated (octahedral with three free coordination sites or tetrahedral with one free coordination site). In several recent publications, it has been inferred that pentacoordinated aluminum ions, which are clearly visible in ^{27}Al NMR spectra of γ-Al_2O_3 would determine most of the surface and bulk

chemistry of this material. The authors proposed pentacoordinated aluminum ions to act as the Lewis acid sites absorbing ethanol and catalyzing its decomposition into ethylene [206], acting as structural promoters for phase transitions [207], for anchoring of platinum oxide [208], as well as for the sintering of supported platinum metal particles [209].

Barrow et al. [210] confirmed the observation of surface penta-coordinated Al species on γ-Al_2O_3 using ^{1}H-^{27}Al Cross Polarization MAS NMR. However, it must be taken into account that ^{27}Al NMR may fail in detecting very distorted low coordination species considered to be essentially "silent" in normal experiments [211,212], being probably responsible for very broad bands, such as in the case of dehydrated zeolites where a broad feature at 67 ppm has been assigned to tri-coordinated Al ions [213]. Accordingly, Wischert et al. [214] stated that even current high-field NMR experiments are not (yet) able to provide a complete picture of the structure of γ-Al_2O_3, and much caution should be exercised when interpreting ^{27}Al NMR spectra. In practice, in the case of aluminas the signal due to surface low coordination Al^{3+} (both surface tetracoordinated and tricoordinated) may be very weak or almost silent, thus being not revealed, taking into account the strong intensity of the signal of tetrahedral Al ion which are present and abundant even in the bulk. The signal of surface penta-coordinated Al^{3+} is well evident also because its amount in the bulk is very low, if any.

Indeed, IR studies using both CO [200,201,215] and pyridine as surface "basic" probes, reveal a significant heterogeneity of the Lewis adsorbed species, suggesting that different Lewis sites, i.e. exposed Al^{3+} with different overall coordination. Some authors simulated the adsorption of pyridine on aluminum oxide clusters and found that the calculated shifts of the vibrational modes of pyridine adsorbed on tri-coordinated Al^{3+} ions (giving a tetrahedral complex) agree with those measured experimentally for pyridine adsorbed on the strongest Lewis sites [216,217] (8a mode at 1624 cm^{-1} and 19b mode at 1456 cm^{-1}). Similarly, adsorbed CO species absorbing at 2230 cm^{-1} is certainly associated to very highly uncoordinated species. Theoretical calculations, in agreement with experimental data, indicate that CO interacting with penta-coordinated Al^{3+} gives rise to species with νCO $\sim$ 2150-2160 cm^{-1}, while CO interacting with tetra-coordinated Al^{3+} gives rise to species with νCO $\sim$ 2210-2180 cm^{-1} [218,219,220]. Thus, bands above 2210 cm^{-1} must be attributed to νCO of carbon monoxide interacting with tri-coordinated Al^{3+}. Similar sites were supposed to be the active sites also for methane dissociation and strongest N_2 adsorption [205,221].

The behavior we observe upon pyridine adsorption suggests that a contribution to the spectra can arise from poly-pyridine species. In fact, the species characterized by the 8a mode at 1624 cm^{-1} and the 19b mode at 1456 cm^{-1} is initially not observed, but starts to form

after outgassing at 473 K, when other species (8a at 1615-10 and 1591 cm^{-1}, 19b at 1447-1441 cm^{-1}) are disappearing. It is possible that part of the lower frequency bands are due to di- or tri-pyridine species that decompose by heating into monopyridine one. This would parallel the behavior of $AlCl_3$ that can coordinate a single pyridine molecule forming the tetrahedral complex $PyAlCl_3$, but also three pyridine molecules forming the octahedral complex Cl_3AlPy_3 [222]. The likely formation at high pyridine vapour pressure of poly-pyridine complexes is a further support to the identification of the strongest Lewis sites of alumina as tricoordinated Al^{3+}.

On the other hand, it must be also considered that surface reconstruction of the structure can occur depending on the conditions. As for example, surface tricoordinated Al species can be formed coming from Al ions in tetrahedral sites exposed on the 110 and 111 surface of on the 110-100 edge of the spinel-type structure (Fig. 5). In the bulk spinel structure, the tetrahedra share a face with an empty octahedron of a non-spinel site (i.e. an interstice which is not occupied in the spinel structure). Surface reconstruction certainly occurs for dehydroxylated surfaces [223]. Thus, the exposed 3-coordinated Al ion may reduce its free energy by slightly shifting down, below the surface, entering this octahedron to increase its coordination to four, five or six. This shift can be reversed in the presence of gas-phase bases, thus producing tetrahedral Al species bonded to the base. A similar hypothesis was proposed by Busco et al [224] to occur on zeolites.

Thus, trigonal Al ions certainly represent the strong Lewis sites of alumina producing tetrahedral species by interacting with bases, even if they may not exist as such but mask themselves as tetrahedral or pentacoordinated species or even as a tetrahedron bonded to an hydroxyl-group.

3.5.2. Acido-basicity and the character of surface hydroxyl- groups of aluminas.

Together with Lewis acid sites, the ionicity of the Al-O bond also results in the presence of surface basic sites. O1s binding energy is relatively high, 531.2 eV [102], but is definitely lower with respect to that of silica. Actually, the true particular sites of aluminas for adsorption and most catalytic reactions are very likely anion-cation couples which have very high activity and work synergistically. The basic counterpart may be oxide anions or hydroxyl species. As an example, alcohol adsorption experiments [225,226] allow the characterization of such sites where dissociative adsorption occurs. CO_2 adsorption forming carbonate and bicarbonate species also reveals these sites [227]. The strong activity of γ-Al_2O_3 for position isomerization of olefins, occurring at low temperature only after

dehydration of the catalyst [228], is likely associated to the strength of the acido-basic couples that allows the formation of surface intermediate allyl species [229]. The strongest among these sites may even dissociated methane and hydrogen [214].

Many studies have been devoted to the multiplicity of the surface hydroxy groups of aluminas. At least five components are usually present in the IR spectrum of the hydroxy groups of aluminas, i.e. at ca 3790, 3770, 3740-3720, 3700-3690 and 3580 cm^{-1}, although in many cases the observed peaks are multiple. A number of different assignments have been proposed for these bands. Surface OH groups can also be revealed by ^{1}H MAS NMR: also in this case a large number of peaks may be observed [210,230,231,232,233,234,235,236].

Although most authors attribute to transitional aluminas essentially Lewis acidic properties, several studies show that some of their multiple surface hydroxy groups also have some Brønsted acidity. Actually, among the pure ionic oxides, aluminas is one of the strongest Brønsted acids. Indeed, protonation of bases at the surface of γ-Al_2O_3 has been reported, such as that of n-butylamine [237] and piperidine [94], i.e. bases stronger than the most used probe, pyridine. The activity of pure γ-Al_2O_3 as a good catalyst of skeletal n-butylene isomerization to isobutylene has been attributed to its medium-strong Brønsted acidity, sufficient to protonate n-butylenes at high temperature, producing carbenium ions, but too low to cause much cracking and coking [238].

The reasons for the really moderate but not always negligible Brønsted acidity of the alumina's OH very likely stay in their stability in the undissociated form, evidenced by the practical impossible dihydroxylation of transitional aluminas, as remarked years ago by Soled [203]. On the other hand, the ionic framework of allumina cannot stabilize the negative charge arising from hydroxyls dissociation, although it could likely stabilize the protonated form of the adsorbed base.

Although the surface chemistry of α-Al_2O_3 is far less investigated than those of transitional aluminas, it seems quite established that also on this polymorph surface Lewis acidity and basicity are present, but far weaker. This could be due to the higher coordination of both species in the bulk that will reduce the number of highly uncoordinated sites at the surface and also the extent of uncoordination of the predominant exposed sites.

3.5.3.. Aluminas as catalysts.

Transition aluminas, mostly denoted as γ-Al_2O_3, but actually being sometimes a mixture of γ-Al_2O_3, δ-Al_2O_3 and θ-Al_2O_3, or of η-Al_2O_3 and θ-Al_2O_3, have wide application as catalysts.

Among the most prominent ones, they are used in the catalytic steps of the Claus process, the production of sulphur from H_2S in the refineries [239].

$H_2S + 2\ SO_2 \rightarrow 3\ S_8 + H_2O$

Aluminas for this application have large surface area (300-400 m^2/g), pore volumes 0.5 ml/g of which 0.1 ml/g due to macroporosity (> 750 Å, with loss on ignition of 5.5-6.5 % wt/wt [240]. They may be promoted by iron to reduce deactivation by sulphation.

Aluminas are very active in the dehydration of alcohols to olefins and to ethers [241], and have been used in the sixties for producing ethylene from dehydration of bioethanol at > 250 °C [242].

$CH_3CH_2OH \rightarrow H_2C=CH_2 + H_2O$

They are applied to produce dimethylether from methanol

$CH_3OH \rightarrow CH_3OCH_3 + H_2O$

at 250–280 °C and 0.04–0.05 MPa, as a first step in the methanol to olefin (MTO) process [243]. To increase the rate of this reaction increasing the density of Lewis acid sites is necessary [244].

As reported by deKlerk [245] aluminas are and have been used largely in the refining of Fischer Tropsh syncrude. In particular thay are used to increase octane number through position isomerization of terminal to internal olefins, for the iskeletal isomerization of n-pentene to isopentene as well as to dehydrate higher alcohols to olefins.

Aluminas are reported to be used in the production of chloromethane from methanol and hydrogen chloride [246]

$CH_3OH + HCl \rightarrow CH_3Cl + H_2O$

All these reactions implying alcohols as reactants are mostly activated by chemisorption of the alcohol through one of its oxygen lone pairs to the Lewis sites of alumina.

Aluminas may be used for the dehydrofluorination of alkylfluorides which are byproducts of the HF catalyzed isobutane / butylene alkylation process. Fluoroalkanes react at 170-220°C, being converted to olefins. HF is adsorbed on the alumina to form aluminum fluoride, regeneration being needed every 6 months [247].

3.5.5 Aluminas as supports of catalysts.

Aluminas find very large application as supports of catalysts. In particular, they are the standard supports for many metal and sulphide catalysts. When applications requiring relatively low reaction temperature (< 500 °C) are considered, such as for hydrotreating with supported sulphides or hydrogenation using platinum, palladium or nickel metals as the

active phases, high surface area γ-, δ- or η-Al_2O_3, can be used. Transitional aluminas are also used as supports of partial oxidation reactions occurring at quite low temperatures, such as e.g. the oxychlorination of ethylene to ethylene dichloride in the process to produce vinyl chloride monomer, performed over alumina supported copper chloride at 300 °C.
These supports, however, are characterized by high acidity and reactivity, thus not applicable when very reactive compunds are present in the reactant mixture. For this reason, less reactive and lower surface area θ- or α-Al_2O_3 are used. This is, e.g. the case of Pd catalysts for 1,3-butadiene hydrogenation, where the oligomerization of the diene on the support has to be avoided. α-Al_2O_3 is also used as the support of silver catalysts for ethylene oxidation to ethylene oxide, where also the reactivity of the support must be limited. θ-Al_2O_3 is a common support for total oxidation of volatile organic compounds (VOC), such as those based again on Pt and Pd, where temperatures of the order of 400-800 °C are produced. Similarly, θ-Al_2O_3 seems to be one of the best supports for Rh used in methane catalytic partial oxidation (CPO) to syngas, a promising new process to produce hydrogen. Stabilized aluminas, such as γ-, δ-, η- and θ-Al_2O_3 containing either silica or alkali, alkali earth or rare earth cations, such as K^+, Ca^{2+}, La^{3+}, are largely used also for applications at medium- high temperature. This is the case for some endothermic reactions such as steam reaforming or partial oxidation reactions using nickel platinum or rhodium catalysts. Also wash-coats of car's catalytic mufflers, based on Pt-Rh or Pd, are based on alumina mixed with ceria, zirconia and lanthana.

3.5.6 Other applications of aluminas. Aluminas find also a number of applications in adsorption [248], in particular for purification treatments of waters [249], of as well as in the field of catalysis, as "binder" or an "active matrix". This is in particular the case of the use of alumina as a "separated" component of the mixture used as transport bed catalysts in the Fluid Catalytic Cracking process. In this case, in fact, the real catalyst component is based on Faujasite zeolites, usually Rare Earth –Y or Mg-HY zeolites (see chapter 7). However, the mixture of powders used in FCC reactors contains several components, as cocatalysts, binders and active matrices. High surface area alumina, or their precursors such as boehmites [250,251], are added to the catalysts to have the role of Nickel scavenger. In fact, the feed to this process usually contain Ni-porfirin compounds that depose somewhere their Ni ions that, reduced to metal, give rise to unwanted dehydrogenating catalytic activity. Ni-porphirins tend to react specifically with alumina, where they are partially stabilized in the bivalent state, thus reducing the amount of Ni metal produced on tha catalyst.

Aluminas are also the precursors for fluorided and chlorided aluminas, which may be produced *in situ* upon halogenation, as well as for silicated aluminas (see below), borated aluminas and other “modified aluminas” produced *ex situ* by chemical treatments

4. Silicated or silica-doped aluminas.

Some commercial aluminas actually contain small amounts of silica mainly for stabilization against the phase transformation to corundum and resistance to coking. Some of these materials are prepared by deposing silica over alumina or its hydroxide precursor. This is the case in particular of the Siralox family of Sasol (previously Condea), whose preparation and characterization has been reported in some detail [252]. Similar materials, denoted as silicated aluminas, are prepared by deposition of orthosilicates (like tetraethoxysilane, TEOS) at the surface of alumina [253,254,255]. According to Trombetta et al. [256] and to Daniell et al. [252] these materials, also denoted as silica-doped aluminas [257] almost independtly of the preparation procedures, have the structure of γ-Al_2O_3, silica being located at least in large part at their surface . This is deduced by the presence of the typical IR spectroscopic features of surface silanol group and also by the presence of Si-O stretching modes at 1100-1050 cm^{-1} that are strongly perturbed by adsorption of bases like pyridine [83].

It is remarkable that the addition of silicate species to alumina (at the surface or in the bulk) gives rise to terminal silanols but does not produce bands in the region of bridging OHs. No relevant Brønsted acidity is observed on these materials [253,255,256,258] although the acidity of the terminal silanol might be slightly enhanced [255,259]. This is explained suggesting that Si-OH groups tend to dissociate over the ionic alumina surface. Silicate species tend to maximize the interaction with the bulk of alumina by orienting three oxygen atoms toward the bulk, while the fourth necessarily stands up, with respect the surface. To limit the free energy, the fourth oxygen standing up bonds with a proton. It seems obvious that it cannot bend to bridge surface aluminum cations. The resulting Brønsted acidity is consequently that of isolated silanols, weak although possibly enhanced by the vicinity of Al ions

The materials rich in alumina reveal the presence of surface Lewis acid sites similar in quality to those of alumina [260]. Some studies, however, indicate that they may be decreased in amounts but some of them are maybe slightly increased in strength [255].

Similar materials are very active for the diethylether (DME) synthesis from methanol at 300 °C and atmospheric pressure [261]. The presence of silica would increase acidity and

resistence to coking. Similar materials are excellent catalysts for the skeletal isomerization of butylenes to isobutylene at 400-450 °C [255,262,263]. A similar catalyst was apparently reported for the ARCO tert-butyl alcohol dehydration process to produce pure isobutylene: the reaction occurs in the vapor phase a 260-370 °C at about 14 bar , with a conversion of 98% [264].

5. Solid state chemistry of aluminum silicates and silico-aluminates.

5.1 Layered aluminosilicate “oxyhydroxides”.

A number of crystalline mixed silicon, aluminum oxides and oxy-hydroxides are known. Kaolinite, halloystite, pyrophillite and donbassite are Si,Al hydroxide compounds. All are layered structures belonging to the phyllosilicate family.

Kaolinite has layers composed of a phyllosilicate sheet constituted by tetrahedral SiO_4 silicate groups sharing three corners, and a sheet containing octahedral $AlO_4(OH)_2$ complexes (1:1 sheet), giving rise to the overall stoichiometry $Al_2Si_2O_5(OH)_4$ (Si:Al ratio =1). Halloysite has essentially the same structure, but the 1:1 unit layers are separated by a monolayer of water not present in kaolinite. Anauxite and dickite also have the same layer structures of kaolinite. Pyrophillite layer structure has two phyllosilicate sheets sandwich an Al-containing octahedral sheet (1:2 sheet), with formula $Al_2Si_4O_{10}(OH)_2$ (Si:Al ratio =2). In all these cases, silicon is tetrahedral while aluminum is fully octahedral.

Al for silicon substitution in the phyllosilicate layer gives rise to a charge defect that must be compensated by cationic species in the interlayer specieIn the case of micas, like e.g. muscovite $KAl_3Si_3O_{10}(OH)_2$, the charge of the layers is balanced by interlayer hydrated potassium ions. In dioctahedral chlorite structures two families of octahedral Al species exist together with tetrahedral Al substituting for silicon in the phyllosilicate sheets. An example is donbassite, with the empyrical formula $[Al_2Si_{4-x}Al_xO_{10}]$ $[Al_{2+x/3}(OH)_8]$ [265] and a typical Si:Al ratio = 0.56, with both octahedral and tetrahedral Al ions.

5.2. Aluminum silicates

The above described alumino-silicate “oxyhydroxides” decompose at moderate temperatures producing mostly amorphous aluminum-silicon mixed oxides and gaseous water. The decomposition of kaolinite produces the so-called “metakaolinite”, which is indeed an amorphous silica-alumina with Si:Al atomic ratio ~ 1. This material is obviously quite impure of metal elements, as the original kaolinite mineral is. Heating of this material produces the progressive crystallization of mullite and usually of cristobalite. In fact,

according to thermodynamics (Fig. 6 [266]), between alumina (corundum) and silica (quartz, tridimite and cristobalite, depending on the temperature) the only intermediate phase that has thermodynamic stability is mullite [267], whose composition ($Al^{VI}_2Al^{IV}_{2+2x}Si_{2-2x}O_{10-x}$) mostly ranges between $3Al_2O_3.2SiO_2$ and $2Al_2O_3.SiO_2$, i.e. with Si/Al a.r. ÷ 0.25-0.33).

Additionally, three crystalline polymorphic forms of aluminum silicates also exist as metastable phases, all with formula Al_2SiO_5 (Si/Al a.r. 0.5) i.e. kyanite, andalusite and sillimanite [268]. Aluminum coordination is octahedral in kyanite and half octahedral and half pentacoordinated in andalusite. In both these cases, isolated tetrahedral sites exist only occupated by silicon as orthosilicate species. The structure of sillimanite consists of chains of edge-sharing AlO_6 octahedra crosslinked by double chains of TO_4 tetrahedra with strict alternation of Si and Al.

The structure of mullite can be derived from that of sillimanite. The further substitution of some Si by Al in the tetrahedral sites, gives rise to O vacancies and the formation of AlO_4 tetrahedra triclusters sharing a common O atom. In the case of high alumina mullite (with Si/Al a.r. 0.25), one every 25 oxygen atom is lost, producing two tetrahedra triclusters, while in the case of low alumina mullite (with Si/Al a.r. 0.33) one every 40 oxygen atom is lost, producing two tetrahedra triclusters.

According to thermodynamics, no solubility exists between corundum and silica (Fig. 6). However, data agree that some solubility exists of silica in metastable spinel-type alumina. A spinel-type phase with composition $6\ Al_2O_3\ .\ SiO_2$, where Si substitutes for Al in tetrahedral coordination, i.e. as a isolate orthosilicate species, has been reported as a metastable form [269]. A spinel phase with the composition of mullite from $2Al_2O_3.SiO_2$ to $Al_2O_3.SiO_2$ is also observed during the crystallization of mullite from amorphous precipitates [270,271] and upon the thermal transformation of kaolinite first to largely amorphous metakaolinite and later to mullite + cristobalite [272,273]. According to Schneider et al. [274] the SiO_2 content of the γ-alumina gradually rises with temperature and reaches a maximum amount of ≈ 18 mole% at 1150°C which corresponds to the following structure: $^{IV}[Si_2Al_6]\ ^{VI}[Al_{12.67}{*}_{3.33}]O_{32}$ where * denotes vacancies. In practice, spinel like phases may exist with maximum Si/Al a.r. < 0.5 - 0.2. It seems interesting to remark that the four known crystalline Si,Al mixed oxides are all Al-rich, with Si:Al ratio ≤ 0.5. Materals with Si:Al > 0.5 are essentially amorphous or biphasic.

5.3 Framework aluminosilicates.

Framework aluminosilicate structures have the common feature to be constituted by a negatively charged $[Si_{1-x}Al_xO_2]^{x-}$ (with $x \leq 0.5$) framework constituted by corner sharing tetrahedra, with charge balancing cations located in "extraframework" voids. In all cases Si/Al a.r. is ≥ 1.

Feldspar structures.

Potassium and sodium feldspars, such as orthoclase, microcline, sanidine and albite, are framework aluminosilicates with formula $MAlSi_3O_8$ (M = Na,K) while calcium feldspar, i.e. anorthite, has the formula $CaAl_2Si_2O_8$. In these cases silicon and aluminum atoms occupy the centers of corner sharing tetrahedra forming an intricate, three dimensional, negatively charged framework. The alkali or alkali earth cations sit within the voids in this structure. In pure anorthite, AlO_4 and SiO_4 tetrahedra alternate regularly forming a fully ordered structure, and calciums are located within an irregular cavity bounded by about 10 oxygens. In alkali feldspar, ordering of Si and Al tetrahedra occurs in low temperature forms. Aluminum locates in one of the two crystallographic positions in microcline while it regularly alternates in the two positions in orthoclase. In the case of "high temperature forms", such as sanidine (another $KAlSi_3O_8$ polymorph) the tetrahedra are randomly mixed but it should occur without production of Al-O-Al bridges [275]. It seems interesting to remark that excess Al could be located in extraframework positions in feldspates [276].

Feldspathoids and "stuffed silicas".

Feldspathoid aluminosilicates have mostly larger Al content than feldspates. Among them, stuffed silicas are framework aluminosilicates whose tetrahedral frameworks retain the basic geometries of crystalline silica polymorphs [277,278,279,280], with a Si:Al ratio ~ 1. As said above, silica structure have low density, associated to the covalence of the bonds. Thus, interstices are present in the structure. As for example, quartz structures contain spaces that can host ions in tetrahedral or in octahedral coordination (Fig.7) In the case of β-eucryptite, $LiAlSiO_4$, the basic framework is that of β-quartz where, however, half Si atoms are substituted by Al, the corresponding charge defect being compensated by "extraframework" Li ions. The monovalent Li^+ cations are located in tetrahedral interstices formed by four oxygen atoms each shared by two tetrahedra, occupied by Al and by Si, respectively [281].Thus, Li atom is surrounded by eight different tetrahedra in β-eucryptite. In Fig. 8, left, the coordination of Mg in a $Mg_{0.5}AlSiO_4$ phase recently described [282] is reported. Here the framework structure is that of α-quartz, and Mg^{2+} occupying octahedral interstices. In the case of the $NaAlSiO_4$ polymorphs nepheline, a stuffed derivative of

tridymite, and carnegierite, a stuffed derivative of cristobalite, Na ions occupy six coordinated sites.

Leucite $KAlSi_2O_6$ can also be considered in the frame of feldspathoids and of zeolites: its framework, analogous to that of analcime (ANA), consists of singly-connected 4-tetrahedra membered rings (4-MR) rings, arranged in chains coiled around tetrad screw axes. Every 4-MR is a part of three mutually perpendicular chains, each parallel to a crystallographic axis. An ordered Si/Al distribution was found [283]. Potassium is coordinated to twelve oxygen atoms in the cubic form while coordination number is reduced to six in the low-temperature tetragonal polymorph.

Zeolites

Zeolites differ from other framework aluminosilicates because the cavities hosting charge balancing cations are larger, allowing several cations being located in the same cage and stay in a highly hydrated form. Cavities are interconnected by channels that give rise to a variety of microporous structures which can be penetrated only by sufficiently small molecules, so giving rise to the “molecular sieving” effect [284]. The cations are exchangeable, so zeolites may also act as cationic exchangers. The Si/Al ratio in natural zeolites is quite variable, typically ranging 1- 6, but in synthetic zeolites it can be much higher, up to ∞. In fact, pure silica zeolites, usually denoted as silicalites, have also been prepared for several zeolite frameworks. Silicalites, obviously, do not contain cations in the cavities.

Cationic zeolites may have Si:Al ratio up to 1, such as is the case of faujasite and A-type zeolite. These materials, although being also metastable phases, have significant thermal stability.

5.4. Silicon and aluminum in aluminosilicate glasses.

The structure of aluminosilicate glasses has been the object of a number of studies applying vibrational spectroscopies (Ir and Raman), solid state NMR spectroscopy and computational techniques. Most of Al ions is in coordination four in glasses with modifier oxides equal to or in excess of alumina, e.g., peralkaline compositions with Si/Al > 1 and Al/Na < 1, and form an integral part of the rigid silicon-oxygen glass network. However, ^{27}Al NMR studies have demonstrated that glasses frequently also contain small amounts of aluminum species in coordination five even when stoichiometry does not need it [285], while minimum amounts of six-coordinated Al ions can also be present. This is likely associated to the remarkably higher densities of SiO_2-Al_2O_3 glasses with respect to silica glass [286,287], see Table 1.

Pentacoordinated aluminum may be especially important in mechanisms of viscous transport in silica-rich melts. ^{17}O NMR, thallium-probe ion luminescence spectroscopy and X-ray photoelectron spectroscopy also show the existence of non-bridging oxygens (NBO) [288], i.e. oxygen species bonded to a single tetrahedral group [289], which may interact with higher coordination aluminum [290]. Additionally tetrahedral triclusters (oxygen shared by three tetrahedral [291,292]) can also balance NBOs to maintain local charge balance [293]. The interplay of these "defect" structures determine several relevant properties of glasses.

5.5. On the Al/Si distribution in aluminosilicates including zeolites. The "Lowenstein rule" and the stability of Al-O-Al bonds in zeolites.

As we have already seen, the silicon to aluminum atomic ratio crystalline aluminum silicates is < 1, and in this case aluminum may have both 4-fold and 6-fold coordination, and also in case 5-fold coordination. In contrast, in most silicoaluminates the Si/Al atomic ratio is ≤ 1 and Al is essentially tetrahedral only. The so-called Löwenstein's rule of "aluminium avoidance" [294] states that the Si and Al location is ordered in silicoaluminates, with strict alternance of them in tetrahedral framework when Si/Al a.r. is ~ 1. Thus, Löwenstein's rule prohibits –Al–O–Al– linkages from occurring in these materials. This rule is substantially obeyed in particular in the case of natural zeolites [295,296] and in most Al-rich zeolites such as NaX [297]. Recently, the strict validity of this rule for zeolites was questioned using density functional theory (DFT) theoretical calculations for protonic zeolites [298]. Previous theoretical calculations mostly agree in showing that "Lowenstein" clusters (without Al-O-Al linkage) are more energetically favorable than "non-Lowenstein" clusters (which contain such bridges) in the gas phase [299]. However, the energetic preference for the Löwensteinian model (with strict validity of the Löwestein rule), with respect to models where this rule is relaxed, was found to be sufficiently small to be overcome by thermal energies at high temperatures, at least for zeolite A [300]. Actually, the existence of Al-O-Al bonds in tetrahedral networks is not impossible, seen the existence of several calcium and strontium aluminates with Al-only tetrahedral networks, as cited above. In practice these bonds can occur as defects, in particular after low temperature preparation preocedures, or be the result of disorder induced by high temperature, but may be precursors for framework dealumination [296].

The situation is different for protonic zeolites. Protonic zeolites with low Si:Al ratio down to 1, as H-LTA and H-FAU zeolites (the latter denoted as HX faujasite) can be prepared with

difficulty and are unstable, suffering very easy dealumination. This behavior provides evidence of the stabilizing effect of cations towards Si;Al tetrahedral structure. Acid zeolites with Si:Al ratio > 5 have usually better stability, depending from the structure (as for e.g. H-FER, H-MOR and H-MFI zeolites) but also dealuminate quite easily, while materials with larger Si:Al ratio, like 30-300, such as ultrastable Y Faujasite (USY), have usually batter stability.

The “stability” of these structures, however, should not be only evaluated in terms of thermodynamics, as mostly done by theoreticians. Taking into account that zeolites are thermodynamically unstable structures and tend to convert into mullite and silica, or to amorfize, the lack of Al-O-Al bonds can be associated to the “kinetic” tendency of such structures to produce dealumination, in particular but not only in the protonated forms. Dealumination is a process implying expulsion of Al ions from the tetrahedral framework, producing “extraframework” Al (or Si-Al oxide) debris, and occurs in the case of Si-O-Al-OH-Si structures, but should occur even easier in the case of Si-O-Al-OH-Al-OH-Si (non Löwenstein) structures.

Zeolite materials with Si/Al a.r. well above 1 exist naturally in cationic forms and/or can be prepared in both cationic and protonic forms. In this case, it becomes relevant to determine the distribution of Al in the tetrahedral framework. In the case of natural zeolites, ordered structures and disordered structures exist [295,296,301]. According to the so-called Dempsey’s rule [302], there is a tendency to ordering to maximize the distance between each aluminum atom is in order to stabilize the frameworks. In case of protonic zeolites, this point may be very relevant for explaining details of catalytic activity. Taking into account that these materials are prepared by low temperature procedure, the distribution apparently depends on kinetics and on the particular structure, and may vary with several different procedure details. To define the Al distribution in this case advanced techniques have been developed recently [303].

6.Protonic zeolites: surface chemistry and catalysis.

Protonic zeolites, i.e. those zeolites where the framework charge is balanced, formally, by protons, find industrial applications as acid catalysts in a large number of hydrocarbon conversion reactions in refinery and petrochemistry (Table 4). The application of these materials is due to three main properties:

i) the strong Brønsted acidity of bridging Si-(OH)-Al sites generated by the presence of aluminium inside the silicate framework and the balancing proton [304,305];

ii) the shape selectivity [306,307] and other confinement effects [308] due to the molecular sieving properties associated to the well-defined crystal pore sizes, where the catalytic active sites are located;

iii) their environmental friendliness, well superior to that of alternative acid catalysts.

6.1 Preparation of protonic zeolites.

The original method for preparing zeolites [309] was based on hydrothermal crystallization of reactive alkali metal aluminosilicate gels at high pH and, typically 100 ° C and ambient pressure. With this method, where alkali cations play the role of directing the formation of the zeolite structure, materials with low to intermediate Si/Al ratios (1 – 5) are produced in the cationic form. Exchange with ammonium ions allows the production of the ammonium forms of zeolites that can be converted into protonic forms by calcination with resulting decomposition of ammonium ions.

After the pioneering work of Barrer [310], new techniques for the preparation of zeolites have been developed, mainly involving the use of “templates” or “organic structure directing agents” (OSDAs) [311,312]. Protonic zeolites are thus prepared at 100-200 °C, using cationic templates that are later decomposed, burnt off or washed off, leaving protons as the only balancing cationic species. With these techniques, the preparation of a number of new protonic zeolites with many different structures has also been obtained. With this method high silica zeolites and, in the absence of aluminum species, a number of purely siliceous zeolites have been prepared. From protonic zeolites, cationic zeolites are produced by cationic exchange.

The addition of fluoride to the reactive gel led to more perfect and larger crystals of known molecular sieve structures as well as new structures and compositions. The fluoride ion also is reported to serve as a template (or SDA) in some cases. Fluoride addition extends the synthesis regime into the acidic pH region.

The cheapest source of silicon is waterglass, i.e. an acqueous sodium silicate solution with small contamination of aluminum. Consequently, it cannot be used to prepare pure silica zeolites. To produce purely siliceous zeolites colloidal silica sols, fumed silicas, precipitated silicas as well as alkoxy-silanes can be used as the Si source. They are more expensive, and, at least for alkoxy silanes, toxicity concerns appear. As for the source of aluminum, Al salts or sodium aluminates are used.

6.2. The bridging hydroxyl group.

The strongly acidic hydroxy groups of zeolites are well characterised by the presence, in the IR spectrum, of moderately sharp and strong bands in the region between 3650 and 3500 cm^{-1} (Fig. 8) as well as by evident ^{1}H MAS NMR peaks in the region 3.6 – 8.0 ppm [86]. With both techniques, it is possible to reveal the acidity of these groups [76]. In fact these spectroscopic signals disappear upon contact with bases like ammonia, pyridines, amines and phosphines, in parallel with the appearance of the features of the corresponding protonated bases. In the presence of weak basic probes (CO, nitriles) a significant perturbation of the spectral characteristics of these groups is evident too.

Both IR and ^{1}H MAS NMR spectra of zeolites distinguish very well from those of silicas (Figs. 2 and 8) and silica aluminas. This is shown, as an example, for the zeolite ferrierite H-FER as compared to the spectrum of a mesoporous silica-alumina (Al-MCM41) in Fig. 9 [313].

The position of the IR band due to bridging OH's is somehow dependent on the size of the zeolite cavities, νOH being generally (but not really always) the lower the smaller the cavity. In particular, the OH stretching band position and width can be influenced by weak H-bondings through the cavities [314]. In the case of zeolites with more than one type of quite different cavities, splitting of the band of the bridging hydroxy groups can be observed. Some authors suggested that a correlation exists between OH stretching frequency and the Si-O(H)-Al bond angle [315]. As for ^{1}H MAS NMR peaks of protonic zeolites, the trend among different studies is for increased chemical shift corresponding to an increase in the intrinsic acid strength [316], i.e., protons are more de-shielded in zeolites perceived to be more acidic. On the other hand, the peak position is also sensitive to location: peaks at 3.6–4.3 ppm are due to bridging OH groups in large cages and channels; peaks at 4.6–5.2 ppm to bridging OH groups in small cages of zeolites, while those at 5.2–8.0 ppm are associated to disturbed bridging OH groups interacting with framework oxygen [86]. Parallel ^{1}H NMR and IR studies show that the IR extintion coefficient of the zeolite's bridging OH's is far higher than for silanol groups, and this allowed Kazansky et al. [317] to propose to use the intensity of the IR band to determine the surface acid strength.

Interestingly, bridging OH's are only detected in the interior of the zeolitic cavities, being the corresponding spectroscopic features (both IR and NMR) absent in any non zeolitic material based on silica and alumina [83,318,319] and also on the external surfaces of different zeolites. Thus, the existence of the bridging hydroxy groups Al–(OH)–Si should imply the existence of the cavity. In other words, the cavities (or the microporous zeolitic framework)

are possibly involved in the generation and/or stabilization of the bridging OH sites, as well as in the strengthening of their acidity [83,320].

Besides “zeolitic” bridging OH’s, additional OH groups are or may be observed in the case of H-zeolites. Terminal silanols similar to those of silica (νOH at 3745±3 cm^{-1}, ^{1}H NMR signal at 1.2-2.2 ppm) have been found to be located at the external surface, while additional features (νOH at ca. 3780 and 3675 cm^{-1}, ^{1}H NMR signal at 2.4–3.6 ppm) are usually attributed to OH’s on extra-framework (EF) alumina or silica-alumina matter. Finally, broad absorptions are also frequently detectable in Al-rich zeolites at lower frequencies (3500-3200 cm^{-1}), likely due to strongly H-bonded OH’s in small cavities, such as Al-rich H-FER [321] and H-CHA with Si/Al atomic ratio of 2 [322], but also H-MFI and H-MWW [10,80] in agreement with the theoretical work of Yan Li et al. [323].

6.3. On the poor stability and strong Brønsted acidity of protonic sites of H-zeolites.

All data confirm that the Brønsted acidity of protonic zeolites is due to the bridging OH groups. The spectroscopic data agree suggesting that such acidic protons are actually linked (in the dry zeolite) through an essentially covalent bond to oxygen atoms bridging between a silicon and an aluminum atom. These sites can thus be considered as “perturbed silanol groups”, where an oxygen lone pair interacts with the nearest Al cation through a Lewis base acid bond. This Lewis acid-base interaction is certainly “favored” thermodynamically and “exothermic”. However, all available data indicate that the basicity of the silanol group, i.e. the availability of the electron lone pairs at oxygen, is extremely weak. Thus this interaction is weak, and definitely weaker as compared to the interaction of the dissociated silanol with Al^{3+} as it occurs in aluminosilicates.

The poor stability of bridging OH’s in alumina-rich environments is also somehow demonstrated by the easy de-alumination of Al-rich zeolites in the protonic form, such as e.g. H-X and H-LTA, in contrast to the strong stability of both Al-rich alkali-zeolites (like Na-X and Na-LTA) and of the highly siliceous protonic zeolites, as USY, and silicalites too. It can be supposed that the stabilization of the bridging OH’s is associated to the existence of the quite rigid and highly covalent silica-based zeolite crystalline framework, the more, the more silica-rich the framework is. In contrast, the Al coordination in silicoaluminates is flexible and variable, where coordination 6, 5 and 4 and, to some extent, even 3, are allowed, easily obtained and well characterized. Some weak interactions of the proton of bridging OH’s with the other oxygen atoms exposed on the zeolite cavities might also give a stabilizing contribution. Recently Otsuga et al. [324] reported on a temperature-dependent

behavior of acidic OH groups on zeolites: gradual shifts in the peak-top position to lower frequencies and decreases in integrated intensity were observed by infrared spectroscopy, more pronounced in the order CHA < MFI < MOR. This behavior was attributed to the dissociation of OH groups to form IR inactive species at high temperatures, with proton migration in other positions.

The substantial instability (poor stability) or the bridging silanol is certainly a factor favoring its intrinsic strong Brønsted acidity. Another reason for high acidity of protonic centers in zeolites is associated to the stabilization of the framework when the proton is lost and the silanol converts into a silicate species. The ionic interaction of silicate, a quite strong base, with the strongly Lewis acidic Al^{3+} ion, is quite strong, like it occurs in all aluminsilicates. On the other hand, the negative charge formally formed on the silicate's oxygen upon proton jump may be somehow "delocalized" on the four nearly equivalent oxygen atoms surrounding the Al cation, as well as over the other siloxane's oxygens by the already cited hyperconjugaton effect.

A fourth powerful effect is related to the stabilization of the protonated base by the "tridimensional solvation" occurring in the zeolite cages by multiple Van der Waals interactions with the walls of the cavities, i.e. with the exposed siloxane bridges (Fig. 10). This differentiates microporous materials from normal porous or mesoporous surfaces, where these solvation effects are certainly less and, overall, weaker.

Several papers report on the slightly stronger Brønsted acidity of silica-rich protonic zeolites with respect to alumina-rich protonic zeolites [325]. This can be explained by the delocalization of the negative charge of the dissociated species over Si-O-Si siloxane bonds due to the hyper-conjugation effect discussed above. This effect is more efficient the more polymerized the silicate species is. Thus, it can explain the slightly stronger acidity of low Al-content zeolites with respect to zeolites richer in Al, due to the lerger "polysilicate" fragments existing in the former than in the latter. This phenomenon, with the delocalization of the negative charge on the siloxane oxygens of the cavities, could also further strengthen the interactions of the cavity walls with the protonated base.

On the other hand, it must also be considered that the molecular traffic may be more hindered on zeolites richer in protons with respect to zeolites with less protons, due to the strong interaction of molecules with more adsorbing sites. This might result in lower catalytic activity even if the acidity is not weaker [326]. Additional effects due to the cavity shapes and sizes (with respect to the base molecular shape and size) may also play a role when the acidities and catalytic activities of different zeolites are compared, as discussed below.

6.4. On the Lewis acidity of protonic zeolites

Lewis acidity in protonic zeolite is due to available coordinatively unsaturated Al^{3+} ions, as shown by the adsorption of molecular probes. Studies using hindered probe molecules demonstrated that Lewis acid sites may occur at the external surface of zeolites, where the "zeolitic" structure in some way vanishes [80,318]. Additionally, Lewis acidity frequently comes from "extraframework" matter, composed by alumina-like or silica-alumina-like debris. In fact, protonic zeolite catalysts may contain, as a result of the preparation, or of an intentional pretreatment, significant amounts of species external to the framework. Several zeolites are actually applied after treatments tending to increase their stability and also, in case, to further enhance surface acidity and shape selectivity effects. These treatments, like steam dealumination, can cause the decrease of the framework Al content and the release from the framework of aluminum-containing species [327] that may contribute in stabilizing the framework, but can also contain additional catalytically active acid sites. These particles can also narrow the size of the zeolite channels or of their mouths, thus improving the shape selectivity effects. Extraframework material is composed by very small particles mostly containing Al cations complexed by oxide ions and/or OH's but sometimes also involving silicate species, being similar to silica-alumina debris [327], likely interacting with the framework walls, located in the cavities or on the external surface. As said, the presence of EF gives rise to the presence of strong additional bands in the IR OH stretching, usually above 3750 cm^{-1} and in the region 3730-3650 cm^{-1}. These species are also responsible for ^{1}H NMR peaks at -0.5- + 0.7 and 1.7-2.7 ppm [86] and reveal medium-strong Brønsted acidity. Similarly, the detection of octahedral Al ions in ^{27}Al NMR techniques is evidence of EF. EF species usually contain exposed Al ions acting as strong Lewis acid sites.

Recently, it has been pointed out the possible activity of framework Al ions as Lewis acid sites [328]. It seems likely that Al ions can behave as other cations do, in framework positions in zeolites. This is the case e.g. of Ti^{4+} in Ti silicalite TS-1 [91] as well as of Sn^{4+} and other cations, that behave as Lewis acids when in substitutional positions in silicalites [329]. It is normally supposed that the access of basic molecules to the framework Al^{3+} ions does not occur mainly because it is hindered by, or competes with, the interaction of the base with the near proton. Nevertheless, in complex pore zeolites it is possible that Al ions can interact with basic molecules when the proton is in position internal to another cavity. This is the case, e.g., of USY faujasite (Figs. 11 and 12), where it has been proposed [328] that framework Al ions can be active in adsorbing bases from the supercage when they are

associated to protons located in the sodalite cavity or in the hexagonal prism. Tetrahedral framework Al ions can enlarge their coordination to five, without any dehydration, by reacting with a base from the other side with respect that where the acidic OH lays. This point has also been discussed on theoretical grounds by Busco et al. some years ago [330].
The data and our interpretations suggest that also extraframework material-free (or nearly free) high silica zeolites may display Lewis acidity and could act as Lewis acid catalysts, due to the activity of framework Al atoms. It has been reported, in particular, that the sample USY (30), an ultra-stable dealuminated Y faujasite, is an excellent catalyst for some fine chemistry reactions most typically catalyzed by homogenous Lewis acids [331].

6.5. Cavity effects in catalysis on protonic zeolites.

The relations between structural parameters and acid strength of hydroxyl groups of zeolites have been object of many discussions. Sastre, Niwa and coworkers concluded that a complex mixture of short- and long-range factors is at play [332]. Its seems quite established today that protonic zeolites have similar Brønsted acid strengths, with a relevant role of local geometric factors differentiating their behavior [333]. Experimental, as well as theoretical, data show that, besides the interactions of the functional groups of the reactive molecules with the zeolites Brønsted sites, the van der Waals interactions of other unreactive groups of atoms with the zeolite cavity walls may be very relevant and stabilize the intermediates. These interactions may vary significantly as a function of the type of the zeolite, the dimension and shape of the cavities as well as the Al and proton content and the presence of EF. Also, they depend on the size and shape of the molecule. These “confinement effects” make the cavities of the single zeolite structures unique solvation and reactivity environments and play relevant role in the catalysis by zeolites [334]. Different catalytic activities would predominantly reflect differences in the size and solvating properties (confinement effect) of their cavities, rather than differences in acid strength [335,336]. As it is well known, shape selectivity is a key phenomenon making forbidden (or strongly inhibited) reactions involving transition states, intermediates and/or products whose size exceeds that of the catalyst cavities [337,338], thus somehow favouring competitive reactions. In contrast, confinement effects can directly favour reactions whose transition states match the cavity size and are stabilized by the cavity [326,339].
An example of “positive” confinement effects is the easy formation of aromatics, such as benzene, toluene and styrene, and the relatively low coking rate occurring on medium-pore zeolites such as H-MFI and LTL, from a number of reactants such as light paraffins and

olefins, methanol, ethanol, vegetable oils, etc. This behaviour, differentiating medium pore zeolites from small pore zeolites and large pore zeolites, could be associated to the optimal size of the cavity for cyclization reactions but too small for extensive coking.

7. Silica-aluminas.

7.1. Preparations and applications of silica-alumina catalysts.

Silica-alumina catalysts have been developed in the thirties, forties and fifties of the 20th century. A number of different preparations have been reported and are used, even industrially, to prepare “silica-alumina” materials. Most of them give rise to fully amorphous solids usually denoted as “amorphous silica-aluminas”, or ASAs, although in some cases (mainly when they are relatively Al-rich) they are not fully amorphous but contain some low-crystallinity γ-alumina phase. Among the many preparations [340,341] we can cite the following:

1. Cogelling. It is basically performed by treating solutions containing both tetravalent silicon and trivalent aluminum at acidic pH (1-3) first (to produce a silica sol) and by adding a base to enhance pH to near 5-9, washing and drying [342]. These materials are characterized by a bulk density near 02-0.6 g/cm^3.
2. In recent years, a number of materials belonging to this system with relevant mesoporosity have been prepared and developed at the industrial level, using structure directing agents to develop porosity [343]. These materials are essentially amorphous SA with non-structural although sometimes ordered mesopores. The surface chemistry of these materials appears to be closely similar to that of amorphous microporous SAs. Among the best known, Al-MCM41 [344,345] and Al-SBA [346,347].
3. Coprecipitation. It is performed by treating solutions containing both tetravalent silicon and trivalent aluminum near neutral pH, washing and drying [348].
4. By the “oil drop method”, mixing an alumina sol and a silica sol and feeding the mixture on top of a forming tower filled with circulating hot oil. This method is reported to be used by UOP to produce spherical silica alumina supports for hydrocracking catalysts [349]
5. Impregnation or grafting of silica gel by an aluminum precursor, drying and calcining [83,350,351,352].
6. Grafting of silica precursors in sufficiently large amounts on alumina or boehmite, drying and calcining [353]. This is the case in particular of the Siralox family of Sasol

(previously Condea), whose preparation and characterization has been reported in some detail [252].

7. Flame hydrolysis of mixed chlorides. This is the procedure to produce catalyst carriers with small aluminum content, Aerosil MOX 80 and 170, produced by Evonik [354]. A similar procedure has been described by Huang et al. [355] and by Gun'ko [356] to produce a set of acidic catalysts.
8. As mixed aerogels, using hydrolysis and supercritical drying of mixed alkoxide solutions, followed by calcination [256,357].

The most typical composition of early silica-alumina cracking catalysts is with a SiO_2/Al_2O_3 molar ratio 10–12 corresponding to a Si/Al ratio of 5-6, and an alumina content of 12–15 wt.% [358,359]. This kind of materials is still commercialized today (as the Aldrich silica-alumina catalyst support, grade 135 [360,361] and Grace silica-alumina Davicat catalyst [362]) and is applied, e.g. for treating Fischer Tropsch products [363]. According to several authors this composition leads to maximum acidity [364] in particular of the Brønsted type [365]. On the other hand, high alumina silica-alumina, with near 30 %wt alumina have also been developed and used as cracking catalysts. Authors report that in this range maximum total acidity and cracking activity occur [366]. Both high-silica and high alumina catalysts are applied, depending on feed and reaction conditions as supports for hydrocracking catalysts [367]: near 50% alumina silica-alumina are reported to be the best for NiMo sulphide catalysts [368,369], although also lower alumina content is reported (e.g. 14% Al_2O_3 the support of a NiW sulphide catalyst) [370]. Silica alumina seems to be also the choice supports of catalyst for mild hydrocracking of Fischer Tropsch waxes. In this case, the feed being sulphur-free, both supported noble metal catalysts (such as Pt/Silica-alumina applied by Shell [371]) and sulphides (either NiMo or CoMo [372]) are applied.

Silica-aluminas represent also useful supports for many other industrial catalysts. We can cite, e.g., Cr-based Phyllips-type olefin oligomerization catalysts [373], unreduced Ni-based catalysts for olefin dimerization (NiO 50% by weight, Si:Al 20÷ 6) [374,375], Pd catalysts the slurry catalytic hydrogenation of ethylanthraquinone in the manufacture of hydrogen peroxide [376], Ni-based catalysts for the front-end hydrogenation of C2 and C3 acetylenics in steam cracked cuts [377,378], Rh-based metathesis catalysts [379], etc.

7.2. On the structure of low Al content silica-aluminas.

Low Al content silica-aluminas (alumina content of 12–15 wt.% corresponding to a Si/Al ratio of 5-4) are generally fully amorphous. Thus, the XRD technique does not give any structural information. ^{27}Al MAS NMR technique is largely applied to investigate their structure. This technique reveals the presence of tetrahedral Al ions (peak at 50–60 ppm), in these cases, with a virtual absence or a very small amount of octahedral Al ions (peaks in the range -10 - +5 ppm [355,380,381,382,383,384,385,386]), usually without significant detection of pentacoordinated Al, that become apparent at relatively high Al contents. Working with catalysts relatively rich in aluminum, Wang et al. [387] proposed recently that pentacoordinated aluminum can have a role in the generation of Brønsted acidity in ASAs. As discussed above for aluminas' characterization, we must take into account that such a technique may fail in detecting very distorted low coordination species considered to be almost "silent" [211,212] in particular for amorphous aluminosilicates [385], being probably responsible for extremely broad bands.

The ^{29}Si MAS NMR spectra of low alumina ASAs show a main peak centered at −110/-100 ppm similar to that found on silicas, denoted as Q4 (i.e. due to a Silicate tetrahedra bonded to four other silicate tetrahedra), that tends to shift to higher (less negative) ppm positions by increasing aluminum content. At very high Al content a peak appears at -80 ppm attributed to tetrahedral Si surrounded by alumina [384,388]. XPS studies confirm the presence of two different Al species: in particular the Al2p signal was found split at 74.4 eV and 76.8 eV [389].

These data are usually interpreted as due to the substitution of Al^{3+} for Si^{4+} in the tetrahedral framework of amorphous silica. However, this substitution necessarily leads to a charge umbalance of this framework that must be compensated.

We may mention that, in the case of protonic zeolites with similar composition, the presence of protons as compensating ions is well evident being associated to strong OH stretching bands in IR and also strong ^{1}H MAS NMR signals due to the bridging silanol group (see above). As already said, IR spectra show, in the case of some high-Al content zeolites, additional broad absorptions in the 3400-3300 cm^{-1} region, assumed to be associated to H-bonded H-bonded OH's [80], whose protons may be not available for acid catalysis but that would also contribute in balancing the framework anionic charge. In the case of ASAs, neither IR (Fig. 13) nor ^{1}H MAS NMR techniques not show evidence of compensating protons.

7.3. Surface chemistry of low-Al-content ASAs.

Starting from the very beginning [390], the catalytic activity for cracking reaction of silica-aluminas was attributed to their acidity. In particular, it was found that both Lewis and Brønsted type acid sites are present on the surface [391,392,393,394].

The presence of remarkable Brønsted acidity of SAs is deduced by the observed protonation of ammonia [395], pyridine [327,396,397,398], amines [399] and phosphines [400] also by the strong H-bonding which nitriles [401,402] and with CO [83,327] detected using IR spectroscopy [83,201,327,394,403,404], MAS NMR techniques [405], TPD [406] and calorimetric measurements [397], by the amine titration method [407] as well as deduced by its catalytic activity. This was originally taken with some surprise, because of the absence of Brønsted acidity apparent in the two pure compounds silica and alumina.

The IR spectra of ASAs activated in vacuum always present a very sharp IR band near 3747 cm^{-1} certainly due terminal silanols, spectroscopically very similar to those of pure silicas and of any silica-containing material. A tail towards lower frequencies is likely due (as on pure silica too) to H-bonded and geminal silanols. Several papers reported on the characterization of the acidity of terminal silanols and the complete absence of bands assignable to bridging OH's [76,83,260,262,327,346,408,409,410]. ^{1}H MAS NMR studies of silica-aluminas prepared with different techniques [381,410,411,412,413,414] usually show a single peak at δ 1.7 - 1.8 ppm assigned to terminal silanols as observed on pure siloicas, with a broader component located at variable positions between 2.5 and 3.8 ppm, attributed to Al-OH's. In contrast the typical bridging OH of zeolites resonates sharp above 3.8 ppm, as cited above.

Some papers emphasized the additional presence of very small bands near 3600 cm^{-1} in the spectra of mesoporous SAs [415-418], supposed to be due to bridging zeolite-type sites. Also theoretical works at least up to the end of nineties, modeled the active site for zeolites and SA in the same way, as Al-(OH)-Si bridging hydroxy groups. Accordingly, it was supposed that the active site for SA and protonic zeolites is the same (i.e. it is constituted by the bridging hydroxy groups bonded to a silicon and an aluminum atom) [419]. On the other hand, Busca [94] previously reported that the Brønsted acidic sites in ASA absorb at 3741 cm^{-1}, while the sites which di not protonate pyridine absorb both at higher and lower frequencies (3746 and 3735 cm^{-1}), all being necessarily terminal. Trombetta et al. [262,344] proposed that nearby Al ions can increase the Brønsted acidity of terminal silanols by bridging their dissociated form thus stabilizing it. Poduval et al. [420] reported data

suggesting that bands typical of bridging OD's might be evident in the spectra of deuterated silica alumina, but are masked on those of undeuterated samples. Garrone et al. [421] reported that small amounts of water adsorbed on mesoporous silica-alumina produce a weak band at 3611 cm^{-1} together with another at 3697 cm^{-1} (symmetric and asymmetric OH stretchings) and that adsorbed water adsorbs CO showing significant protonic acidity. Blanchard et al. [362] more recently confirmed that the presence of some water in the line give rise to stronger adsorption of CO on silica-alumina. Sanchez Escribano et al [201] however, showed that water does not modifies the Brønsted acidity of ASA with respect to pyridine protonation, being thus an intrinsic property of this material. On the other hand, water vapour is reported to act as a poison for silica-alumina acid catalysts. Cairon [422] confirmed the previous data showing very strongly acidic terminal silanols on amorphous SA but emphasized the complexity of the corresponding absorptions.

Bevilacqua et al [83] investigated the surface hydroxy groups and the surface acidity of silica, silicalite, mesoporous and microporous SAs, silicated aluminas, aluminated silicas and silicalite, and of some zeolites, by IR spectroscopy. CO, pyridine and lutidine have been used as molecular basic probes. The data suggest that bridging hydroxy group Si – OH – Al are fully stable structures only in the cavities of zeolites, where they produce the strong bands at 3630-3500 cm^{-1} well correlated with the framework Al content. Extremely small bands near 3610 cm^{-1} may be found on some SA samples only (mostly prepared in organic media) and on aluminated silicas after activation by outgassing, thus being not due to adsorbed water. These bands certainly correspond to very few OH groups, and impurities (like bicarbonates) might contribute to their formation. It has been suggested that, in disordered mesoporous or microporous amorphous materials, zeolite-like pores may accidentally form and host zeolite-like bridging hydroxy- groups. The conclusion [83] was that terminal silanols whose acidity is enhanced by nearby Al^{3+} Lewis acid sites represent the predominant Brønsted acid sites in non-zeolitic materials based on combinations of silica and alumina. Part of these sites may be located in the internal cavity of small pores, even having molecular (or zeolitic) size but, due to the flexibility of the amorphous structure, this does not change significantly their structure and acidity.

This approach was considered and developed by Chizallet et al. [423,424] on the basis of theory and experiment. These authors confirmed the possible existence and strong acidity of pseudobridging OH's formed by the interaction of a silanol groups with the fifth coordinative valency of tetrahedrally coordinated Al or Si atoms.

Data from Hensen et al. [425] confirmed the existence of a small number (< 10 μmol/g) of very strong Brønsted acid sites on silica-aluminas together with a second family of weaker Brønsted acid sites (50-250 μmol/g), suggesting that they *might* arise from the interaction of silanol groups with strong Lewis acid sites. Huang et al. [355] observed the formation of very strong Brønsted sites on flame derived silica-alumina and concluded that they may be associated to silanols interacting with one tetracoordinated Al ion and a second pentacoordinated Al ion. More recently the same group reported evidence of pentacoordinate aluminum being involved in the Brønsted sites in ASA's [387].
As observed since many years, strong Lewis acid sites also exist at the surface of low aluminum content ASAs. The spectrum of adsorbed pyridine is simpler on ASAs with respect to that observed on γ-Al_2O_3: In practice, one only strongly adsorbed species is found whose typical absorptions are similar but at little lower frequencies than those observed on aluminas. The 8a mode is found at 1622 cm-1 with respect to 1624 cm-1 found on γ-Al_2O_3. The position of these bands is almost identical to those observed on zeolites and attributed to pyridine interacting with framework Al^{3+} [328]. According to these data, it seems likely that Lewis acidity of ASAs is essentially associated to similar Alions, which are already tetrahedral bonded in the silica framework and can expand their coordination to five by bonding a base.

Studies show that ASAs do not display any relevant surface basicity and/or nucleophilicity. In particular, CO_2 adsorption does not produce any carbonate or bicarbonate species, occurring only through molecular adsorption on surface OH's and on Lewis acid sites [201].

7.4. On the structure of low-Al-content ASAs: the Al-stuffed silica model.

It is clear that the fundamental structure of ASAs is a disordered tetrahedral network very similar to that of amorphous silica. In this framework, aluminum for silicon sostitition occurs to a moderate extent. Charge compensation for the resuting negative charge does not came from rpotons. Thus, charge compensation can either be obtained by loss of oxide ions, producing e.g. tetrahedra triclusters as proposed to occur for glasses [291,292], or by additional presence of extra-framework aluminum cations.
As discussed above, silica frameworks leave interstitial sites that can be occupied by balancing cations. This occurs with alkali and alkali hearth cations in the structures of the so-called "stuffed silicas", where such ions occupy tetrahedral or octahedral sites in the structure of crystalline silica polymorphs (quartz, cristobalite, tridimite). Amorphous silicas are slightly less dense than crystalline polymorphs, thus their disordered structures certainly

also contain similar interstices likely in higher amounts. On the other hand, the Al^{3+} ion is smaller in size than alkali and alkali earth ions. Thus, Al^{3+} ions can be located in similar interstices, either tetrahedral or octahedral, or even with coordination five. When located in tertrahedral interstices, these interstitial "extraframework" Al^{3+} ions are nearly indistinguishable from substitutional tetrahedral Al^{3+} ions. When in tetraherdral interstices, Al^{3}+ will be located near five to eight framework tetrahedra, three of which can be occupied by Al^{3+} ions, the others by silicon. In practice, this would create some clusters of AlO_4 tetrahedra in a framework that is mainly formed by SiO_4 tetrahedra. Clustering of Al tetrahedra may justify the inhomogeneity of Al distribution in silica-aluminas observed by Sarbu and Delmon [426]. A typical composition of such low-alumina ASAs is Al_2O_3 15 %wt, which corresponds to a Si/Al at. ratio near 4. A possible ideal composition is then $Si_{16}(Al_F)_3(Al_{EF})O_{38}$, where A_F and A_{EF} indicate framework tetrahedral Al^{3+} and "extraframework" compensating Al^{3+}, respectively. This means that one "extraframework" compensating Al^{3+} ion is present every 19 tetrahedra at most, with respect to one monovalent alkali ion per two tetrahedra as it occurs in stuffed silica silicolauminates.

This model can justify an all-tetrahedral coordination for aluminum (when tetrahdedral interstices are occupied by Al^{3+}), but also justifies the presence of aluminum ions in coordination 5 and 6 when it occupies larger interstices. This probably depends on preparation procedure and on the Si/Al ratio. The model proposed here also justifies the possible preparation of acid catalyst by simple deposition of aluminum compounds over amorphous silica, producing materials that can be denoted as "aluminated silicas".

With this "stuffed amorphous silica" model for ASA, no alumina-like oxygen atoms exist, i.e. do not exist Al-O-Al groups in an alumina-like environment. This explains the lack of nucleophilic and/or basic sites on low alumina ASA, as found by CO_2 adsorption [201], in contrast to the nucleophilicity of alumina's surface hydroxyls and oxide species, and the acidobasicity of alumina catalysts. The Lewis acidity of ASAs is probably mostly due to framework Al ions, as proposed above, being the extraframework interstitial Al ions less in number and probably mostly not exposed at the surface. Nevertheless, it seems likely that interstitial Al ions can be located just below the surface and can accidentally be nearby a silanol group. The interaction of such Al^{3+} ion with the silanol group is weak, just because the basicity of the silanol's oxygen is very weak and the structure is flexible, not forcing this interaction. However, when a base is available, the silanol's proton can jump to protonate it and the nearby interstitial Al^{3+} can enlarge its coordination sphere to bridge the silanol

anionic form (Fig. 14). This process can certainly strongly stabilize the system, allowing proton jump.

This explains why ASAs show terminal silanols able to protonate pyridine, are more active than aluminas as Brønsted acid catalysts, but are less active than aluminas as Lewis acidic and/or acidobasic catalysts.

7.5. Alumina-rich silica-alumina materials: solid state and surface chemistry.

In agreement with these data, the “coprecipitation” and cogelling of significant amounts alumina (> 20%) with silica gives rise to materials quite refractory to crystallization with a large amount of pentacoordinated Al found by ^{27}Al MAS NMR [381,427]. A similar situation occurs when aluminas are modified with large amounts of silicas, as in the preparation of the materials of the Siralox family. These materials tend to crystallize partially to spinel type alumina (γ-Al_2O_3 and θ-Al_2O_3 [428]). These materials are essentially biphasic being roughly constituted by mixtures of an amorphous phase (essentially an ASA phase) together with asilica-covered alumina phase. The balance of Lewis to Brønsted acid is shifted further towards Lewis acidity, due to the contribution of alumina Lewis acidity. However, the total acidity amount increases by increasing the alumina amount.

8.Conclusions.

The data reported above and the proposed interpretations allow to give a somehow comprehensive picture of the surface and bulk chemistry of the materials belonging to the SiO_2-Al_2O_3 system. The main key points are the covalency and rigidity of the SiO_4 tetrahedra and the ionicity the Al-O bonds and resulting elasticity of the coordination spheres around Al^{3+}. The Lewis acidity in the system are associated to the small size and moderately high charge of the Al^{3+} ion, resulting in its ability to modify its coordination and to strongly bond n-bases. On alumina, tri-coordinated by the vicinity of Al^{3+} ions can form by dehydration as well as by substitution of surface OH’s and may act as very strong Lewis sites. On silica-aluminas as well as on zeolites both tetrahedral Al ions substitutional for silicon in te silica-like framework, as well as “extraframework” and interstitial Al ions contribute to Lewis acidity. The Brønsted acidity in the system arises from the moderate acidity of the silanol group that may be strongly enhanced by the vicinity of Al^{3+} ions, mainly due to the stabilization by the Al^{3+} ions of the dissociated form of silanol (silicate anion). The rigidity of the silica-rich zeolite frameworks contribute to the formation of the bridging silanols (that are essentially an instable structure) thus generating very strong Brønsted acidity.

Table 1. Densities (specific gravity) of phases in the SiO_2-Al_2O_3 system.

Phase		Density g/cm^3
Corundum	α-Al_2O_3	3.98
γ-Al_2O_3		3.65
Kyanite	Al_2SiO_5	3.61
Sillimanite	Al_2SiO_5	3.24
Mullite	$Al_{4+2x}Si_{2-2x}O_{10-x}$	3.11-3.26
Andalusite	Al_2SiO_5	3.15
Low-quartz	SiO_2	2.65
$(SiO_2)_{1-x}$-$(Al_2O_3)_x$ glasses (x ÷ 25-60)		2.43-2.81
High-quartz (> 573°C)	SiO_2	2.53
Low-cristobalite (< 200 - 270°C)	SiO_2	2.32
Low-tridymite	SiO_2	2.26-2.27
High-tridymite (> 200 - 450°C)	SiO_2	2.22-2.26
High-cristobalite (> 200 - 270°C)	SiO_2	2.20
Silica glass	SiO_2	2.21
Fumed amorphous silica	SiO_2	2.20
Precipitated silica	SiO_2	1.9-2.1
Stöber silica	SiO_2	2.04-2.10
Silicalite-1	SiO_2	1.80
Silica gel	SiO_2	1.80-2.20
Mesoporous silica	SiO_2	1.60-2.20

Table 2. Some relevant industrial applications of amorphous silica as catalyst support.

Reaction	Catalyst composition	Reaction conditions
SO_2 oxidation to SO_3	5-10 % V_2O_5 / 10-25 % M_2SO_4 (M= K, Cs) /SiO_2	380-500°C, 1-2 bar [140]
Propene ammoxidation to acrylonitrile	Bi, Fe, Cr, Ni, Co, Mg molybdates supported on silica	450°C, 1.5 bar [141]
Hydrogenation of vegetable oils to margarine	22% Ni, 4% SiO_2 dispersed in hydrogenated edible fats	180-230 °C, 2-6 bar [142]
Acetylene hydrogenation reaction in VCM process	< 1% Pd/SiO_2	25-100 °C, 20-35 bar [143]
Various hydrogenations	Cu/SiO_2, Ni/SiO_2	[144, 145]
Olefin oligomerization	~ 50 % H_3PO_4/SiO_2 (Kieselguhr)	50-200°C, 10-40 bar [144]
Olefin metathesis	8% WO_3/SiO_2	250-400°C, 30 bar [147]
Olefin sterospecific polymerization	1% Cr^{II} / SiO_2 Phillips process	100 °C, 25 bar [148]

Table 3. Crystal data of aluminum hydroxides, oxy-hydroxides and oxides.

Mineral name	Formula	Space Group	Z
Bayerite	α-$Al(OH)_3$	$P2_1/n$	8
Gibbsite	γ-$Al(OH)_3$	$P2_1/n$	8
Nostrandite	$Al(OH)_3$	$P\bar{1}$	4
Doyleite	$Al(OH)_3$	$P\bar{1}$ or P1	2
Diaspore	α-AlOOH	Pbnm	4
Boehmite	γ-AlOOH	$P2_1/c$ or $Cmc2_1$	4
Tohdite	$5Al_2O_3 .H_2O$	doubtful	
	γ-Al_2O_3	$Fd\bar{3}m$ *	10,66
	δ-Al_2O_3	$P\bar{4}m2$ *	16
	θ-Al_2O_3	C2/m	4
	η-Al_2O_3	$Fd\bar{3}m$	10.66
	κ-Al_2O_3	$Pna2_1$	8
	χ-Al_2O_3	doubtful	
Corundum	α-Al_2O_3	$R\bar{3}c$	6

*Alternative models have been proposed

Table. 4 . industrial application of some acidic zeolites.

Zeolite usual name	IZA code	Main cavities	Reaction	Phase	Temp. Pressure	
Ferrierite	H-FER	10 MR 4.2x5.4 8 MR 3.5x4.8 intersecting	olefins isomerisation	G	350 °C	Lyondell – CDTech
ZSM-5	H-MFI	10 MR 5.3x5.6 10 MR 5.1x5.5 intersecting	benzene alkylation to ethylbenzene	G	390-450 °C 15-20 bar.	Mobil-Badger
			toluene disproportionation	G	420-480 °C, 20-40 bar,	Mobil
			olefins oligomerization	G	200-350 °C 10-50 bar	Mobil Lurgi
beta	H-BEA	12 MR 7.6x6.4 12 MR 5.5x5.5 intersecting	benzene alkylation to cumene	L	150-200 °C 10-40 bar.	UOP Polimeri Europa-ENI
mordenite	H-MOR	12 MR 6.5x7.0 8 MR 3.4x4.8 side pokets	benzene alkylation to cumene	L	150-200 °C 10-40 bar.	Dow-Kellogg
			C8 aromatics isomerizaton	G	370-430°C 7-15 bar	
			alkane isomerization	G	200 °C. 15-30 bar	Sud Chemie
MCM-22	H-MWW	12 MR 7.1 capped 10 MR elliptical	benzene alkylation to cumene and ethylbenzene	L	150-200 °C 10-40 bar.	Mobil
Faujasite	H-FAU (HY)	12 MR 7.4x7.4 intersecting	fluid catalytic cracking	G	500-750 °C 2 bar	Grace, BASF
			isobutene alkylation	L	40-90°C	Akzo Nobel, Lurgi

Figure captions.

Figure 1. Models for surface species in amorphous siolicas.

Figure 2. FT-IR spectra of silica gel (A) and fumed silica (B) after outgassing at 300 K (a), 473 K (b), 673 K (c), 873 K (d). In the inset: the two samples outgassed at 873 K, enlarged.

Figure 3. Model for ammonia adsorption on silica.

Figure 4. Most common evolution paths for phase transformations of aluminum hydroxides and oxides upon heat treatment in the preparation of catalytic materials

Figure 5.Model for strongest Lewis acid sites on gamma-alumina. A: cutting of the spinel-type structure along 111 plane. B: model for surface reconstruction. C: Top view of the site.

Figure 6. Phase diagram for the SiO_2-$Al2O_3$ system, reprinted with permission from Ref. [266].

Figure 7. Coordination of interstitial ions in stuffed silica compounds: Mg^{2+} α-quartz framework of $Mg_{0.5}AlSiO_4$ and Li^+ in the ß-quartz framework of $LiAlSiO_4$ (β-eucryptite). reprinted with permission from Ref.[282].

Figure 8. IR spectra of the surface hydroxyl- groups of protonic zeolites and other materials belonging to the SiO_2-$Al2O_3$ system

Figure 9. IR spectra and 1H MAS NMR spectra of H-FER zeolite and Al-containing MCM-41 mesoporous silica-alumina. NMR spectra are reprinted with perfmission from Ref. [313].

Figure 10. Model for pyridine adsorption on protonic zeolites.

Figure 11. Structure of faujasite with location of the different tetrahedral crystallographic positions.

Figure 12. Model for pyridine adsorption on Brønsted sites of H-USY when the proton is located in the small cavities (sodalite cage or hexagonal prism) and pyridine adsorbs from the supercage (left), or when both proton and pyridine are located in the supercage (in the middle).

Figure 13. Skeletal IR spectra of silica, amorphous silica-alumina and gamma alumina.

Figure 14. Model for ammonia protonation on silica-alumina.

References

[1] Vogt ETC. Weckhuysen, BM Fluid catalytic cracking: recent developments on the grand old lady of zeolite catalysis, Chem Soc Rev 2015; 44(20): 7342-7370

[2] *The Houdry Process*, ACS, 1996, available on Internet https://www.acs.org/content/dam/acsorg/education/whatischemistry/landmarks/houdry/the-houdry-process-catalytic-conversion-commemorative-booklet.pdf accessed september 1st 2018.

[3] Hudec P, FCC Catalyst - Key Element In Refinery Technology, 45th International Petroleum Conference, June 13, 2011, Bratislava, Slovak Republic, available on Internethttp://www.vurup.sk/sites/default/files/downloads/46_ft_hudec-fcc.pdf accessed september 1st 2018.

[4] Wilson JW, Fluid Catalytic Cracking Technology and Operations, Pennwell Publishing, Tulsa, 1997.

[5] Eberly, PE Jr., Kimberlin, CNJr., Miller WH, Drushel, V Coke Formation on Silica-alumina Cracking Catalysts. Ind. &Eng. Chem. Proc. Des. Dev., 1966; 5 (2): 193-198.

[6] Lloyd L, *Handbook of Industrial Catalysts*, Springer, 2011, pp. 182-183

[7] Flaningen EM, Zeolites and Molecular Sieves. An Historical Perspective, in *Introduction to Zeolite Science and Practice,* Jacobs PA, Flanigen EM, Jansen JC, van Bekkum H eds, Elsevier , 2001, pp. 11-36.

[8] Avidan AA, Origin, development and scope of FCC catalysis, in *Fluid Catalytic Cracking: Science and Technology,* Magee JS, Mitchel MM eds, Elsevier, 1993, pp. 1-40

[9] Fletcher RP, The History of Fluidized Catalytic Cracking: A History of Innovation: 1942-2008, in Flank WH, Abraham MA, Matthews MA, eds, Innovations in Industrial and Engineering Chemistry, ACS Symposium Series, Vol. 1000, 2009, ACS, pp 189–249.

[10] Busca G, Acid Catalysts in the Industrial Hydrocarbon Chemistry, Chem. Rev. 2007; 107: 5366-5410.

[11] Vermeiren W, Gilson JP, Impact of zeolites on the petroleum and petrochemical industry, Topics in Catalysis, 2009; 52 (9): 1131-1161

[12] Primo A, Garcia H, Zeolites as catalysts in oil refining, *Chem. Soc. Rev*., 2014; **43 (22):** 7548-7561

[13] Busca G, Structural, surface and catalytic properties of aluminas, Advances in Catalysis, 2014; 57: 319-404.

[14] Peratello S, Molinari M, Bellussi G, Perego C, Olefins Oligomerization: Thermodynamics and kinetics over a mesoporous silica-alumina, Catal. Today 1999, 52 (2-3), 271–277.

[15] Grace Davison, Silica/Alumina Supports https://e-catalysts.com/supportsearch/tutorials/silicaalumina.htm, accessed september 1st, 2018

[16] Scherzer J, Gruia AJ, Hydrocracking Science and Technology, CRC press, 1996.

[17] J. A. Anderson and M. F. Garcia eds., Supported metals in catalysis, World Scientific, 2nd ed., 2011.

[18] Montebelli A, Tronconi E, Orsenigo C, Ballarini N Kinetic and Modeling Study of the Ethylene Oxychlorination to 1,2-Dichloroethane in Fluidized-Bed Reactors, Ind. Eng. Chem. Res. 2015; 54 (39): 9513–9524

[19] Vedrine JC, Metal Oxides in Heterogeneous Catalysis, Elsevier, 2018.

[20] Sannita E, Aliakbarian B, Casazza AA, Perego P, Busca G, Medium-. temperature conversion of biomass and wastes into liquid products, a review.Renew. Sustain. En. Rev. 2012, 16(8), 6455-6475.

[21] Ennaert T, Van Aelst J, Dijkmans J, De Clercq R, Schutyser W, Dusselier M, Verboekend D, Sels BF. Potential and challenges of zeolite chemistry in the catalytic conversion of biomass Chem Soc Rev. 2016; 45(3):584-611.

[22] Serrano DP, Aguado J, Escola JM, Developing Advanced Catalysts for the Conversion of Polyolefinic Waste Plastics into Fuels and Chemicals, ACS Catal. 2012, 2(9),1924–1941.

[23] Perego C, Bagatin R, Tagliabue M, Vignola R Zeolites and related mesoporous materials for multi-talented environmental solutions Micro Mesop Mater 2013; 166:37–49

[24] Provis JL Activating solution chemistry for geopolymers, in Provis JL, Van Deventer JSJ, eds., Geopolymers, structure, processing, properties and industrial applications, CRC Press, 2009, p. 50-71.

[25] Nauroth P, Kuhlmann R, Turk G, Becker A, Process for preparing precipitated silica, US Patent 4857289 A (1989) to Degussa.

[26] Wilhelm S, Kind M, Influence of pH, Temperature and Sample Size on Natural and Enforced Syneresis of Precipitated Silica, Polymers 2015; 7(12): 2504–2521

[27] Lagaly G, Crystalline silicic acids and their interface reactions, Adv. Colloids Interface Sci 1979; 11(2): 105-148.

[28] Beneke K, Lagaly G, A hydrated potassium layer silicate and its crystalline silicic acid *Amer. Miner*. 1989; **74(1-2):** 224-229.

[29] Borowski M, Marler B, Gies H, The crystal structure determination of the crystalline layered silicic acid H-RUB-18, Zeit. Kristall., Crystall. Mater. 2002; 217: 233-241

[30] Rieck HP, Crystalline silicic acid, its salts, and processes for their preparation, US4581213 to Hoechst (1984)

[31] Faust SD, Aly OM, Chemistry of Water Treatment, 2nd Ed., CRC press, 1998, p.224

[32] Shannon RD, Revised effective ionic radii and systematic studies of interatomic distances in halides and chalcogenides, Acta Cryst. 1976; A32(5): 751-767

[33] Tossell JA, N. Sahai N, Calculating the acidity of silanols and related oxyacids in aqueous solution.Geochim. Cosmochim. Acta, 2000; 64: 4097– 4113,

[34] Sulpizi M, Gaigeot MP, Sprik M, The Silica–Water Interface: How the Silanols Determine the Surface Acidity and Modulate the Water Properties *J. Chem. Theory Comput.* 2012; **8(3)**: 1037−1047.

[35] Weinhold F, West R, The Nature of the Silicon–Oxygen Bond, Organometallics, 2011; 30 (21): 5815–5824

[36] Passmore J, Rautiainen JM, On The Lower Lewis Basicity of Siloxanes Compared to Ethers, *Europ. J. Inorg. Chem.* 2012 (36): 6001-6010.

[37] Weinhold F, West R, Hyperconjugative Interactions in Permethylated Siloxanes and Ethers: The Nature of the SiO Bond, J. Am. Chem. Soc., 2013, 135(15), 5762–5767

[38] U. Kalapathy U, Proctor A, Shultz J, A simple method for production of pure silica from rice hull ash, Biores. Tech., 73(3),257-62 (2000).

[39] Abu Bakar R, Yahya R, Gan SN, Production of High Purity Amorphous Silica from Rice Husk, Procedia Chem. 2016 19. 189-195

[40] Schlomach J, Kind M, Investigations on the semi-batch precipitation of silica, J. Colloid Interf. Sci. 2004; 277(2): 316-326

[41] Winyall ME, Silica Gel preparation and properties, in Applied Industrial Catalysis, vol. 3, Leach BE ed., Academic Press, New York, 1984.

[42] http://www.grace.com/Products/Sylobead/

[43] Kresge CT, Leonowicz ME, Roth WJ, Vartuli JC, Beck JS. Ordered mesoporous molecular sieves synthesized by a liquid-crystal template mechanism. Nature, 1992; 359(6397): 710—712

[44] Yanagisawa T, Shimizu T, Kuroda K, Kato C, The preparation of alkyl-trimethylammonium-kaneinite complexes and theirconversion to microporous materials, Bull. Chem.Soc. Jpn. 1990, 63, 988-992.

[45] Martens JA, Jammaer J, Bajpe S, Aerts A, Lorgouillou Y, Kirschhock CEA, Simple synthesis recipes of porous materials Microp.Mesopor. Mater. 2011; 140: 2–8

[46] Zhao L, Qin H, Wu R, Zou H, Recent advances of mesoporous materials in sample preparation J. Chromatogr. A, 2012; 1228: 193– 204

[47] Tanev PT, Pinnavaia J, A neutral templating route to mesoporous molecular sieves. Science 1995;267:865–7.

[48] Stöber W, Fink A, Bohn E, controlled growth of monodisperse silica spheres in the micron size range, J. Colloid Interface Sci. 1968; 26: 62–69.

[49] Plumeré N, Ruff A, Speiser B, Feldmann V, Mayer HA, Stöber silica particles as basis for redox modifications: Particle shape, size, polydispersity, and porosity, J. Colloid Interface Sci. 2012; 368: 208–219

[50] Du X, He J, Spherical silica micro/nanomaterials with hierarchical structures: synthesis and appòlications, Nanoscale, 2011; 3: 3984-4002

[51] Briesen H, Fuhrmann A, Pratsinis SE, The effect of precursor in flame synthesis of SiO_2, Chem. Eng. Sci. 1998; 53(24): 4105—4112

[52] Wang LH, Tsai BJ, The sintering and crystallization of colloidal silica gel, Mater. Lett. 2000; 43: 309–314

[53] Griffen DT, Silicate Crystal Chemistry, Oxford University Press, 1992

[54] Davila LP, Risbud SH, Shackelford JF, Quartz and silicas, in Shackelford JF, Doremus RH eds, Ceramic and Glass Materials, Springer, 2008, pp. 71-86

[55] Busca G The surface acidity of solid oxides and its characterization by IR spectroscopic methods. An attempt at systematization, Phys. Chem. Chem. Phys 1999; 1: 723-736.

[56] E. M. Flanigen EM, Bennett JM, Grose RW, Cohen JP, Patton RL, Kirchner RM, Smith JV, Silicalite, a new hydrophobic crystalline silica molecular sieve, Nature, 1978; 271: 512–516

[57] Bibby DM, Milestone NB, Aldridge LP, Silicalite-2, a silica analogue of the aluminosilicate zeolite ZSM-11 Nature 1979; 280: 664 - 665

[58] Fernández AB. Marinas A, Blasco T, Fornés V, Corma A. Insight into the active sites for the Beckmann rearrangement on porous solids by in situ infrared spectroscopy, J. Catal. 2006, 243, 270-277

[59] Camblor MA, Corma A, Diaz-Cabanas MJ, Baerlocher C. Synthesis and Structural Characterization of MWW Type Zeolite ITQ-1, the Pure Silica Analog of MCM-22 and SSZ-25, *J. Phys. Chem. B.;* **1998**, *102(1),* 44-51.

[60] Camblor MA, Corma A, Lightfoot P, Villaescusa LA, Wright PA, Synthesis and Structure of ITQ-3, the First Pure Silica Polymorph with a Two-Dimensional System of Straight Eight-Ring Channels, Angew. Chem. Int. Ed. 1997; 36: 2659-2661.

[61] Corma A, Rey F, Rius J, Sabater MJ, Valencia S. Supramolecular self-assembled molecules as organic directing agent for synthesis of zeolites, Nature, 2004, 431, 287.

[62] Kuperman A, Nadimi S, Oliver S, Ozin GA, Garces JM, Olken MM Non-aqueous synthesis of giant crystals of zeolites and molecular sieves, Nature 1993; 365: 239-242.

[63] Wragg DS, Morris R, Burton AW, Zones SI, Ong K, Lee G, The synthesis and structure of SSZ-73: an all-silica zeolite with an unusual framework topology, Chem. Mater. 2007; 19(16): 3924-3932

[64] Gajan D, Copéret C, Silica-supported single-site catalysts: to be or not to be? A conjecture on silica surfaces, New J. Chem., 2011; 35: 2403–2408

[65] Dimitrov V, Komatsu T, Correlation among electronegativity, cation polarizability, optical basicity and single bond strength of simple oxides, J. Solid State Chem. 2012; 196: 574–578

[66] Bancroft GM, Nesbitt HW, Ho R, Shaw DM, Tse JS, Biesinger MC, Toward a comprehensive understanding of solid-state core-level XPS linewidths: experimental and theoretical studies on the Si 2p and O 1s linewidths in silicates Phys. Rev. 2009, B 80, 075405.

[67] Nesbitt HW, Bancroft GM, High resolution core and valence level XPS studies of the properties (structural, chemical and bonding) of silicate minerals and glasses, Rev. Miner. Geochem. 2014; 78: 271-329.

[68] Simonsen ME, Sønderby C, Li Z, Søgaard EG, XPS and FT-IR investigation of silicate polymers J. Mater. Sci. 2009; 44: 2079-2088.

[69] Kennedy GJ, Afeworki M, Calabro DC, Chase CE, Smiley, RJ Jr., ^{1}H MAS NMR techniques for the quantitative determination of hydrogen types in solid catalysts and supports Appl. Spectrosc. 2004; 58: 698-704.

[70] Murray DK, Differentiating and characterizing geminal silanols in silicas by (29)Si NMR spectroscopy J. Colloid Interface Sci. 2011; 352 163-170.

[71] Morrow BA, Cody IA, Infrared studies of reactions on oxide surfaces. 5. Lewis acid sites on dehydroxylated silica, J. Phys. Chem. 1976; 80(18): 1995-1998.

[72] Navrocki J, The silanol group and its role in liquid chromatography, J. Chromatogr. 1997; 779: 29-71.

[73] Zhuravlev LT, The surface chemistry of amorphous silica. Zhuravlev model, Colloids Surf. A: Physicochem. Eng. Asp., 2000; 173: 1-38.

[74] Potapov, VV, Zhuravlev LT, Concentration of various forms of water in silica precipitated from a hydrothermal solution, J. Volcanology Seismology, 2007; 5: 310-318.

[75] Rimola A, Costa D, Sodupe M, Lambert JF, Ugliengo P, Silica surface features and their role in the adsorption of biomolecules: computational modeling and experiments, Chem. Rev. 2013 ; 113(6): 4216-4313.

[76] Hadjiivanov KI, Identification and Characterization of Surface Hydroxyl Groups by Infrared Spectroscopy, Advan. Catal. 2014; 57: 99-318.

[77] Hoffmann P, Knözinger E, Novel aspects of mid and far IR Fourier spectroscopy applied to surface and adsorption studies on SiO_2, Surf. Sci. 1987,188,181-198.

[78] Morrow BA, Mc Farlan AJ, Surface vibrational modes of silanol groups on silica, J. Phys. Chem. 1992; 92: 1395-1400.

[79] Morrow BA, Cody IA, Infrared studies of reactions on oxide surfaces. 6. Active sites on dehydroxylated silica for the chemisorption of ammonia and water, J. Phys. Chem. 1976; 80(18):1998-2004

[80] Busca G, Location and Accessibility of Hydroxy Groups in Silico-aluminate Porous Materials as Studied by IR Spectroscopy, Current Phys. Chem., 2012; 2: 136-150.

[81] Gallas JP, Goupil JM, Vimont A, Lavalley JC, Gil B, Gilson JP, Miserque O, Quantification of water and silanol species on various silicas by coupling IR spectroscopy and in-situ thermogravimetry, Langmuir, 2009, 25, 5825-5834

[82] Ghiotti G, Garrone E, Morterra C, Boccuzzi F, Infrared study of low temperature adsorption. 1. Carbon monoxide on aerosil. An interpretation of the hydrated silica spectrum, J. Phys. Chem, 1979; 83(22) 2863-2869.

[83] Bevilacqua M, Montanari T, Finocchio E, Busca G, Are the active sites of protonic zeolites generated by the cavities ?, Catal. Today 2006; 116: 132-142.

[84] Burneau A, Barres O, Gallas JP, Lavalley JP, Comparative study of the surface hydroxyl groups of fumed and precipitated silicas. 2. Characterization by infrared spectroscopy of the interactions with water, Langmuir, 1990; 6(8): 1364-1372.

[85] Hartmeyer G, Marichal C, Lebeau B, Rigolet S, Caullet P, Hernandez J, Speciation of silanol groups in precipitated silica nanoparticles by ^1H MAS NMR Spectroscopy, J. Phys. Chem. C, 2007; 111: 9066–9071.

[86] Jiang Y, Huang J, Dai W, Hunger M, Solid-state nuclear magnetic resonance investigations of the nature, property, and activity of acid sites on solid catalysts, Solid State Nuclear Magnetic Resonance, 2011; 39(3-4): 116-141.

[87] Kim HN, Lee SK, Atomic structure and dehydration mechanism of amorphous silica: Insights from ^{29}Si and ^{1}H solid-state MAS NMR study of SiO_2 nanoparticles, Geochim. Cosmochim. Acta 2013; 120: 39–64

[88] Fubini B, Fenoglio I, Ceschino R, Ghiazza M, Martra G, Tomatis M, Borm P, Schins R, Bruch J, Relationship between the state of the surface of four commercial quartz flours and their biological activity in vitro and in vivo, Int. J. Hyg. Environ. Health 2004; 207; 89 ± 104

[89] Fenoglio I, Ghiazza M, Ceschino R, Gillio F, Martra G, Fubini B, The role of nature and structure of the surface sites in the biological response to silica particles, in Bliz JP, Gun'ko VM eds., Surface Chemistry in Biomedical and Environmental Science, Kluwer, Amsterdam, pp. 287-298.

[90] Zecchina A, Bordiga S, Spoto G, Marchese L, Petrini G, Leofanti G, Padovan M, Silicalite characterization. 2. IR spectroscopy of the interaction of carbon monoxide with internal and external hydroxyl groups, J. Phys. Chem. 1992; 96(12): 4991-4997.

[91] Astorino E, Peri J, Willey RJ, Busca G,, Spectroscopic characterization of silicalite-1 and titanium silicalite-1, J. Catal., 1995; 157: 482-500.

[92] Armaroli T, Bevilacqua M, Trombetta M, Milella F, Gutièrrez Alejandre A, Ramirez Solis J, Notari B, Willey RJ, Busca G,, A study of the external sites of MFI-type zeolitic materials through the FT-IR investigation of the adsorption of nitriles, Appl. Catal. A Gen., 2001; 216: 59-71.

[93] Flego C, Dalloro L, Beckmann rearrangement of cyclohexanone oxime over Silicalite-1: an FT-IR spectroscopic study, Micropor. Mesopor. Mater. 2003; 60: 263-271.

[94] Busca G, Spectroscopic characterization of the acid properties of metal oxide catalysts, Catal. Today, 1998; 41: 191-206.

[95] Parida SK, Dash S, Patel S, Mishra BK, Adsorption of organic molecules on silica surface, Advan. Colloid Interface Sci. 2006;121(1-3): 77–110.

[96] Bennici S, Aroux A, Thermal analysis and calorimetric methods, in S.D. Jackson and J.S.J. Hargreaves eds., Metal oxide catalysis, Wiley, 2009, pp. 391-442 .

[97] Fan HF, Li F, Zare RN, Lin KC, Characterization of two types of silanol groups on fused-silica surfaces using evanescent-wave cavity ring-down spectroscopy, Anal. Chem. 2007; 79(10): 3654-3661.

[98] Buszewski B, Bocian S, Rychlicki G, Matyskac M, Pesek J, Determination of accessible silanols groups on silica gel surfaces using microcalorimetric measurements, J. Chromatogr. A 2012; 1232: 43–46.

[99] Comas-Vives A, Amorphous SiO_2 surface models: energetics of the dehydroxylation process, strain, ab initio atomistic thermodynamics and IR spectroscopic signatures, Phys. Chem. Chem. Phys., 2016; 18: 7475-7482.

[100] Pfeiffer-Laplaud M, Costa D, Tielens F, Gaigeot MP, Sulpizi M, Bimodal Acidity at the Amorphous Silica/Water InterfaceJ. Phys. Chem. C 2015; 119(49): 27354−27362

[101] Liu X, Cheng J, Lu X, Wang R, Surface acidity of quartz: understanding the crystallographic control, Phys. Chem. Chem. Phys. 2014; 16: 26909-26916.

[102] Dimitrov V, Komatsu T, Classification of Simple Oxides: A Polarizability Approach J. Solid State Chem. 2002; 163(1): 100-112.

[103] Alam AU, Howlader MMR, Deen MJ, Oxygen Plasma and Humidity Dependent Surface Analysis

of Silicon, Silicon Dioxide and Glass for Direct Wafer BondingECS J. Solid State Science Tech., 2013; 2(12): P515-P523.

[104] Bordes Richard E, Courtine P, Optical Basicity: A scale of acidity/basicity of solids and its application to oxidation catalysis, in Metal oxides, chemistry and applications, Fierro JLG ed., Taylor &Francis, 2006, pp. 319-352.

[105] Busca G, Bases and Basic Materials in Chemical and Environmental Processes. Liquid versus Solid Basicity, Chem. Rev. 2010; 110: 2217–2249

[106] Xie Z, Bau R, Reed CA, Isolation of a protonated silanol: $But_3Si(OH_2)^+$, J. Chem. Soc. Chem. Commun. 1994; 2519-2510.

[107] Cypryk M, Ab initio study of the basicity and propensity of siloxanols towards hydrogen bond formation, J. Organomet. Chem. 1997; 545-6: 483-493.

[108] Storozheva EN, Sekushin VN, Tsyganenko AA, FTIR Spectroscopy Evidence for the Basicity Induced by Adsorption, Catal. Lett. 2005; 107: 185-188.

[109] Tsyganenko AA, Storozheva E, Manoilova O, Lesage T, Daturi M, Lavalley JC, Brønsted acidity of silica silanol groups induced by adsorption of acids, Catal. Lett. 2000; 70: 159-163.

[110] Cypryk M, Apeloig Y, Mechanism of the acid-catalyzed Si-O bond cleavage in siloxanes and siloxanols. A theoretical study, Organometallics, 2002; 21: 2165–2175

[111] Lokwood GK, Garofalini SE, Bridging oxygen as a site forproton adsorption on the vitreous silica surface, J. Chem. Phys. 2009; 131: 074703.

[112] McCrate JM, Ekerdt JG, Langmuir, Titration of free hydroxyl and strained siloxane sites on silicon dioxide with fluorescent probes, 2013; 29: 11868-11875.

[113] Chew TL, Ahmad AL, Bhatia S, Ordered mesoporous silica (OMS) as an adsorbent and membrane for separation of carbon dioxide (CO2), Advan. Colloid Interface Sci. 2010; 153(1-2): 43–57

[114] Pham TD, Xiong R, Sandler SI, Lobo RF, Experimental and computational studies of the adsorption of CO_2 and N_2 on Pure Silica Zeolites, Micropor. Mesopor. Mater. 2014; 185: 157–166

[115] Morrow BA, Devi A, Infra-red studies of reactions on oxide surfaces. Part 1.—Boron trifluoride on silica, J. Chem. Soc. Faraday Trans. I, 1972, 68, 403-422.

[116] Morrow BA, Cody IA, Lee LSM, Infrared studies of reactions on oxide surfaces. 7. Mechanism of the adsorption of water and ammonia on dehydroxylated silica. J. Phys. Chem., 1976; 80: 2761-2767.

[117] Marrone M, Montanari T, Busca G, Conzatti L, Costa G, Castellano M, Turturro A, An FT-IR Study of the Reaction of Triethoxysilane (TES) and of bis[3-triethoxysilylpropyl-]tetrasulphane (TESPT) with the Surface of Amorphous Silica, J. Phys. Chem. B., 2004; 108: 3563-3572.

[118] Hamzaoui, B, Bendjeriou-Sedjerari A, Pump E, Abou-Hamad E, Sougrat R, Gurinov A, Huang KW, Gaian D, Lesage A, Emsley L, Basset JM, Atomic-level organization of vicinal acid–base pairs through the chemisorption of aniline and derivatives onto mesoporous SBA15, Chem. Sci. 2016; 7: 6099-6105.

[119] Armandi M, Bolis V, Bonelli B, Otero Areán C, Ugliengo P, Garrone E, Silanol-Related and Unspecific Adsorption of Molecular Ammonia on Highly Dehydrated SilicaJ. Phys. Chem. C 2011; 115 (47): 23344–23353

[120] Papirer E, Adsorption on Silica Surfaces, Dekker, 2000

[117] Pacchioni G, Skuja L,. Griscom DL, eds., Defects in SiO_2 and Related Dielectrics: Science and Technology, Springer, 2000

[122] Sushko PV, Mukhopadhyay S, Mysovsky AS, Sulimov VB, Taga A, Shluger AL, Structure and properties of defects in amorphous silica: new insights from embedded cluster calculations, J. Phys.: Condens. Matter 2005; 17: S2115

[123] Yue Y, Song Y, Zuo X, First principles study of oxygen vacancy defects in amorphous SiO_2, AIP Adances 2017; 7: 015309

[124] Musso F, Ugliengo P, Solans-Monfort X, Sodupe M, Periodic DFT Study of Radical Species on Crystalline Silica Surfaces, J. Phys. Chem. C 2010, 114, 16430–16438

[125] Uchino T, Takahashi M, Yoko T, Structure and generation mechanism of the peroxy-radical defect in amorphous silica Phys Rev Lett. 2001;86(20):4560-3.

[126] Capron N, Carniato S, Lagraa A, Boureau G, Local density approximation and generalized gradient approximation calculations for oxygen and silicon vacancies in silica, J. Chem. Phys. 2000; 112(21): 9543

[127] McCrate JM, Ekerdt JG, Detection of low-density surface sites on silica: experimental evidence of intrinsic oxygen-vacancy defects, Chem. Mater. 2014, 26, 2166−2171

[128] Parmaliana A, Arena F, Frusteri F, Martínez-Arias A, López Granados M, Garcia Fierro JM, Effect of Fe-addition on the catalytic activity of silicas in the partial oxidation of methane to formaldehyde, Appl. Catal. A: Gen.2002; 226: 163–174

[129] Ono T, Nakamura M, Unno K, Oyun A, Ohnishi J, Kataoka M, Fujio K, Partial oxidation of CH_4 over Al/silica catalysts using molecular oxygen, J. Mol. Catal. A: Chem. 2008; 285: 169–175.

[130] Armor JN, Zambri PM, Silica as an oxidation catalyst, J. Catal 1982; 73: 57-65

[131] Pinelli D, Trifirò F, Vaccari A, Giamello E, Pedulli G, Nature of active sites in catalytic ammoximation of cyclohexanone to the corresponding oxime on amorphous silica: E.P.R. investigations, Catal. Lett. 1992;13(1-2): 21–26

[132] Kamitori Y, Hojo M, Masuda R, Izumi T, Tsukamoto S, Silica gel as an effective catalyst for the alkylation of phenols and some heterocyclic aromatic compounds, J. Org. Chem., 1984; 49 (22): 4161–4165

[133] Hojo M, Masuda R, Silica Gel as a Catalyst for the Condensations of aromatic compounds with RSCl, $RSCH_2Cl$ and S_2Cl_2, Synt. Commun. 1975; 5(3): 173-176

[134] Jin Y, Li J, Peng L, Gao C, Discovery of neat silica gel as a catalyst: an example of S → O acetyl migration reaction, Chem. Commun., 2015; 51: 15390

[135] Wang H, Zhang C, He H, Wang L, Glucose production from hydrolysis of cellulose over a novel silica catalyst under hydrothermal conditions, J. Envir. Sci. 2012; 24 (3): 473-478

[136] Phung TK, Proietti Hernandez L, Busca G, Conversion of ethanol over transition metal oxide catalysts: effects of tungsta addition on the catalytic behavior of titania and zirconia, Appl. Catal. A, Gen. 2015; 489: 180-187.

[137] Ge C, Li Z, Chen G, Qin Z, Li X, Dou T, Dong M, Chen J, Wang J, Fan W, Kinetic study of vapor-phase Beckmann rearrangement of cyclohexanone oxime over silicalite-1, Chem. Eng. Sci. 2016; 153: 246–254.

[138] Halasz I, ed., Silica and Silicates in Modern Catalysis, Transworld Research Network, Kerala, India,2010

[139] Soled S, Silica-supported catalysts get a new breath of life, Science, 2015; 350, 1171-1172

[140] Lloyd L, Handbook of Industrial Catalysts Springer, 2011, pp. 35-38

[141] Brazdil JF, Designing multifunctionality into single phase and multiphase metal-oxide-selective propylene ammoxidation catalysts, Catalysts 2018; 8: 103

[142] Catalysts for Edible Oil hydrogenation, brochure, www.jmcatalysts.com

[143] Woike U, Kammerhofer P, Vinnolit vinyl chloride and suspension polyvinyl chloride technologies in Meyers RA, ed., Handbook of Petrochemicals Production Processes, McGraw-Hill, 2005, p. 18.3-36.

[144] Lloyd L, Handbook of Industrial Catalysts Springer, 2011, pp. 73-118

[145] Busca G, Heterogeneous Catalytic Materials, Elsevier, 2014, pp. 297-344.

[146] Van Der Merwe W, Conversion of Spent Solid Phosphoric Acid Catalyst to Environmentally Friendly Fertilizer, Environ. Sci. Technol. 2010, 44, 1806–1812.

[147] Lefbvre T, in Khosravi E, Szymanska-Buzar T, Ring opening metathesis and related chemistry, NATO science series, Kluwer, 2002, pp. 247-262.

[148] Chromium CatalystsIn ed, Introduction to Industrial Polyethylene: Properties, Catalysts, Processes, 2010 Scrivener Publishing LLC, pp. 61-70

[149] Minakata S, Komatsu M, Organic Reactions on Silica in Water, Chem. Rev. 2009; 109: 711–724

[150] Peters D, Bock J, Jacobs H, Hexaaminaluminiumiodidmonoammoniakat — $[Al(NH_3)_6]I_3NH_3$ — Darstellung und kristallstruktur J. Less Common Met. 1989; 154(2), 243-250.

[151] Tomasik P, Ratajewicz Z, Pyridine metal complexes, Wiley, 1985, pp. 61-99.

[152] Dimitrov A, Heidemann D, Khallow KI, Kemnitz E, Syntheses and Characterization of Salts with the $[Al(D)_4F_2]^+$ Cation (D = Pyridine or Water), Inorg. Chem. 2012, 51(21), 11612−11622

[153] Yin HY, Lai J, Tang J, Shang Y, Zhang JL, A Cryptand-Type Aluminum Tris(salophen) Complex: Synthesis, Characterization, and Cell Imaging Application Inorganics 2018; 6; 20, pp. 1-11

[154] Milione S, Milano G, Cavallo L, Pentacoordinated Organoaluminum Complexes: A Computational Insight, Organometallics, 2012; 31 (24): 8498–8504

[155] Radzewich CE, Guzei IA, Jordan RF, Three-Coordinate Cationic Aluminum Alkyl Complexes Incorporating Diketiminate Ligands, J. Am. Chem. Soc. 1999; 121: 8673-8674

[156] Floris F, Persico M, Tani A, Tomasi J, Free energies and structures of hydrated cations, based on effective pair potentials, Chem. Phys. 1995; 195: 207-220

[157] Wasserman E, Rustad JR, Xantheas SS, Interaction potential of in water from first principles calculations, J. Chem. Phys. 1997; 106: 9769-9780.

[158] Casey WH, Large aqueous aluminum hydroxide molecules, Chem. Rev., 2006; 106:1-16.

[159] Shafran KL, Perry CC, A systematic investigation of aluminium ion speciation at high temperature. Part. 1. Solution studies, Dalton Trans. 2005, 2098-2105.

[160] Sipos P, The structure of Al(III) in strongly alkaline aluminate solutions — A review, J. Mol. Liq. 2009;146: 1–14

[161] Violante A, Huang PM, Formation mechanism of aluminum hydroxide polymorphs, Clays Clay Min. 1993; 41: 590-597..

[162] Wefers K, Mitra C, Oxides and hydroxides of aluminum, Alcoa Laboratories, 1987.

[163] Evonik, AEROXIDE ® Alu C, https://products-re.evonik.com/www2/uploads/productfinder/AEROXIDE-Alu-C-EN.pdf

[164] Sakashita S, Araki Y, Shiomada H, Effects of surface orientation of alumina supports on the catalytic functionality of molybdenum sulfide catalysts Appl. Catal. A Gen. 2001; 215: 101–110.

[165] Busca G, The surface of transition aluminas. A critical Review, Catal. Today, 2014; 226: 2-13.

[166] Li Y, Lousada CM, Korzhavyi PA, The nature of hydrogen in γ-alumina, J. Appl. Phys. 2014; 115(20): 203514

[167] Samain L, Jaworski A, Edén M, Ladd DM, Seo DK, Garcia-Garcia FJ, Häussermann U, Structural analysis of highly porous γ-Al_2O_3, J. Solid State Chem. 2014; 217: 1-8.

[168] Hansen MR. Jakobsen HJ, Skibsted, J, Structural environments for boron and aluminum in alumina-boria catalysts and their precursors from ^{11}B and ^{27}Al single- and double-resonance MAS NMR experiments, J. Phys. Chem. C, 2008; 112: 7210-7222.

[169] Pecharromán C, Sobrados I, Iglesias JE, González-Carreño T, Sanz J, Thermal evolution of transitional aluminas followed by NMR and IR spectroscopies J. Phys. Chem. B 1999; 103: 6160-6170

[170] Zhou, R.-S.; Snyder, R.L.; Structures and transformation mechanisms of the η-, γ- and θ- transition aluminas, Acta Crystallographica B 1991; 47: 617-630.

[171] Gleizes AN, Samélor D, Vahlas C, Sarou-Kanian V, Florian P, Massiot D, Temperature Dependent 4-, 5- and 6-Fold Coordination of Aluminum in MOCVD-Grown Amorphous Alumina Films: From Local Coordination to Material Properties, Advan. Sci. Technol. 2014; 91: 123-133

[172] Eklund P, Sridharan M, Singh G, Singh G, Bøttiger J, Thermal stability and phase transformations of γ-/amorphous-Al2O3 thin films, Plasma Process. Polym. 2009; 6: S907–S911

[173] Skibsted J, Henderson E, Jakobsen HJ, Characterization of calcium alumínate phases in cements by ^{27}Al MAS NMR spectroscopy Inorg. Chem. 1993; 32: 1013-1027

[174] Santamaría-Pérez D, Vegas A, The Zintl-Klemm concept applied to cations in oxides. I. The structures of ternary aluminates, Acta Cryst. 2003; B59: 305-323;

[175] Depmeier W, Aluminate sodalite $Ca_8[Al_{12}O_{24}](WO_4)_2$ at room temperature. Acta Crystallogr., 1984; C40:226 42.

[176] S.M. Antao, I. Assan, J.B. Parise, Chromate aluminate sodalite, $Ca_8[Al_{12}O_{24}](CrO_4)_2$: phase transitions and high-temperature structural evolution of the cubic phase, The Canadian Mineralogist 2004; 42: 1047-1056.

[177] Stephenson DA, Moore PB. The crystal structure of grandidierite, (Mg,Fe)A13SiBO9. Acta Cryst 1968; B24:1518-1522.

[178] Bennett JM, Cohen JM, Artioli G, Pluth JJ, Smith JV, Crystal structure of AlPO4-21, a framework aluminophosphate containing tetrahedral phosphorus and both tetrahedral and trigonal-bipyramidal aluminum in 3-, 4-, 5-, and 8-rings, Inorg. Chem., 1985; 24 (2): pp 188–193

[179] Bleam WF, Dec SF, Frye JS, 27A1 Solid-state nuclear magnetic resonance study of five-coordinate aluminum in augelite and senegalite, Phys Chem Minerals 1989; 16:817-820

[180] Simon S, van Moorsel JGMP, Kentgens APM, de Boer E, High fraction of penta-coordinated aluminium in amorphous and crystalline aluminium borates Solid State Nuclear Magnetic Resonance 5 (1995) 163-173

[181] Massiot D, Kahn-Harari A, Michel D, Muller D, Taulelle F, Aluminium-27 MAS NMR of Al2Ge2O7 and LaAlGe2O7: Two pentacoordinated aluminium environments, Magn. Res. Chem. 1990; 28: S82-S88.

182 Turcu FRV, SamosonA, Maier M, Trandafir DL, SimonS, High Fraction of Penta-Coordinated Aluminum and Gallium in Lanthanum–Aluminum–Gallium Borate, J. Am. Ceram. Soc., 2016; 99 (8): 2795–2800

[183] Skinner LB, Barnes AC, Salmon PS, Hennet L, Fischer HE, Benmore CJ, Kohara S, Weber JKR, Bytchkov A, Wilding MC, Parise JB, Farmer TO, Pozdnyakova I, Tumber SK, Ohara K, Joint diffraction and modeling approach to the structure of liquid alumina Phys. Rev. B 2013; 87: 024201

[184] Sierka M, Döbler, Sauer J, Santambrogio G, Brümmer M, Wöste L, Janssens E, Meijer G, Asmis KR, Unexpected Structures of Aluminum Oxide Clusters in the Gas Phase, Angew. Chem. Int. Ed. 2007, 46, 3372 –3375

[185] van Bokhoven JA, van der Eerden AMJ, Koningsberger DC, Three-coordinate aluminum in zeolites observed with In situ X-ray Absorption Near-Edge Spectroscopy at the Al K-edge: flexibility of aluminum coordinations in zeolites, J. Am. Chem. Soc., 2003; 125 (24): 7435–7442

[186] Brunetti B, Piacente V, Scardala P, Torsion vapor pressures and sublimation enthalpies of aluminum trifluoride and aluminum trichloride, J. Chem. Eng. Data 2009; 54: 940–944

[187] Bernasconi L, Madden PA, Wilson M, Ionic to molecular transition in $AlCl_3$: an examination of the electronic structure PhysChemComm, 2002; 5(1): 1–11.

[188] Pullmann P, Hensen K, Röntgenstrukturbestimmung von $AlCl_3$-pyridin-addukten: der strukturelle aufbau im trans-dichlorotetrakis(pyridin)aluminium(III)-tetrachloroaluminat(III) und im trichlorotris(pyridin)aluminium(III), Z. Naturforsch. 1982; 371: 1312-1315

[189] Dimitrov A, Heidemann D, Kemnitz E, F/Cl-exchange on AlCl3-pyridine adducts: synthesis and characterization of trans-difluoro-tetrakis-pyridine-aluminum-chloride, $[AlF_2(Py)_4]^+Cl^-$, Inorganic Chemistry, 2006; 45 (26): 10807-10814

[190] Sobota P, Mustafa MO, Utko J, Lis T, The crystal structure and properties at $[AlCl_3(C_6H_5COOC_2H_5]$, J. Organomet. Chem. 1989; 368(3): 257-262

[191] Hormnirun P, Marshall EL, Gibson VC, Pugh RI, White AJP, Study of ligand substituent effects on the rate and stereoselectivity of lactide polymerization using aluminum salen-type initiators, PNAS 2006; 103(42) 15343–15348.

[192] Saito S, Yamamoto H, Designer Lewis acid catalysts—bulky aluminium reagents for selective organic synthesis, Chem. Commun., 1997; 1585-6.

[193] Czympiel L, Pfrommer J, Tyrra W, Schafer M, Mathur S, Ligand modulated chemical and structural implications in four-, five- and six-fold coordinated aluminum heteroaryl alkenolates, Inorg. Chem. 2015; 54: 25-37.

[194] Morterra C, Magnacca G., A case study: surface chemistry and surface structure of catalytic aluminas, as studied by vibrational spectroscopy of adsorbed species, Catal. Today, 1996; 27: 497-532.

[195] Gervasini A, Auroux A, Thermodynamics of adsorbed molecules for a new acid-base topochemistry of alumina, J. Phys. Chem. 1993; 97: 2628-2639.

[196] Bolis V, Cerrato G, Magnacca G, Morterra C, Surface acidity of metal oxides. Combined microcalorimetric and IR-spectroscopic studies of variously dehydrated systems, Thermochim. Acta, 1998; 312: 63-77.

[197] Guillaume D, Gautier S, Despujol J, Alario F, Beccat P, Characterization ofacid sites on γ-alumina and chloineted γ-alumina by PNMR of adsorbed trimethylphosphine, Catal. Lett. 1997; 4: 213-218.

[198] Moroz IB, Larmier K, Liao WC, Copéret C,Discerning γ‑alumina surface sites with Nitrogen-15 dynamic nuclear polarization surface enhanced NMR spectroscopy of adsorbed pyridine, J. Phys. Chem. C 2018; 122: 10871−10882

[199] Velthoen MEZ, Nab S, Weckhuysen BM, Probing acid sites in solid catalysts with pyridine UV-Vis spectroscopy, Phys Chem Chem Phys. 2018;20(33):21647-21659.

[200] Gribov EN, Zavorotynska O, Agostini G, Vitillo JG, Ricchiardi G, Spoto G, Zecchina A, FTIR spectroscopy and thermodynamics of CO and H_2 adsorbed on γ-, δ- and α-Al_2O_3, Phys. Chem. Chem. Phys. 2010; 12: 6474–6482.

[201] Sanchez Escribano V, Garbarino G, Finocchio E, Busca G, γ-alumina and amorphous silica-alumina: structural features, acid sites and the role of adsorbed water,Topics in Catal. 2017; 60: 1554-1564.

[202] Phung TK, Lagazzo A, Rivero Crespo MA, Sanchez Escribano V, Busca G, A study of commercial transition aluminas and of their catalytic activity in dehydration of ethanol, J. Catal. 2014; 311: 102-114.

[203] Soled S, γ-Al_2O_3 viewed as a defect oxyhydroxide, J. Catal 1983; 821: 252-257.

[204] Lundie DT, McInroy AR, Marshall R, Winfield JM, Jones P, Dudman CC, Parker SF, Mitchell C, Lennon D, Improved description of the surface acidity of eta-alumina, J. Phys. Chem. B 2005,;109(23): 11592–11601.

[205] Wischert R, Copéret C, Delbecq F, Sautet P, Dinitrogen: a selective probe for tri-coordinate Al "defect" sites on alumina, Chem. Commun. 2011, 47, 4890–4892.

[206] Hu JZ, Xu S, Kwak JH, Hu MY, Wan C, Zhao Z, Szanyi J, Bao X, Han X, Wang Y, Peden CHF, High field ^{27}Al MAS NMR and TPD studies of active sites in ethanol dehydration using thermally treated transitional aluminas as catalysts, J. Catal. 2016; 336: 85–93

[207] Kwak JH, Hu J, Lukaski A, Kim DH, Szanyi J, Peden CHF, Role of pentacoordinated Al^{3+} Ions in the high temperature phase transformation of γ-Al_2O_3, J. Phys. Chem. C, 2008; 112(25): 9486-9492.

[208] Kwak JH, Hu JZ, Mei D, Yi CW, Kim DH, Peden CHF, Allard LF, Szanyi J, Coordinatively unsaturated Al^{3+} centers as binding sites for active catalyst phases of platinum on gamma-Al_2O_3, Science, 2009; 325: 1670-1673.

[209] Mei D, Kwak JH, Hu JZ, Cho SJ, Szanyi J, Allard LF, Peden CHF, Unique role of anchoring penta-coordinated Al^{3+} sites in the sintering of γ-Al_2O_3-supported Pt catalysts, J. Phys. Chem. Letters 2010; 1 : 2688-2691.

[210] Barrow NS, Scullard A, Collis N, Dynamic nuclear polarisation enhanced solid-state nuclear magnetic resonance studies of surface modification of γ-Alumina, Johnson Matthey Technol. Rev. 2016; 60: 90-97.

[211] Flemming RL, Terskikh V, Ye E, Aluminum environments in synthetic Ca-Tschermak clinopyroxene ($CaAlAlSiO_6$) from Rietveld refinement, ^{27}Al NMR, and first-principles calculations, Amer. Miner. 2015; 100: 2219–2230.

[212] Zhao Z, Xu S, Hu MY, Bao X, Peden CHF, Hu J, Investigation of aluminum site changes of dehydrated zeolite H-Beta during a rehydration process by high-field solid-state NMR J. Phys. Chem. C 2015; 119(3): 1410−1417

[213] Brus J, Kobera L, Schoefberger W, Urbanov M, Klein P, Sazama P, Tabor E, Sklenak S, Fishchuk AV, Dědeček J, Structure of framework aluminum Lewis sites and perturbed aluminum atoms in zeolites as determined by 27Al{1H} REDOR (3Q) MAS NMR spectroscopy and DFT/molecular mechanics, Angew. Chem. Int. Ed. 2015; 54: 541 –545

[214] Wischert R, Florian P, Copéret C, Massiot D, Sautet P, Heterolytic splitting of H_2 and CH_4 on γ-alumina as a structural probe for defect sitesj. Phys. Chem. C 2014; 118: 15292−15299.

[215] Szanyi J, Kwak JH, Dissecting the steps of CO2 reduction: 1. The interaction of CO and CO_2 with γ-Al_2O_3: an in situ FTIR study, Phys. Chem. Chem. Phys., 2014;16: 15117-15125

[216] Nastova I, Skapin T, Pejov L, Effect of partial fluorination on the Lewis sites of microcrystalline γ-alumina studied by adsorption of pyridine as a probe molecule: a quantum chemical cluster model study, Surface Sci. 2011, 605, 1525-1536.

[217] Kassab E, Castellà-Ventura M, Theoretical study of pyridine and 4,4‘-Bipyridine adsorption on the Lewis acid sites of alumina surfaces based on ab initio and density functional cluster calculations, J. Phys. Chem. B 2005, 109, 13716-13728.

[218] Neyman KM, Nasluzov VA, Zhidomirov GM, A density functional study of CO adsorption on three- and five-coordinate Al in oxide systems, Catal. Lett. 1996; 40 (1-2): 183-188

[219] Casarin M, Maccato C, Vittadini A, Theoretical Study of the Chemisorption of CO on Al_2O_3(0001), Inorg. Chem. 2000; 39: 5232-5237

[220] Rohmann C, Metson JB, Idriss H, DFT study of carbon monoxide adsorption on α-Al_2O_3(0001), Surface Science 2011; 605: 1694–1703.

[221] Wischert R, Copéret C, Delbecq F, Sautet P, Optimal water coverage on alumina: a key to generate Lewis acid–base pairs that are reactive towards the C-H bond activation of methane, Angew. Chem. Int. Ed. 2011, 50, 3202-3205.

[222] Krahl Th, Stösser R, Kemnitz E, Scholz G, Feist M, Silly G, Buzaré JY, Structural insight into aluminum chlorofluoride (ACF), Inorg Chem 2003; 42:6474-6483.

[223] Sohlberg K, Pantelides ST, Pennycook SJ, Surface reconstruction and the difference in surface acidity between γ- and η-alumina, J. Am. Chem. Soc. 2001; 123: 26-29.

[224] Busco C, Bolis V, Ugliengo P, Masked lewis sites in proton exchanged zeolites: a computational and microcalorimetric investigation, J. Phys. Chem. 2007; 111: 5561-5567.

[225] Busca G, Rossi PF, Lorenzelli V, Benaissa M, Travet J, Lavalley JC, Microcalorimetric and FT-IR spectroscopic studies of methanol adsorption on Al_2O_3, J. Phys. Chem., 1985, 89, 5433-5439.

[226] Knözinger H, Krietenbrink H, Müller, HD, Schulz W, Proceedings of the 6th Int. Congr. Catal., London, 1976, Vol. I, p. 183.

[227] Garbarino G, Prasath Parameswari Vijayakumar R, Riani P, Finocchio E, Busca G, Ethanol and diethyl ether catalytic conversion over commercial alumina and lanthanum-doped alumina: reaction paths, catalyst structure and coking, Appl. Catal. B Envir. 2018; 236: 490-500.

[228] Corado A, Kiss A, Knözinger H, Müller D, Catalytic isomerization of olefins on alumina: II. Catalyst deactivation and its effects on the mechanismJ. Catal. 1975; 37: 68–80.

[229] Busca G, Finocchio E, Lorenzelli V, Trombetta M, Rossini SA, Infrared study of olefin allylic activation on magnesium ferrite and alumina catalysts, J. Chem. Soc. Faraday Trans. 1 1996; 92: 4687–4693.

[230] Mastikhin VM, Mudrakovsky IL, Nosov AV, ^{1}H NMR magic angle spinning (MAS) studies of heterogeneous catalysis, Prog. Nucl. Magn. Reson. Spectrosc. 1991; 23: 259-299.

[231] DeCanio EC, Edwards JC, Bruno JW, Solid-State ^{1}H MAS NMR characterization of γ-alumina and modified γ-aluminas, J. Catal. 1994; 148: 76-83.

[232] Deng F, Wang G, Du Y, Ye C, Kong Y, Li X, Double resonance NMR studies on the surface modification of hydroxyls on γ -alumina by sodium, Solid State Nucl. Magn. Res. 1997; 7: 281-290.

[233] Qu L, Zhang W, Kooyman PJ, Prins R, MAS NMR, TPR, and TEM studies of the interaction of NiMo with alumina and silica-alumina supports, J. Catal. 2003; 215: 7–13.

[234] Huittinen N, Sarv P, Lehto J, A proton NMR study on the specific sorption of yttrium(III) and europium(III) on gamma-alumina [γ-Al_2O_3], J. Colloid Interf. Sci. 2011; 361: 252–258.

[235] Ferreira AR, Küçükbenli E, de Gironcoli S, Souza WF, Chiaro SSX, Konstantinova E, Leitão AA, Structural models of activated γ-alumina surfaces revisited: Thermodynamics, NMR and IR spectroscopies from ab initio calculations, Chem. Phys. 2013; 423: 62–72.

[236] Delgado M, Delbecq F, Santini CC, Lefebvre F, Norsic S, Putaj P, Sautet P, Basset JM, Evolution of structure and of grafting properties of γ-alumina with pretreatment temperature, J. Phys. Chem. C 2012; 116: 834–843.

[237] Ramis G, Busca G, FTIR spectra of adsorbed n-butylamine, J. Mol. Struct. 1989; 193: 93-100

[238] Trombetta M, Busca G, Rossini S, Piccoli V, Cornaro U, FT-IR studies on light olefin skeletal isomerization catalysis. Part I: the interaction of C4 olefins with pure γ - alumina, J. Catal., 1997, 168, 334-348.

[239] Zagoruiko AN, Shinkarev VV, Vanag SV, Bukhtiyarova GA, Catalytic processes and catalysts for production of elemental sulfur from sulfur-containing gases, Catalysis in Industry, 2010; 2(4): 343–352

[240] BASF, Claus Catalysts, brochure, available on the web www.basf.com

[241] Pines H, Manassen J, The mechanism of dehydration of alcohols over alumina catalysts, Advan Catal Relat. Subj. 1966;16: 49-93

[242] Morschbacker A, Bio-ethanol based ethylene, J. Polymer Rev. 2009; 49: 79-84.

[243] Liu Z, Sun C, Wang G, Wang Q, Cai G, New progress in R&D of lower olefin synthesis, Fuel Proc. Technol., 2000, 62, 161-172.

[244] Kim SM, Lee YJ, Bae JW, Potdar HS, Jun KW, Synthesis and characterization of a highly active alumina catalyst for methanol dehydration to dimethyl ether, Appl. Catal. A: Gen. 2008; 348(1): 113-120

[245] de Klerk A, Key catalyst types for the efficient refining of Fischer–Tropsch syncrude: alumina and phosphoric acid, Catalysis, 2011, 23, 1–49

[246] Schmidt SA, Kumar N, Zhang B, Eränen K, Murzin DY, Salm T, Preparation and characterization of alumina-based microreactors for application in methyl chloride synthesis, Ind. Eng. Chem. Res., 2012; 51(12): 4545–4555

[247] http://www.basf.com/group/corporate/en/brand/HF_200XPHF (10.12.2012)

[248] http://www.catalysts.basf.com/p02/USWeb-Internet/catalysts/en/content/microsites/catalysts/prods-inds/adsorbents/act-alum-adsorb (10.12.2012)

[249] Kasprzyk-Hordern B, Chemistry of alumina, reactions in aqueous solution and its application in water treatment, Advan. Colloid Interface Sci. 2004; 110: 19–48

[250] Madon R, Harris DH, Xu M, Stockwell D, Lerner B, Dodwell GW,.FCC catalysts for feeds containing nickel and vanadium , US patent 6716338 to Engelhard Corporation (2001)

[251] Harris DH, Xu M, Stockwell D, Madon R, FCC catalysts for feeds containing nickel and vanadium , US patent 6673235, to Engelhard Corporation (2002)

[252] Daniell W, Schubert U, Glöckler R, Meyer A, Noweck K, Knözinger H, Enhanced surface acidity in mixed alumina-silicas: a low-temperature FTIR study, Appl. Catal. A Gen. 2000; 196: 247–260.

[253] Niwa M, Hibino T, Murata H, Katada N, Murakami Y, A silica monolayer on alumina and evidence of lack of acidity of silanol attached to alumina, J. Chem. Soc. Chem. Commun. 1989; 289-290.

[254] Basini L, Aragno A, Raffaelli A, Vibrational infrared spectroscopic studies of 1-butene skeleton isomerization at the surface of a silicated alumina in a micro-plug flow reactor, J. Phys. Chem., 1995; 95 (1): 211-218.

[255] Finocchio E, Busca G, Rossini S, Cornaro U, Piccoli V, Miglio R. FT-IR characterization of silicated aluminas, active olefin skeletal isomerization catalysts,, Catal Today 1997;33: 335-352.

[256] Trombetta, M.; Busca G,; Willey, R.J. Characterization of silica-containing aluminum hydroxide and oxide aerogels, J. Colloids Interface Sci., 1997, 190, 416-426.

[257] Mardkhe MK, Lawson J, Huang B, Handly ED, Woodfield BF, A statistical approach to control porosity in silica-doped alumina supports, Micropor. Mesopor. Mat., 2015; 210: 116-124.

[258] Mouat AR, George C, Kobayashi T, Pruski M, van Duyne RP, Marks TJ, Stair PC, Highly Dispersed SiO_x/Al_2O_3 Catalysts illuminate the reactivity of isolated silanol sites, Angew. Chem. Int. Ed. 2015; 54: 13346 –13351

[259] Niwa M, Katada N, Murakami Y, Thin silica layer on alumina: evidence of the acidity in the monolayer, J. Phys. Chem., 1990; 94 (16): 6441–6445

[260] Phung TK, Busca G, Ethanol dehydration on silica-aluminas: active sites and ethylene/ diethyl ether selectivities, Catal. Commun. 2016; 68:110-116.

[261] Yaripour F, Baghaei F, Schmidt I, Perregaard J, Catalytic dehydration of methanol to dimethyl ether (DME) over solid-acid catalysts, Catal. Commun. 2005, 6, 147-152.

[262] M. Trombetta, Busca G, S. Rossini, V. Piccoli, U. Cornaro, A. Guercio, R. Catani, R.J.Willey, FT-IR studies on light olefin skeletal isomerization catalysis: III. Surface acidity and activity of amorphous and crystalline catalysts belonging to the SiO_2-Al_2O_3 system J. Catal. 179 (1998) 581–596.

[263] Butler AC, Nicolaides CP, Catalytic skeletal isomerization of linear butenes to isobutene, Catal. Today 1993; 18: 443-471.

[264] Weissermel K, Arpe HJ, Industrial Organic Chemistry, 3rd ed., 1997, VCH Weinheim, p. 70.

[265] Bailey SW, Lister JS, Structures, compositions,and X-ray diffraction identification of dioctahedral chlorites, Clays Clay Min. 1989; 37(3) 193-202.

[266] Mao H, Selleby M, Sundman B, Phase equilibria and thermodynamics in the Al_2O_3–SiO_2 system, J. Am Ceram. Soc. 2005; 88(9): 2544-2551

[267] Schneider H, Schreuer J, Hildmann B, Structure and properties of mullite—A review, J. Eur. Ceram. Soc. 2008; 28: 329–344.

[268] Aryal S, Rulis P, Ching WY, Density functional calculations of the electronic structure and optical properties of aluminosilicate polymorphs (Al_2SiO_5), Amer. Mineral. 2008; 93:114-123

[269] Okada K, Otsuka N, Characterization of the spinel phase from SiO_2-Al_2O_3 xerogels and the formation process of mullite, J. Am. Ceram. Soc. 1986; 69: 652-656.

[270] Cassidy DJ, Woolfrey JL, Bartlett JR, The effect of precursor chemistry on the crystallisation and densification of sol–gel derived mullite gels and powders, J. Sol–Gel Sci.Tech. 1997; 10: 19–30

[271] Chakraborty AK, Formation of Silicon-Aluminum Spinel, J. Am. Ceram. Soc. 1979; 62: 120–124

[272] Worrall WE, Clays and Ceramic Raw Materials, Halsted Press, New York, NY, 1975, pp. 151–152

[273] Chakraborty AK, Phase transformation of kaolinite clay, Springer India, New Delhi, 2014, p.183.

[274] Schneider H, Voll D, Saruhan B, Schmücker M, Schaller T, Sebald A, Constitution of the γ-alumina phase in chemically produced mullite precursors, J. Eur. Ceram. Soc.1994; 13(5): 441-448

[275] Sánchez-Muñoz L, Sanz J, Sobrados I, Gan Z, Medium-range order in disordered K-feldspars by multinuclear NMR, Am. Miner. 2013; 98 (11-12): 2115-2131.

[276] Kyono A, Kimata M, Hatta T, Aluminum position in Rb-feldspar as determined by X-ray photoelectron spectroscopy, Naturwissenschaften 2003; 90: 414-418.

[277] Buerger MJ, Derivative crystal structures. J. Chem. Phys. 1947;15: l-16.

[278] Buerger MJ, The stuffed derivatives of the silica structures, Am. Min. 1954; 39: 600-615

[279] Palmer DC, Stuffed derivatives of the silica polymorphs, Rev. Miner. Geochem., January 1994; 29: 83-122

[280] Douglas BE, Stuffed Derivatives of Close-Packed Structures J. Chem. Ed.2007; 84: 1846-1852.

[281] Pillars WW, Peacor DR, The crystal structure of beta eucryptite as a function of temperature, Am. Min. 1973; 58: 681-690.

[282] Xu H, Heaney PJ, Yu P, Huifang X, Synthesis and structure of a stuffed derivative of α-quartz, $Mg_{0.5}AlSiO_4$, Amer. Miner. 2015; 100(10): 2191–2198.

[283] Kohn SC, Henderson CMB, Dupree R, Si-Al ordering in leucite group minerals and ion-exchanged analogues: An MAS NMR study, Am. Miner.1997; 82: 1133-1140.

[284] Barrer RM Zeolites and clay minerals as sorbents and molecular sieves. Academic Press, New York, 1978.

[285] Stebbins JF, Kroeker S, Lee SK, Kiczenski TJ, Quantification of five- and six-coordinated aluminum ions in aluminosilicate and fluoride-containing glasses by high-field,high-resolution ^{27}Al NMR, J. Non-Cryst. Solids 2000; 275: 1-6.

[286] Okuno M, Zotov N, Schmucker M, Schneider H, Structure of SiO_2-Al_2O_3 glasses: combined X-ray diffraction, IR and Raman studies, J. Non-Cryst. Solids 2005; 351: 1032-1038.

[287] Rosales-Sosa GA, Masuno A, HigoY, Inoue H, Crack-resistant Al_2O_3–SiO_2 glasses Scientific Reports 2016; 6:23620.

[288] Onorato PIK, Alexander MN, Struck CW, Tasker GW, Uhlmann DR, Bridging and nonbridging oxygen atoms in alkali aluminosilicate glasses, J. Am. Cer. Soc. 1985; 68(6):C-148 - C-150

[289] Jaworski A, Stevensson B, Edén M, Direct ^{17}O NMR experimental evidence for Al–NBO bonds in Si-rich and highly polymerized aluminosilicate glasses Phys. Chem. Chem. Phys., 2015; 17: 18269-18272.

[290] Stebbins JF, Oglesby JV, Lee SK, Oxygen Sites in Silicate Glasses: A New View from Oxygen-17 NMR Chem. Geol. 2001; 174: 63– 75

[291] Schmücker M, Schneider H, New evidence for tetrahedral triclusters in aluminosilicate glasses, J. Non-Cryst. Solids 2002; 311: 211–215.

[292] Xiang Y, Du J, Smedskjaer MM, Mauro JC, Structure and properties of sodium aluminosilicate glasses from molecular dynamics simulations, The Journal of Chemical Physics 2013; 139: 044507

[293] Jakse N, Bouhadja M, Kozaily J, Drewitt JWE, Hennet L, Neuville DR, Fischer HE, Cristiglio V, Pasturel A, Interplay between non-bridging oxygen, triclusters, and fivefold Al coordination in low silica content calcium aluminosilicate melts, Appl. Phys. Lett. 2012; 101: 201903.

[294] Löwenstein W, The distribution of aluminum in the tetrahedra of silicates and aluminates Am. Mineral. 1954, 39, 92-96.

[295] Gottardi G, Alberti A, Silicon aluminium ordering in the framework of zeolites. Bull. Geol. Soc. Finland 1985; 57 (1-2): 197—206.

[296] Alberti A, Crystal chemistry of Si-Al distribution in natural zeolites, Namba S, Tatsumi T, Inui Teds, Chemistry of Microporous Crystals, Stud. Surf. Sci. Catal. 1991; 60: 107-122.

[297] Porcher F, Souhassou M, Dusausoy Y, Lecomte, The crystal structure of a low-silica dehydrated NaX zeolite Eur. J. Mineral. 1999; 11: 333-343.

[298] Fletcher RE, Ling S, Slater B, Violations of Löwenstein's rule in zeolites Chem. Sci., 2017; 8(11): 7483-7491

[299] Yang CS, Mora-Fonz JMM, Catlow CRA, Stability and Structures of Aluminosilicate Clusters, J. Phys. Chem. C 2011; 115: 24102–24114

[300] Bell RG, Jackson RA, Catlow RRA, Löwenstein's rule in zeolite A: A computational study. Zeolites 1992; 12: 870-871.

[301] Ambruster T, Gunter ME, Crystal structures of natural zeolites, Rev. Miner. Geochem. 2001; 45(1): 1-67.

[302] Dempsey E, Kühl GH,Olson DH, Variation of the lattice parameter with aluminum content in synthetic sodium faujasites. Evidence for ordering of the framework ions, J. Phys. Chem. 1969; 73: 387-390

[303] Perea DE,Arslan J, Liu J, Ristanović Z, Kovarik L, Arey BW, Lercher JA, Bare SR, Weckhuysen BM, Determining the location and nearest neighbours of aluminium in zeolites with atom probe tomography, Nature Commun. 2015; 6: 7589.

[304] Bordiga S, Lamberti C, Bonino F, Travert A, Thibault-Starzyk A, Probing zeolites by vibrational spectroscopies, Chem Soc Rev 2015; 44:7262–7341

[305] Katada N, Analysis and interpretation of acidic nature of aluminosilicates, Mol. Catal. 2017; in press, available on internet

[306] Chen NY, Garwood WE, Dwye FG, Shape Selective Catalysis in Industrial Applications, Dekker, New York, 2nd ed., 1996.

[307] Guisnet M, Gilson JP, eds., Zeolites for Cleaner Technologies, Imperial College Press 2002.

[308] Sastre G, Corma A, The confinement effect in zeolites, J. Mol. Catal. A: Chem. 2009; 305: 3–7

[309] Breck DW, Zeolite Molecular Sieves: Structure, Chemistry and Use, Wiley,New York, NY, 1974

[310] Vaughan DEW, Contributions of R. M. Barrer to zeolite synthesis, Stud. Surf. Sci. Catal. 2007; 170: 87-95.

[311] Martinez C, Corma A, Inorganic molecular sieves: Preparation, modification and industrial application in catalytic processes, Coord. Chem. Rev. 255 (2011) 1558-1580.

[312] Huo Q, Synthetic Chemistry of the Inorganic Ordered Porous Materials, in Xu R, Pang W, Huo Q, eds, Modern inorganic synthetic chemistry, Elsevier, 2011, p. 339-373.

[313] Marthala VRR, Hunger M, Kettner F, Krautscheid H, Chmelik C, Kärger J, Weitkamp J, Solvothermal synthesis and characterization of large-crystal all-silica, aluminum-, and boron-containing ferrierite zeolitesChem. Mater. 2011, 23, 2521–2528

[314] Eichler U, Brändle M, Sauer J, Predicting absolute and site specific acidities for zeolite catalysts by a combined quantum mechanics/interatomic potential function approach, J. Phys. Chem. B, 1997; 101 (48) 10035-10050.

[315] Schroder KP, Sauer J, Leslie M, Catlow CRA, Thomas JM, Bridging hydrodyl groups in zeolitic catalysts: a computer simulation of their structure, vibrational properties and acidity in protonated faujasites (H-Y zeolites), Chem. Phys. Lett. 1992; 188: 320-325.

[316] Simperler A, Bell RG, Anderson MW, Probing the Acid Strength of Brønsted Acidic Zeolites with Acetonitrile: An Atomistic and Quantum Chemical Study, J. Phys. Chem. B. 2004; 108: 7142-7151.

[317] Kazansky VB, Seryk AI, Semmer-Herledan V, Fraissard J, Intensities of OH IR stretching bands as a measure of the intrinsic acidity of bridging hydroxyl groups in zeolites, Phys. Chem. Chem. Phys. 2003; 5: 966-969.

[318] Montanari T, Bevilacqua M, Busca G, Use of nitriles as probe molecules for the accessibility of the active sites and the detection of complex interactions in zeolites through IR spectroscopy, Appl. Catal. A: Gen. 2006; 307: 21-29

[319] Freitas C, Barrow NS, Zholobenko V, Accessibility and location of acid sites in zeolites as probed by Fourier transform infrared spectroscopy and magic angle spinning nuclear magnetic resonance, Johnson Matthey Technol. Rev. 2018; 62(3), 279-290.

[320] Busca G, Acidity and basicity of zeolites: a fundamental approach, Micropor. Mesopor. Mat. 2017; 254: 3-16.

[321] Domokos L, Lefferts L, Seshan K, Lercher JA, The importance of acid site locations for n-butene skeletal isomerization on ferrierite J. Mol. Catal.A: Chem. 2000; 162: 147-157.

[322] Regli L, Zecchina A, Vitillo JG, Cocina D, Spoto G, Lamberti C, Lillerud KP, Olsbye U, Bordiga S, Hydrogen storage in chabazite zeolite frameworks. Phys. Chem. Chem. Phy.. 2005; 7: 3197-3203.

[323] Li Y, Guo W, Fan W, Yuan S, Li J, Wang J, Jiao H, Tatsumi T, A DFT study on the distributions of Al and Brönsted acid sites in zeolite MCM-22, J. Mol. Catal. A: Chem, 2011; 338: 24-32.

[324] Osuga R, Yokoi T, Doitomi K, Hirao H, Kondo, JN, Infrared investigation of dynamic behavior of Brønsted acid sites on zeolites at high temperatures, J. Phys. Chem. C, 2017, 121 (45), pp 25411–25420

[325] Bartohomeuf D, Zeolite acidity dependence on structure and chemical environment. Correlations with catalysis, Mater. Chem. Phys. 1987; 17: 49-55.

[326] Phung TK, Proietti Hernández L, Lagazzo A, Busca G, Dehydration of ethanol over zeolites, silica alumina and alumina: Lewis acidity, Brønsted acidity and confinement effects, Appl. Catal. A: Gen., 2015; 493: 77-89

[327] Matsunaga Y, Yamazaki H, Yokoi T, Tatsumi T, Kondo JN, IR Characterization of homogeneously mixed silica−alumina samples and dealuminated Y zeolites by using pyridine, CO, and propene probe molecules, J. Phys. Chem. C 2013; 117: 14043−14050

[328] Phung TK, Busca G, On the Lewis acidity of protonic zeolites, Appl. Catal. A Gen. 2015; 504: 151-157

[329] Moliner M, State of the art of Lewis acid-containing zeolites: lessons from fine chemistry to new biomass transformation processes, Dalton Trans. 2014; 43: 4197-4208.

[330] Busco C, Bolis V, Ugliengo P, Masked lewis sites in proton exchanges zeolites: a computational and microcalorimetric investigation, J. Phys. Chem. C Lett., 2007; 111(15) 5561-5567.

[331] Sheldon RA, Arends I, Hanefeld U, Green Chemistry and Catalysis, Wiley, Weinheim, 2007, pp. 59-60.

[332] Sastre G, Katada N, Niwa M, Computational study of Brønsted Acidity of mordenite. effect of the electric field on the infrared OH stretching frequencies, J. Phys. Chem. C, 2010; 114 (6):15424–15431

[333] Xu B, Sievers C, Hong SB, Prins R, van Bokhoven JA, Catalytic activity of Brønsted acid sites in zeolites: intrinsic activity, rate-limiting step, and influence of the local structure of the acid sites, J. Catal. 2006; 244: 163-168.

[334] Gounder R, Iglesia E, Effects of partial confinement on the specificity of monomolecular alkane reactions for acid sites in side pockets of mordenite, Angew. Chem. Int. Ed. 2010; 49: 808 –811

[335] Gounder R, Jones AJ, Carr RT, Iglesia E, Solvation and acid strength effects on catalysis by faujasite zeolites, J. Catal. 2012;286:214–223

[336] Simonetti DA, Carr RT, Iglesia E, Acid strength and solvation effects on methylation, hydride transfer, and isomerization rates during catalytic homologation of C1 species, J. Catal. 2012; 285; 19-30

[337] Weisz PB, Frilette VJ, Intracrystalline and molecular-shape-selective catalysis by zeolite salts, J. Phys. Chem. 1960; 64: 382-382.

[338] Smit B, Maesen TLM, Towards a molecular understanding of shape selectivity, Nature 2008; 451: 671-678.

[339] Gounder R, Iglesia E, The roles of entropy and enthalpy in stabilizing ion-pairs at transition states in zeolite acid catalysis, Acc. Chem. Res. 2012; 45:229-238.

[340] de Boer JH, Constitution and properties of silica-alumina-catalysts, Disc. Faraday Soc. 1971; 52: 109–112.

[341] Chamonnot A, In Raybaud P, Toulhoat H, Catalysis by Transition Metal Sulphides, Technip, 2013, pp. 225-247.

[342] Timken HKC, Method for preparing a highly homogeneous amorphous silica-alumina composition, US patent 6,872,685 B2, 2005, to Chevron USA. Inc.

[343] Perego C, Millini R, Porous materials in catalysis: challenges for mesoporous materials, Chem. Soc. Rev., 2013; 42: 3956–3976.

[344] Trombetta M, Busca G, Lenarda M, Storaro L, Pavan M, An investigation of the surface acidity of mesoporous Al-containing MCM-41 and of the external surface of ferrierite through pivalonitrile adsorption Appl. Catal. A: Gen. 1999; 182 (2): 225-235

[345] Suzuki K, Aoyagi Y, Katada N, Choi M, Ryoo R, Niwa M, Acidity and catalytic activity of mesoporous ZSM-5 in comparison with zeolite ZSM-5, Al-MCM-41 and silica-alumina Catalysis Today 2008; 132, 38-45.

[346] Luan Z, Fournier JA, In situ FTIR spectroscopic investigation of active sites and adsorbate interactions in mesoporous aluminosilicate SBA-15 molecular sieves, Microp. Mesop. Mat. 2005; 79: 235-240.

[347] Koekkoek AJJ, Van Veen JAR, Gerrtisen PB, Giltay P, Magusin PCMM, Hensen EJM, Brønsted acidity of Al/SBA-15, Microp. Mesop. Mat. 2012; 151: 34-43.

[348] Gutzeit CL, Woodbury NJ, Preparation of silica-alumina base, US patent 2,735,801, 1956, assigned to Socony, Mobil Oil Company, Inc.

[349] Scherzer J, Gruia AJ, Hydrocracking Science and Technology, Dekker, New York, 1996, pp. 57-58.

[350] Horton WB, Maatman RW, Cumene cracking catalyzed by impregnated and cogelled silica-alumina, J. Catal. 1964; 3: 113-122

[351] Caillot M, Chaumonnot A, Digne M, Van Bokhoven JA, Creation of Brønsted acidity by grafting aluminum isopropoxide on silica under controlled conditions: determination of the number of Brønsted sites and their turnover frequency for m-xylene isomerization, 6 (2014), pp. 832–841

[352] Locus R, Verboekend D, d'Halluin M, Dusselier M, Liao Y, Nuttens N, Jaumann T, Oswald S, Mafra L, Giebeler L, Sels B, Synthetic and catalytic potential of amorphous mesoporous aluminosilicates prepared by postsynthetic aluminations of silica in aqueous media, ChemCatChem 2018; 10: 1385 – 1397

[353] Katada N, Kawaguchi Y, Takeda K, Matsuoka T, Uozumi N, Kanai K, Fujiwara S, Kinugasa K, Nakamura K, Suganuma S, Nanjo M, Dealkylation of alkylpolycyclic aromatic hydrocarbon over silica monolayer solid acid catalyst, Appl. Catal. A: Gen., 2017; 530: 93-101

[354] https://www.aerosil.com/sites/lists/IM/Documents/Catalyst-Carrier-Newsletter-09-EN.pdf

[355] Huang J, van Vegten N, Jiang Y, Hunger M Baiker A. Increasing the Brønsted Acidity of Flame-Derived Silica/Alumina up to Zeolitic Strength. Angew. Chem. Int. Ed., 2010; 49: 7776–7781.

[356] Gun'ko VM, Blitz JP, Gude K, Zarko VI, Goncharuk EV, Nychiporuk YM, Leboda R, Skubiszewska-Zięba J, Osovskii VD, Ptushinskii YG, Mishchuk OA, Pakhovchishin SV, Gorbik PP, Surface structure and properties of mixed fumed oxides, J.Colloid Interf. Sci 2007; 314 (1): 119–130

[357] Tamon H, Sone T, Mikami M, Okazaki M, Preparation and characterization of silica–titania and silica–alumina aerogels, J. Colloid Interf. Sci. 1997; 188: 493–500

[358] Shearon WH, Fullem WR, Silica-Alumina Petroleum Cracking Catalyst, Ind. Eng. Chem., 1959; 51 (6): 720–726

[359] Van Bokhoven JA, Strong Brønsted Acidity in Alumina-Silicates: Influence of Pore Dimension, Steaming and Acid Site Density on Cracking of Alkanes, in Ordered Porous Solids, Recent Advances and Prospects Valtchev V, Mintova S, Tsapatsis M, 2009, Pages 651–668

[360] Phongsawat W, Netivorruksa B, Suriye K, Dokjampa S, Praserthdam P, Panprano J, Production of propylene from an unconventional metathesis of ethylene and 2-pentene over Re_2O_7/SiO_2-Al_2O_3 catalysts, J. Nat. Gas Chem. 2012; 21(1): 83–90

[361] Debecker DP, Stoyanova M, Rodemerck U, Léonard A, Su BL, Gaigneaux EM, Genesis of active and inactive species during the preparation of MoO_3/SiO_2–Al_2O_3 metathesis catalysts via wet impregnation, Catal. Today 2011; 169: 60–68.

[362] Blanchard J, Kraft JM, Dupont C, Sayaga C, Takahashi T, Yasuda H, On the influence of water traces on the acidity measurement of amorphous aluminosilicates, Catal. Today 2014; 226: 89–96

[363] de Klerk A, Effect of oxygenates on the oligomerization of Fischer− Tropsch olefins over amorphous silica− alumina, Energy Fuel, 21 (2007), pp. 625–632

[364] Holm VCF, Bailey GC, Clark A, Acidity Studies of Silica-Alumina Catalysts, J. Phys. Chem. 1959; 63 (2): 129-133.

[365] Schwarz JA, Russell BG, Harnsberger HF, A study of pyridine adsorbed on silica-alumina catalysts by combined infrared spectroscopy and temperature-programmed desorption, J. Catal. 1978; 54: 303-317.

[366] Erickson H, US patent 2,872,410, Improved silica-alumina catalysts and their use in hydrocarbon cracking processes, to Sinclair Refining Company, 1959.

[367] Bridge AG, Mukherjee UK, Hydrocracking for superior fuels and lubes production, in Handbook of petroleum refining processes, R.A. Meyers ed., McGraw Hill, 2005, 3rd ed., 7.3-7.22

[368] Scherzer J, Gruia AJ, Hydrocracking Science and Technology, Dekker, New York, 1996, pp. p. 29

[369] Dik PP, Klimov OV, Budukva SV, Leonova KA, Pereyma VYu, Gerasimov EYu, Danilova IG, Noskov AS, Silica-alumina based nickel-molybdenum catalysts for vacuum gas oil hydrocracking aimed at a higher diesel fraction yield, Catal. Ind. 2014; 6 (3): 231-238.

[370] Sadighi S, Modeling a vacuum gas oil hydrocracking reactor using axial dispersion lumped kinetics Petroleum & Coal 2013;55(3):156-168.

[371] de Klerk A, Furimsky E, Catalysis in the Refining of Fischer-Tropsch Syncrude, The Royal Society of Chemistry, Cambridge, 2010, pp. 193-209

[372] Collins JP, Font Freide JJHM, Nay B, A History of Fischer-Tropsch wax upgrading at BP—from catalyst screening studies to full scale demonstration in Alaska, J. Nat. Gas Chem., 2006; 15: 1-10.

[373] Weckhuysen BM, Schoonheydt RA, Olefin polymerization over supported chromium oxide catalysts, Catal. Today 1999; 51:215-221

[374] Brückner A, Bentrup U, Zanthoff H, Maschmeyer D, The role of different Ni sites in supported nickel catalysts for butene dimerization under industry-like conditions, J. Catal. 2009; 266(1): 120–128

[375] Finiels A, Fajula F, Hulea V, Nickel-based solid catalysts for ethylene oligomerization – a review, Catal. Sci. Technol., 2014; 4: 2412–2426

[376] Chemical Catalysts Brochure, Johnson Matthey, http://www.jmprotech.com/images-uploaded/files/72052%20Chemical%20Catalysts%20Brochure%20PTrb%20c2014%20web.pdf

[377] Bowen CP, Stone & Webster ethylene technology, in Meyers RA ed., Handbook of Petrochemicals Production Processes , McGraw-Hill, 2005, p.6.21-50.

[378] Borsos S, Ronczy S, KBR SCORE™ ethylene technology in Meyers RA, ed., Handbook of Petrochemicals Production Processes , McGraw-Hill, 2005, p.6.51-63.

[379] Valla M, Stadler D, Mougel V, Copéret C, Switching on the metathesis activity of Re Oxo Alkylidene surface sites through a tailor-made silica-alumina support, Angew. Chem. Int. Ed. 2016, 55,1124 –1127

[380] Man PP, Peltre MJ, Barthomeuf D, Nuclear magnetic resonance study of the dealumination of an amorphous silica–alumina catalyst, J. Chem. Soc. Faraday Trans., 1990; 86(9): 1599-1602

[381] De Witte BM, Grobet PJ, Uytterhoeven JB, Pentacoordinated aluminum in noncalcined amorphous aluminosilicates, prepared in alkaline and acid medium J. Phys. Chem. 1995; 99: 6961-6965.

[382] Chen TH, Houthoofd K, Grobet PJ, Toward the aluminum coordination in dealuminated mordenite and amorphous silica-alumina: A high resolution ^{27}Al MAS and MQ MAS NMR study, Micropor. Mesopor. Mater. 2005;86 (1-3): 31-37

[383] Xu B, Sievers C, Lercher JA, Rob van Veen JA, Giltay P, Prins R, van Bokhoven JA, Strong Brønsted acidity in amorphous silica−aluminas, J. Phys. Chem. C, 2007; 111 (32): 12075–12079.

[384] Kima YT, Jung KD, Park ED, Gas-phase dehydration of glycerol over silica–alumina catalysts, Appl. Catal. B: Environ. 2011; 107: 177–187

[385] O'Neil Parker ,Jr., Wegner S, Aluminum in mesoporous silica–alumina, Micropor. Mesopor. Mater. 2012; 158: 235–240

[386] Hensen EJM, Poduval DG, Magusin PCMM, Coumans AE, Veen JAR, Formation of acid sites in amorphous silica-alumina, J. Catal. 2010;269 (1): 201-218

[387] Wang Z, Jiang Y, Lafon O, Trébosc J, Kim KD, Stampfl C, Baiker A, Amoureux JP, Huang J, Brønsted acid sites based on pentacoordinated aluminum species, Nature Commun. 2016; 7, 13820.

[388] Okada K, Tomita T, Kameshima Y, Yasumori A, MacKenzie KJD, Porous properties of coprecipitated Al_2O_3-SiO_2 xerogels prepared from aluminium nitrate nonahydrate and tetraethylorthosilicate, J. Mater. Chem. 1999; 9:1307–1312.

[389] Bicker R, Deger H, Herzog W, Riesert K, Pulm H, Hohlneicher JG, Freund HJ, X-ray photoelectron spectroscopy study of silica-alumina catalysts used for a new pyridine synthesis. J. Catal. 1985; 94:69-78

[390] Plank CJ, Activity of silica-alumina cracking catalysts, Anal Chem., 1952; 24 (8): 1304–1306

[391] Danforth JD, The structure of silica–alumina cracking catalysts, J. Phys. Chem., 1955; 59 (6): 564–566

[392] Gray TJ, The nature of silica-alumina catalysts, J. Phys. Chem., 1957; 61 (10): 1341–1343

[393] Holm VCF, Bailey GC, Clark A, Acidity studies of silica-alumina catalysts J. Phys. Chem., 1959; 63 (2): 129–133

[394] Cant NW, Little LH, Lewis and Brønsted acid sites on silica-alumina, Nature 1966;211: 69-70.

[395] Basila MR, Kantner TR, Infrared spectrum of ammonia adsorbed on silica-alumina, J. Phys. Chem., 1967; 71 (3): 467–472

[396] Parry EP, An infrared study of pyridine adsorbed on acidic solids. Characterization of surface acidity, J. Catal. 1963; 2: 371-379

[397] Cardona-Martinez N, Dumesic JA, Applications of adsorption microcalorimetry to the study of heterogeneous catalysis, Advan. Catal., 1992; 38: 149-244.

[398] Maciel GE, Haw JF, Chuang S, Hawkins BL, Early TA, McKay DR, Petrakis L, NMR studies of pyridine on silica-alumina, J. Am. Chem. Soc.1983; 105 (17): 5529-5535.

[399] Gay ID, Liang S, Investigation of surface acidity by ^{13}C NMR adsorption of amines on silica, alumina, and mixed silica-alumina J. Catal. 1976;4: 306-313

[400] Baltusis L, Frye JS, Maciel GE, P-31 NMR study of trialkylphosphine probes adsorbed on silica- alumina, J. Am. Chem. Soc.. 1987; 109 (1) 40-46.

[401] Scokart PO, Rouxhet PG, Comparison of the acid-base properties of various oxides and chemically treated oxides, J. Colloid Interface Sci. 1982; 86: 96-104.

[402] Boehm HP, Knözinger H, Nature and estimation of functional groups on solid surfaces, in Catalysis, Science and Technology, Anderson JR, Boudart M eds., Vol. 4, Springer, Berlin, 1983, p. 39-207.

[403] Basila MR, An infrared study of a silica-alumina surface, J. Phys. Chem., 1962; 66 (11):2223–2228

[404] Peri JB, Effect of fluoride on surface "acid" sites on .gamma.-alumina and silica-alumina J. Phys. Chem., 1968; 72 (8): 2917–2925

[405] Zheng A, Liu SB, Deng F, Acidity characterization of heterogeneous catalysts by solid-state NMR spectroscopy using probe molecules, Solid State Nucl. Magn. Res. 2013; 55-56: 12–27

[406] Mardkhe MK, Keyvanloo K, Bartholomew CH, Hecker WC, Alam TM, Woodfield BF, Acid site properties of thermally stable, silica-doped alumina as a function of silica/alumina ratio and calcination temperature Appl. Catal. A: Gen. 2014; 482: 16–23

[407] Roy BC, Rahman MS, Rahman MA, measurement of surface acidity of amorphous silica-alumina catalyst by amine titration method, J. Appl. Sci. 2005; 5(7):1275-1278

[408] Luan Z, Fournier JA, In situ FTIR spectroscopic investigation of active sites and adsorbate interactions in mesoporous aluminosilicate SBA-15 molecular sieves, Micropor. Mesopor. Mat. 2005; 79: 235–240.

[409] Bonelli B, Onida B, Chen JD, Galarneau A, Di Renzo F, Fajula F, Garrone E, Spectroscopic characterisation of the strength and stability of the acidic sites of Al-rich microporous micelle-templated silicates Micropor. Mesopor. Mater. 2004; 67: 95-106.

[410] Crépau G, Montouillout V, Vimont A, Mariey L, Cseri T, Maugé F, Nature, Structure and strength of the acidic sites of amorphous silica alumina: an IR and NMR Study, J. Phys. Chem. B, 2006;110: 15172-15185.

[411] Brunner E. Characterization of solid acids by spectroscopy, Catal. Today, 1997; 38: 361-376.

[412] Heeribout L, Vincent R, Batamack P, Dorémieux-Morin C, Fraissard J,. Brønsted acidity of amorphous silica–aluminas studied by ^{1}H NMR, Catal. Lett. 1998; 53: 23-31.

[413] Luo Q, Deng F, Yuan Z, Yang J, Zhang M, Yue Y, Ye C, Using trimethylphosphine as a probe molecule to study the acid sites in Al−MCM-41 materials by solid-state NMR spectroscopy, J. Phys. Chem B, 2003; 107: 2435-2442.

[414] Xu MC, Wang W, Seiler M, Buchholz A., Hunger M, Improved Brønsted Acidity of Mesoporous [Al]MCM-41 Material Treated with Ammonium Fluoride, J Phys. Chem. B, 2002; 106(12): 3202-3208.

[415] Morin S, Ayrault P, El Mouahid S, Gnep NS, Guisnet M, Particular selectivity of m-xylene isomerization over MCM-41 mesoporous aluminosilicates, Appl. Catal. A General, 1997; 159: 317-331.

[416] Corma A, Grande MS, Gonzalez-Alfonso V, Orchilles AV, Cracking activity and hydrothermal stability of MCM-41 and its comparison with amorphous silica-alumina and a USY zeolite, J. Catal. 1996; 159: 375-382.

[417] Di Renzo F, Chiche B, Fajula F, Viale S, Garrone E, Mesoporous MCM-41 aluminosilicates as model silica-alumina catalysts: spectroscopic characterization of the acidity, Stud. Surf. Sci. Catal., 1996; 101: 851-860.

[418] Góra-Marek K, Datka J, IR studies of OH groups in mesoporous aluminosilicates, Appl. Catal. A General, 2006; 302: 104-109.

[419] Zamaraev KI, Thomas JM, Structural and mechanistic aspects of the dehydration of isomeric butyl alcohols over porous aluminosilicate acid catalysts Advan. Catal. 1996; 41: 335-358.

[420] Poduval DG, van Veen JAR, Rigutto MS, Hensen EJM, Brønsted acid sites of zeolitic strength in amorphous silica-alumina, Chem. Commun., 2010; 46: 3466-3468.

[421] Garrone E, Onida B, Bonelli B, Busco C, Ugliengo P, Molecular water on exposed Al^{3+} cations is a source of acidity in silicoaluminas, J. Phys. Chem. B 2006; 110: 19087-19092.

[422] Cairon O, Large heterogeneity of Brønsted acid sites in ASA and USY zeolites: evidencing a third acidic component, Phys. Chem. Chem. Phys., 2010; 12: 6333-6336

[423] Chizallet C, Raybaud P, Pseudo-bridging silanols as versatile Brønsted acid sites of amorphous aluminosilicate surfaces, Angew. Chem. Int. Ed., 2009; 48: 2891-2893.

[424] Chizallet C, Raybaud P, Acidity of amorphous silica-alumina: from coordination promotion of Lewis sites to proton transfer, ChemPhysChem 2010; 11: 105-108.

[425] Hensen EJM, Poduval DG, Degirmenci V, Ligthart DAJM, Chen W, Maugé F, Rigutto MS, Veen JARV, Acidity characterization of amorphous silica-alumina Journal of Physical Chemistry C 2012; 116 (40): 21416-21429

[426] Sarbu C, Delmon B, Nanoscale composition inhomogeneity in silica-aluminas prepared by various methods, Appl. Catal. A Gen. 1999; 185(1): 85-97

[427] Miller JM, Lakshmi LJ, Spectroscopic characterization of sol gel-derived mixed oxides, J. Phys. Chem. B 1998; 102: 6465-6470

[428] Pakharukova VP, Shalygin AS, Gerasimov EY, Tsybulya SV, Martyanov ON, Structure and morphology evolution of silica-modified pseudoboehmite aerogels during heat treatment, J. Solid State Chem. 2016; 233: 294–302

Densities of

Phase	**Density g/cm^3**
Corundum	3.98
γ-Al_2O_3	3.65
Kyanite	3.61
Sillimanite	3.24
Mullite	3.17
Andalusite	3.15
Low-quartz	2.65
$(SiO_2)_{1-x}$-$(Al_2O_3)_x$ glasses (x ÷ 25-60)	2.43-2.81
High-quartz (> 573°C)	2.53
Low-cristobalite (< 200 - 270°C)	2.32
Low-tridymite	2.26-2.27
High-tridymite (> 200 - 450°C)	2.22-2.26
High-cristobalite (> 200 - 270°C)	2.20
Silica glass	2.21
Fumed amorphous silica	2.20
Precipitated silica	1.9-2.1
Stöber silica	2.04-2.10
Silicalite-1	1.8

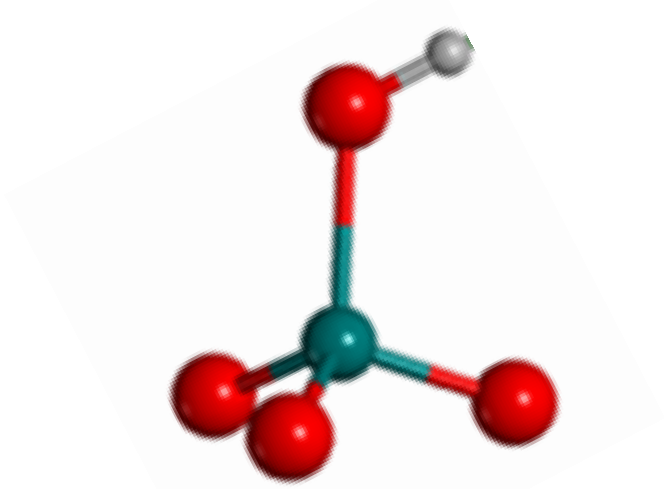

Isolated silanol

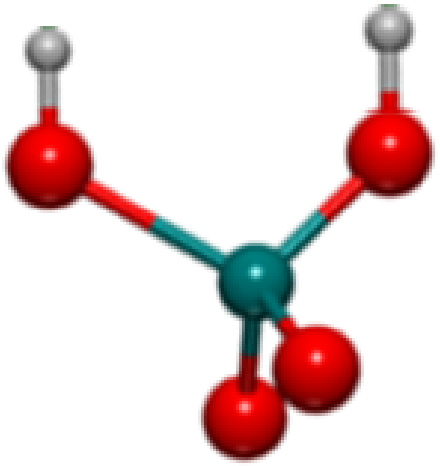

Geminal silanols

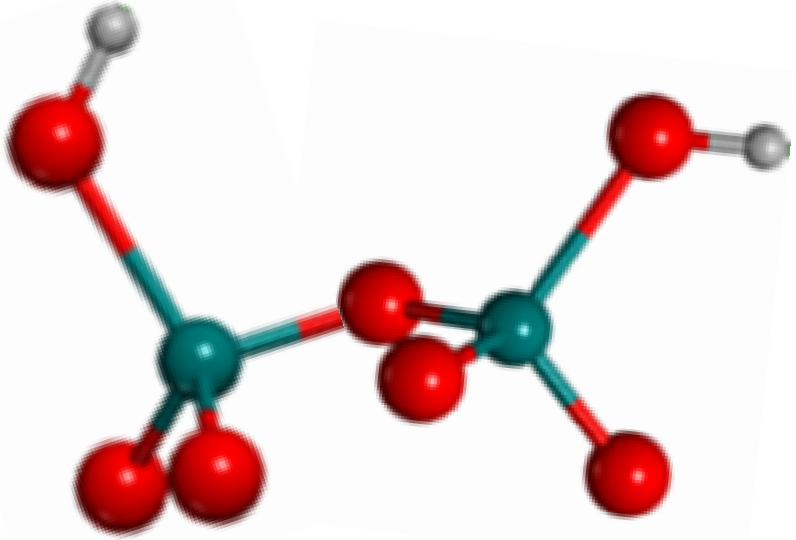

Vicinal silanols

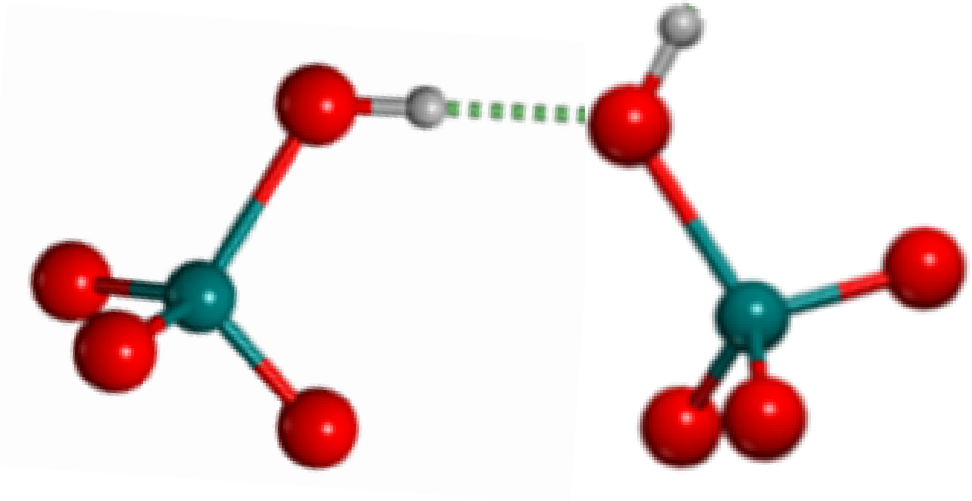

H-bonded silanols

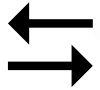

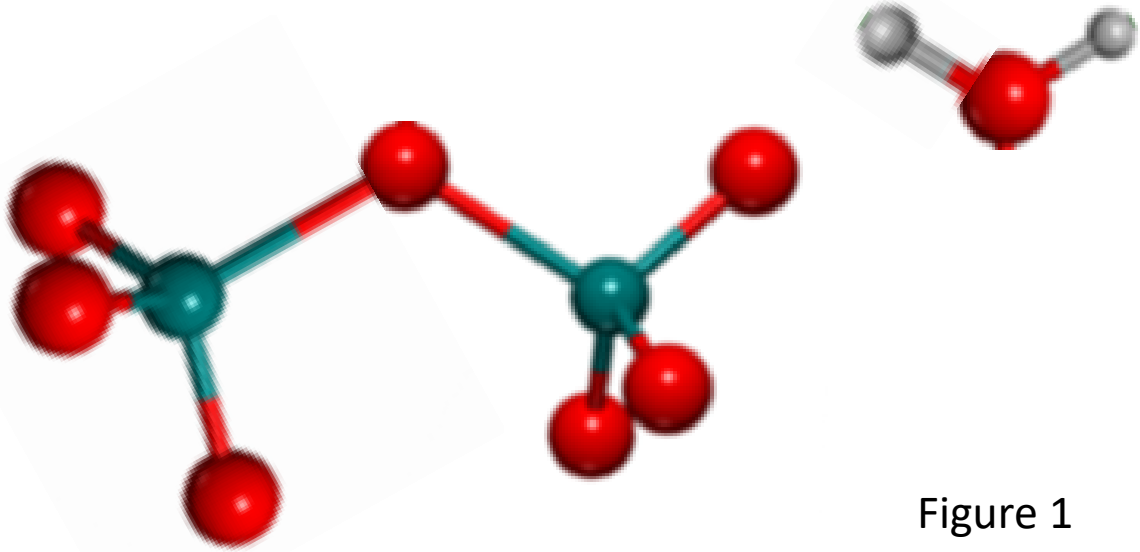

Siloxane bridge

Figure 1

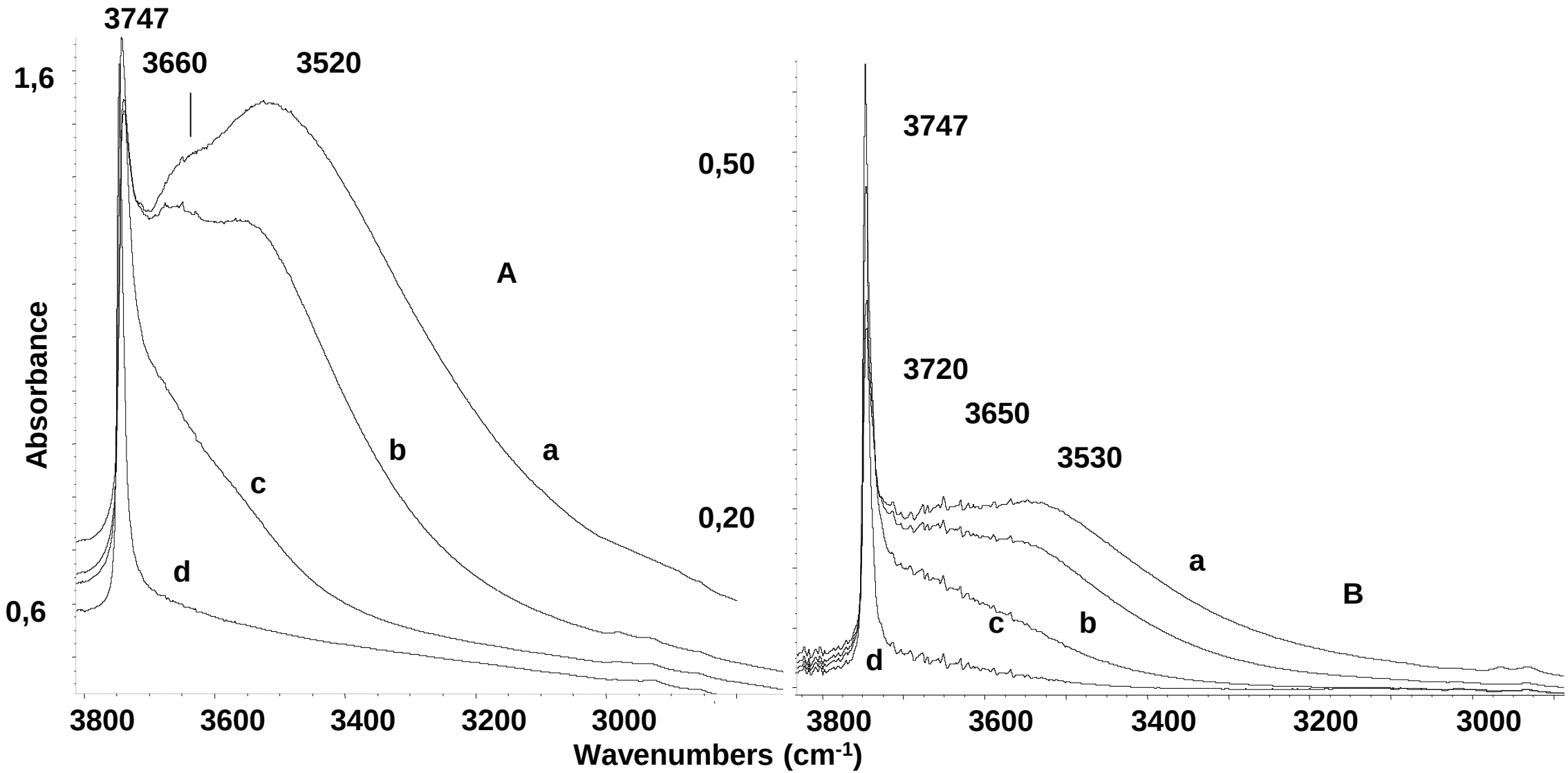
3747
3660
3520
1,6
0,50
A
Absorbance
b
a
c
0,20
d
0,6
3747
3720
3650
3530
a
B
c
b
d
3800
3600
3400
3200
3000
3800
3600
3400
3200
3000
Wavenumbers (cm-1)

Figure 2

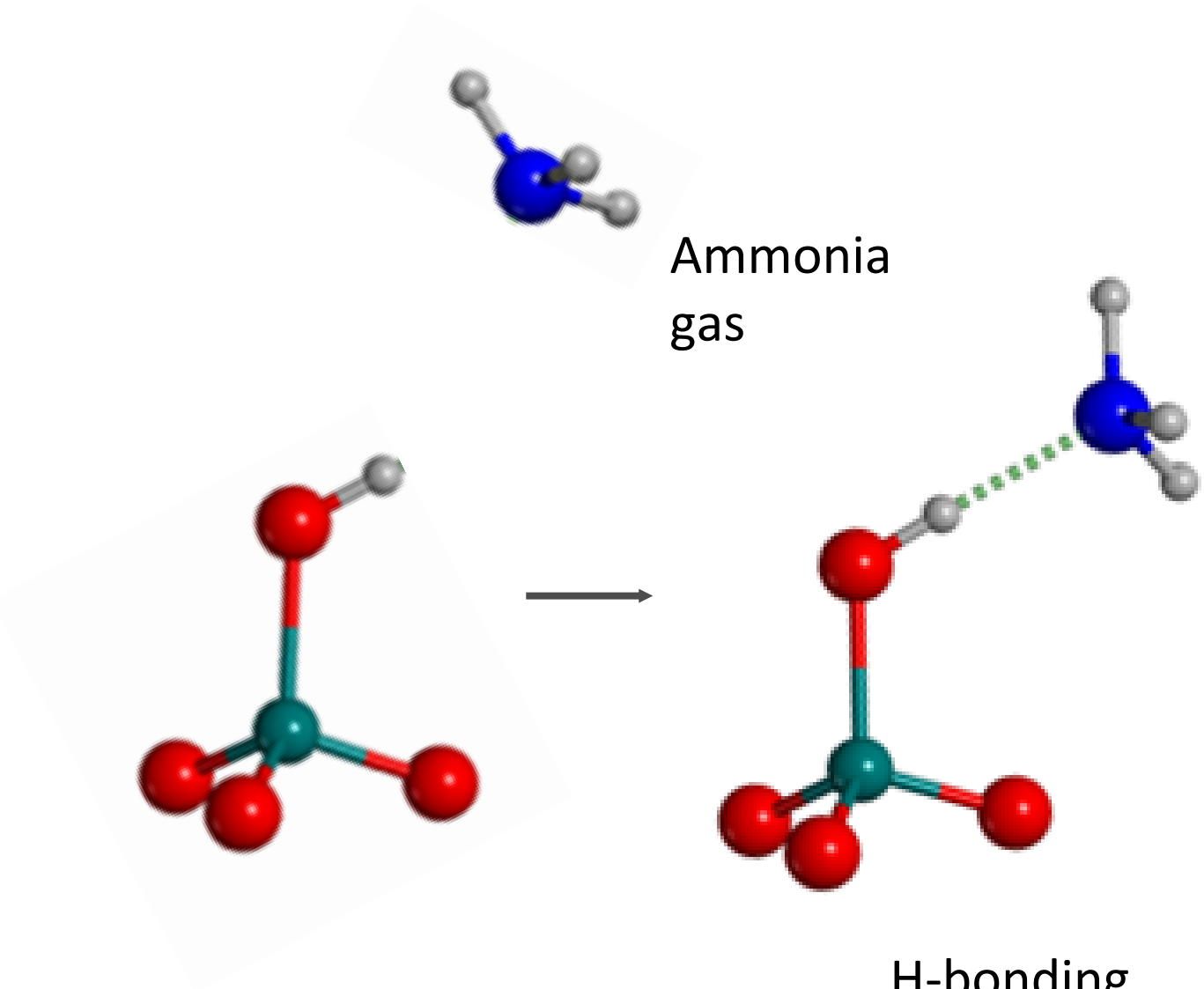

Figure 3

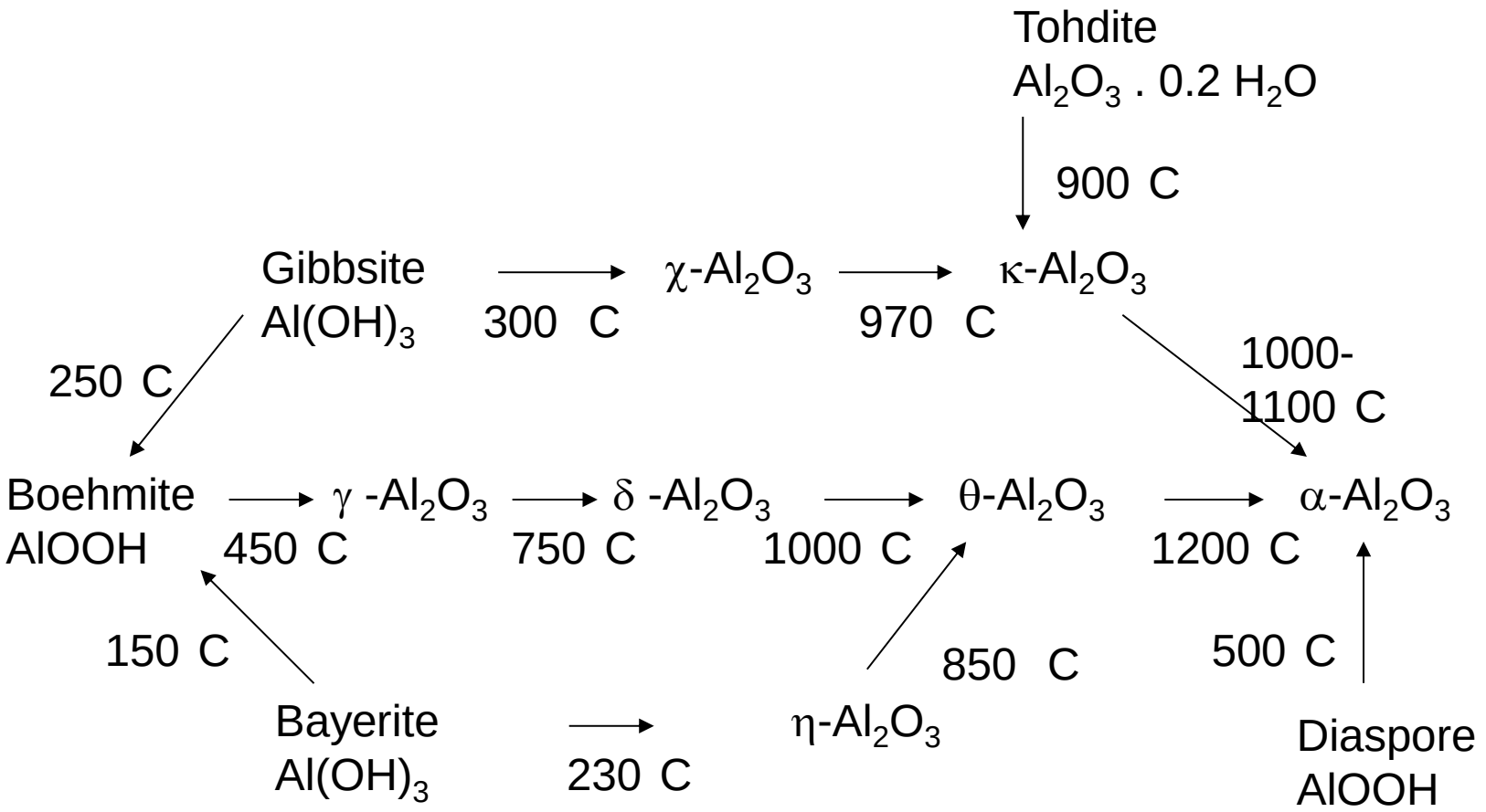
Tohdite
Al_2O_3 . 0.2 H_2O
900 C
Gibbsite
$Al(OH)_3$
300 C
χ-Al_2O_3
970 C
κ-Al_2O_3
250 C
1000-
1100 C
Boehmite
AlOOH
450 C
γ -Al_2O_3
750 C
δ -Al_2O_3
1000 C
θ-Al_2O_3
1200 C
α-Al_2O_3
150 C
850 C
500 C
Bayerite
$Al(OH)_3$
230 C
η-Al_2O_3
Diaspore
AlOOH

Figure 4

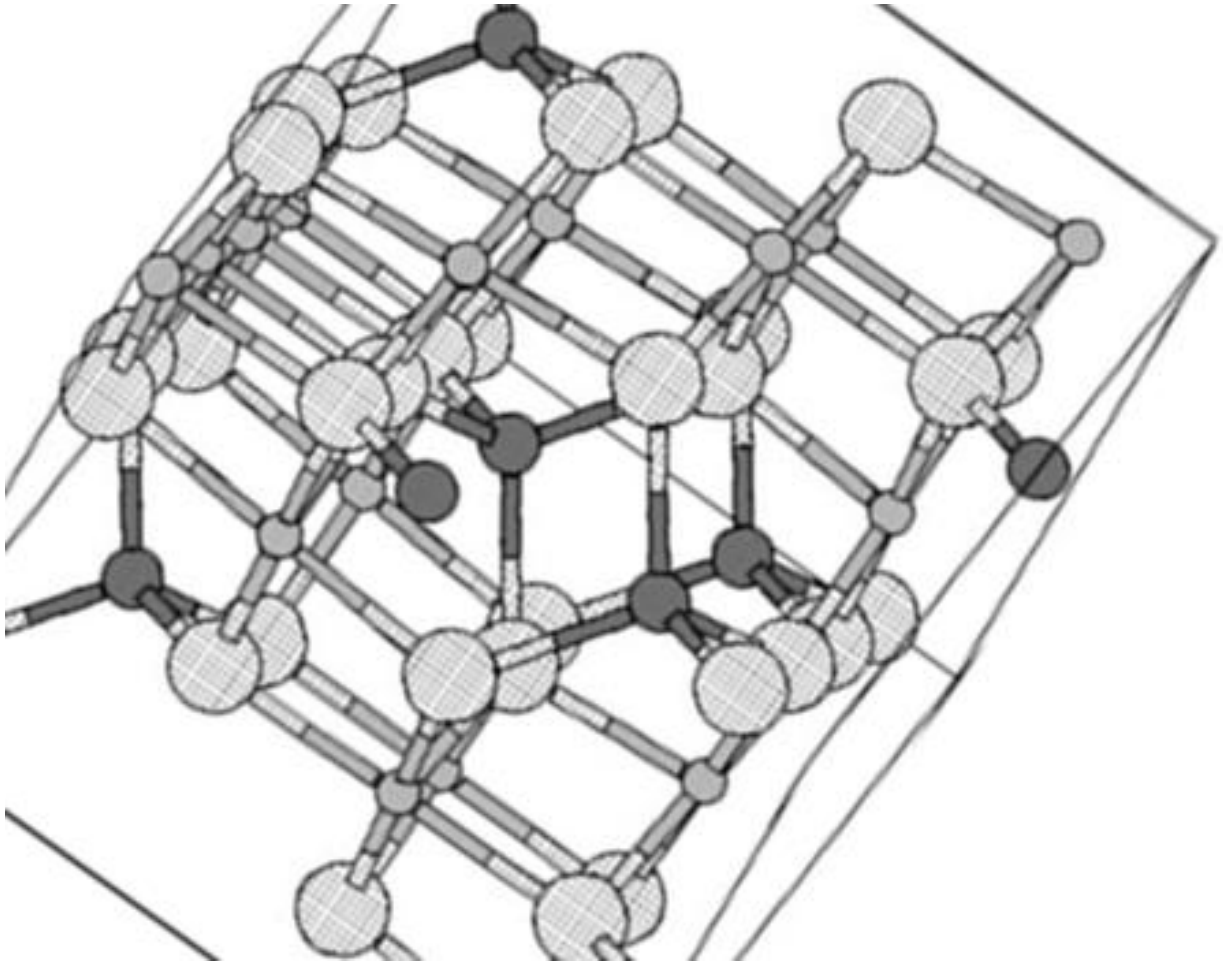

A

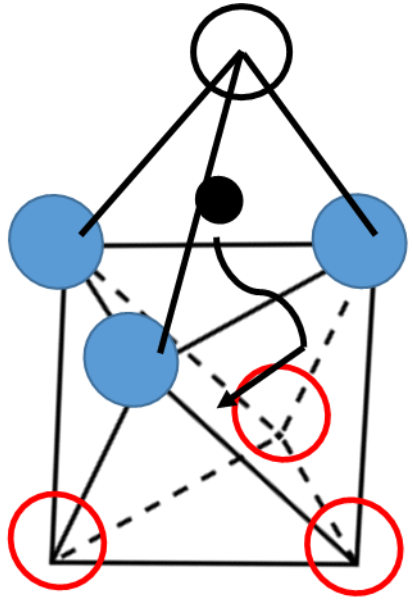

B

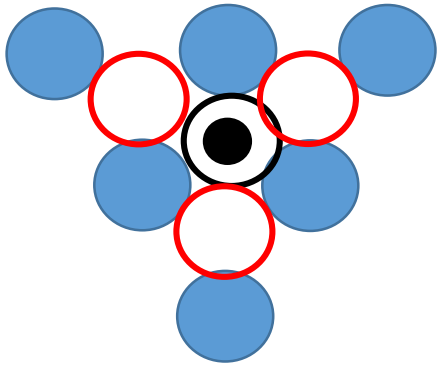

C

Figure 5

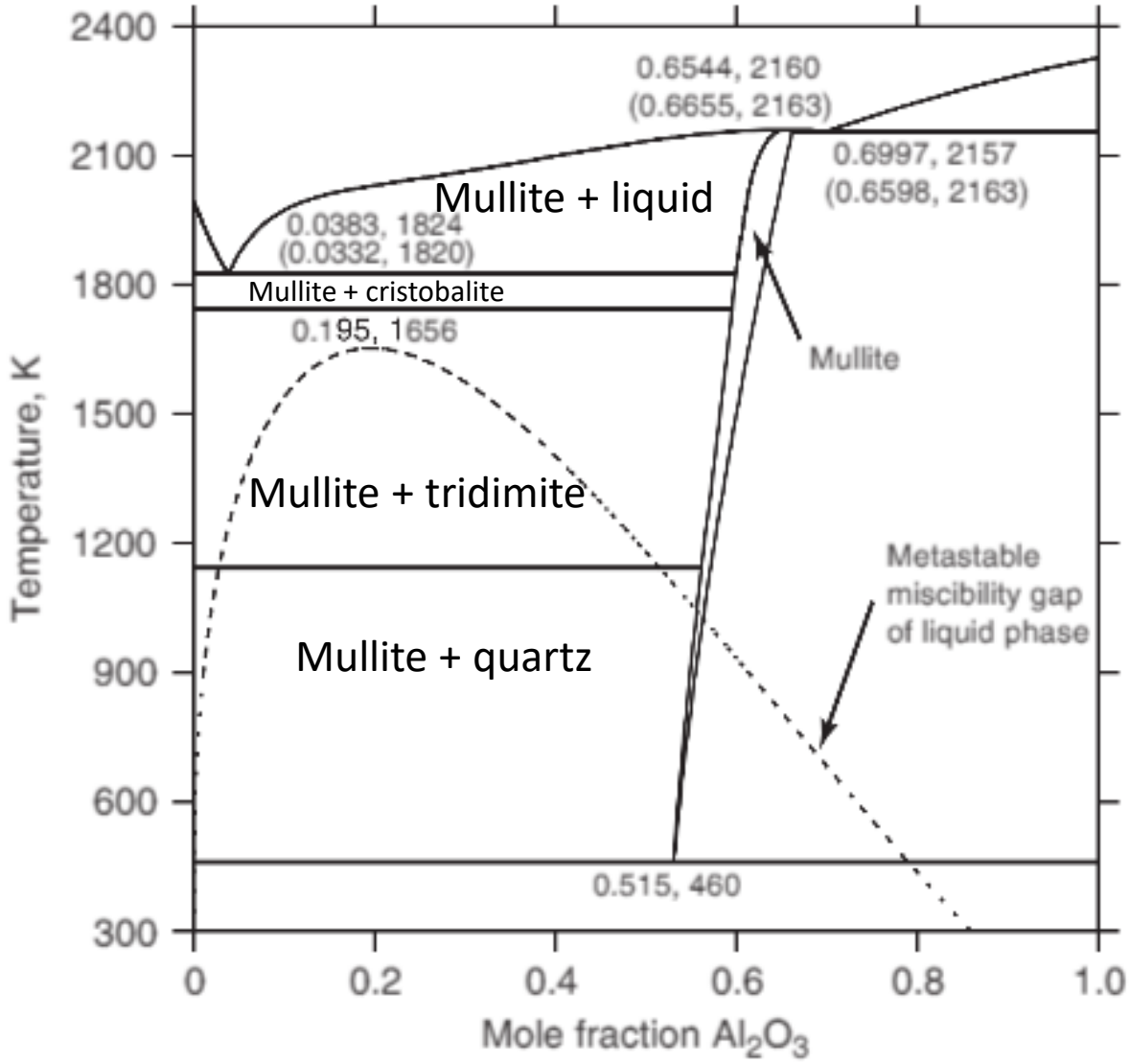
2400
2100
1800
1500
1200
900
600
300
Temperature, K
0
0.2
0.4
0.6
0.8
1.0
Mole fraction Al_2O_3
0.6544, 2160
(0.6655, 2163)
0.6997, 2157
(0.6598, 2163)
Mullite + liquid
0.0383, 1824
(0.0332, 1820)
Mullite + cristobalite
0.195, 1656
Mullite
Mullite + tridimite
Metastable
miscibility gap
of liquid phase
Mullite + quartz
0.515, 460

Figure 6

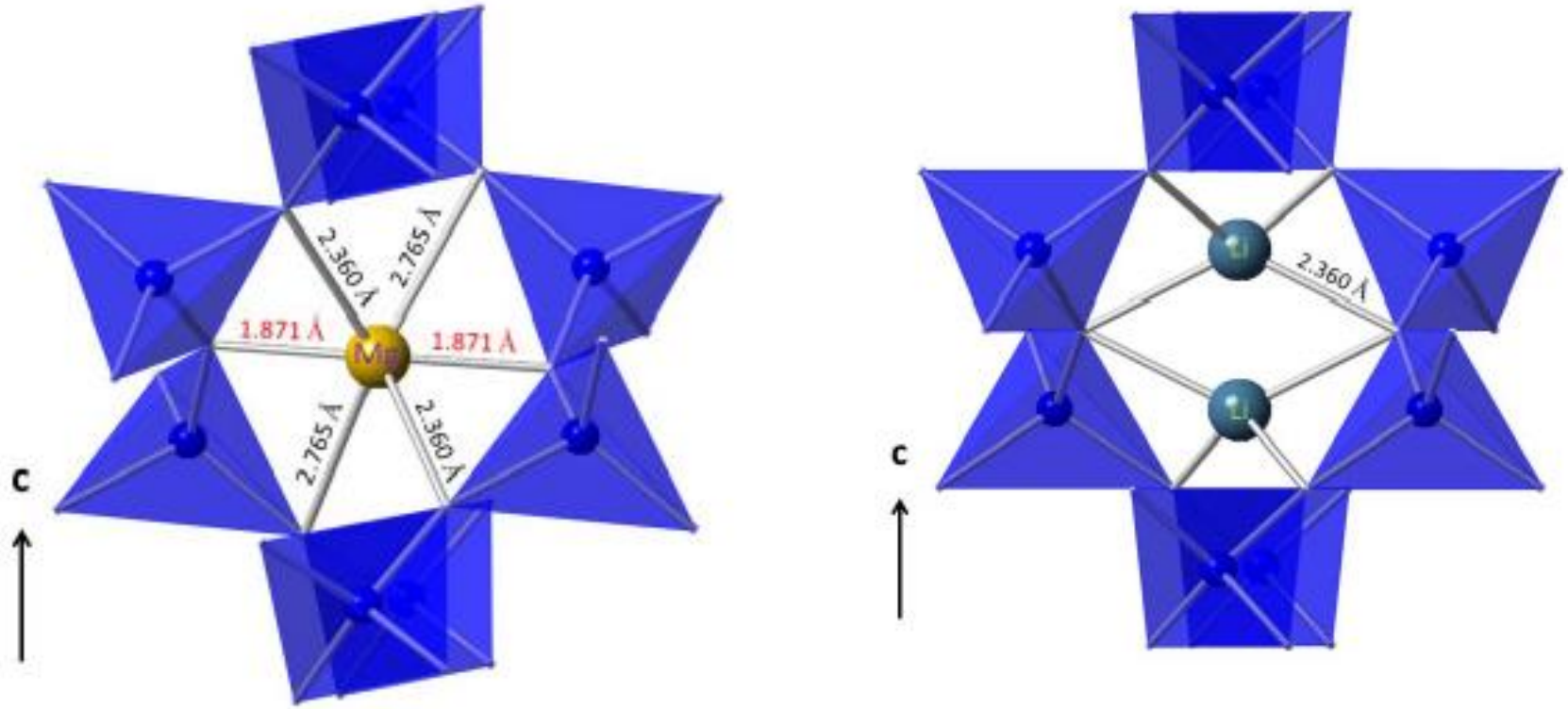

Figure 7

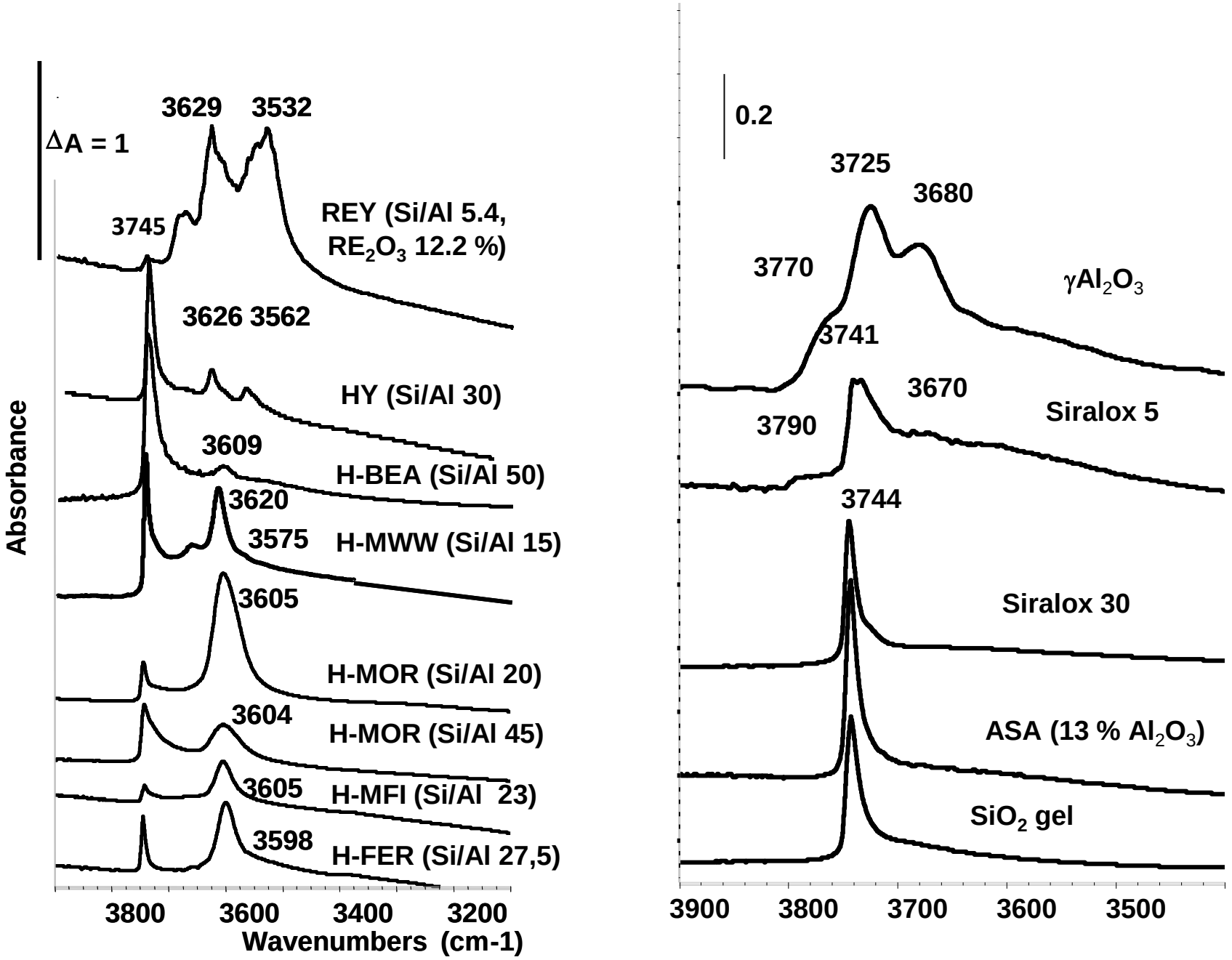
ΔA = 1
3629
3532
3745
REY (Si/Al 5.4,
RE2O3 12.2 %)
3626 3562
HY (Si/Al 30)
3609
H-BEA (Si/Al 50)
3620
3575
H-MWW (Si/Al 15)
3605
H-MOR (Si/Al 20)
3604
H-MOR (Si/Al 45)
3605
H-MFI (Si/Al 23)
3598
H-FER (Si/Al 27,5)
Absorbance
3800
3600
3400
3200
Wavenumbers (cm-1)
0.2
3725
3680
3770
γAl2O3
3741
3670
3790
Siralox 5
3744
Siralox 30
ASA (13 % Al2O3)
SiO2 gel
3900
3800
3700
3600
3500

Figure 8

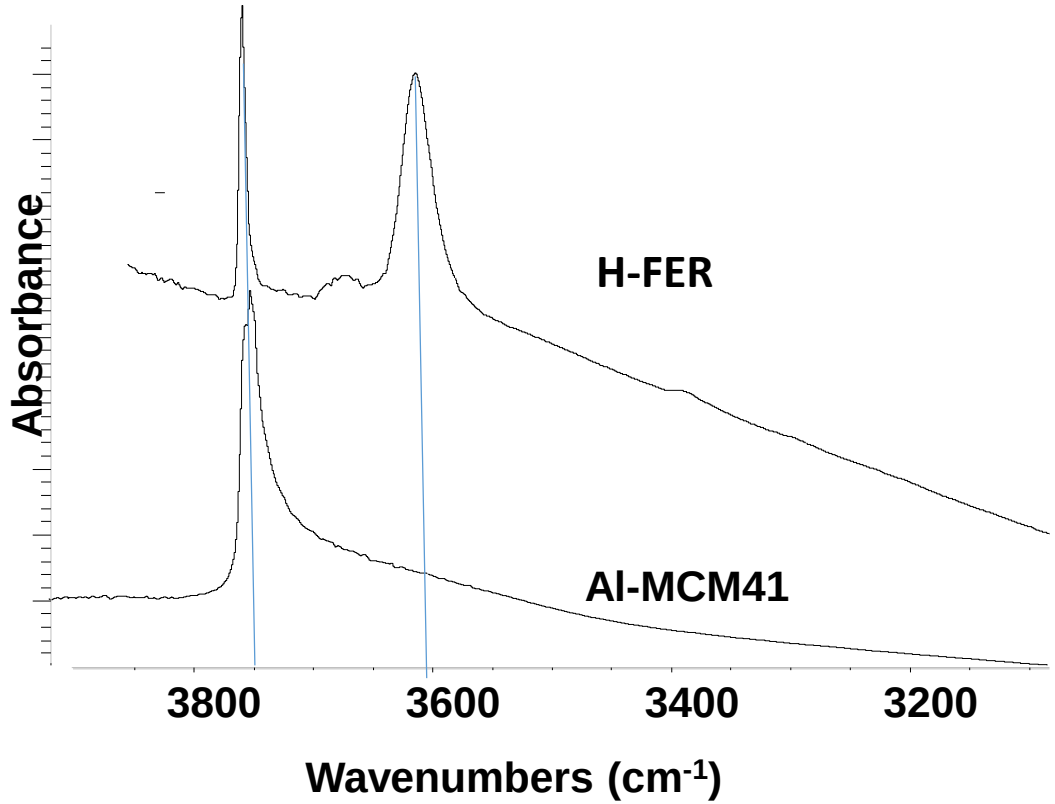
Absorbance
H-FER
Al-MCM41
3800
3600
3400
3200
Wavenumbers (cm-1)

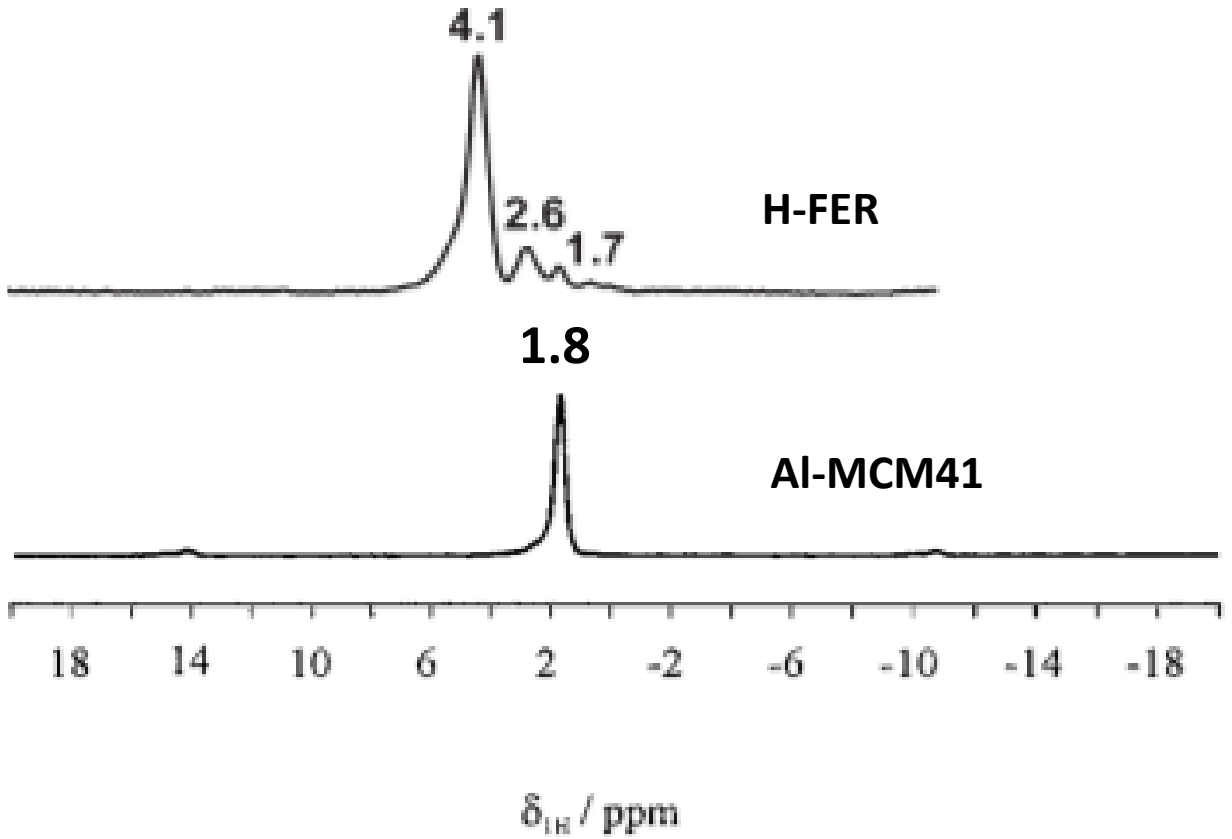
4.1
2.6
1.7
H-FER
1.8
Al-MCM41
18
14
10
6
2
-2
-6
-10
-14
-18
δ1H / ppm

Figure 9

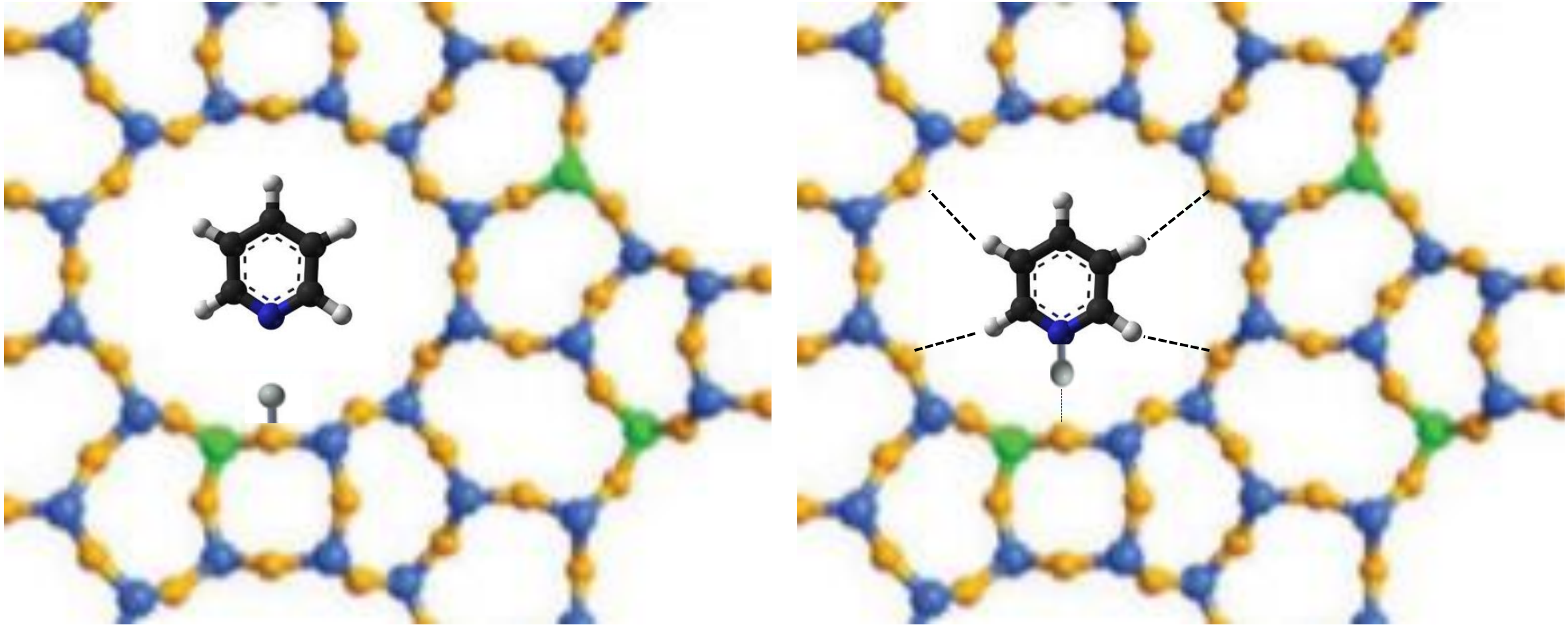

Figure 10

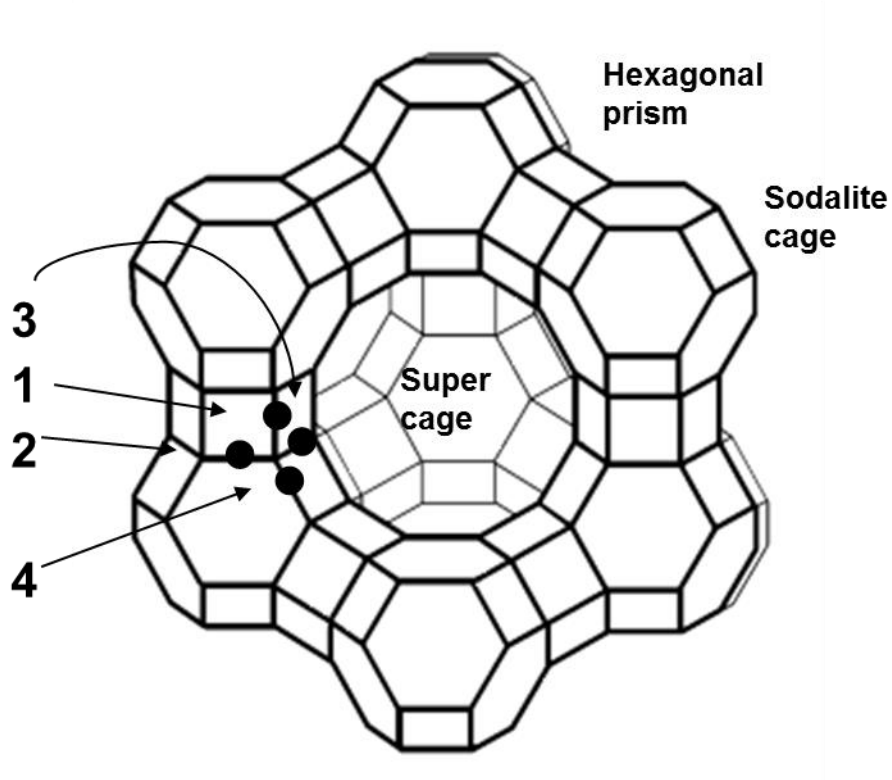

Figure 11

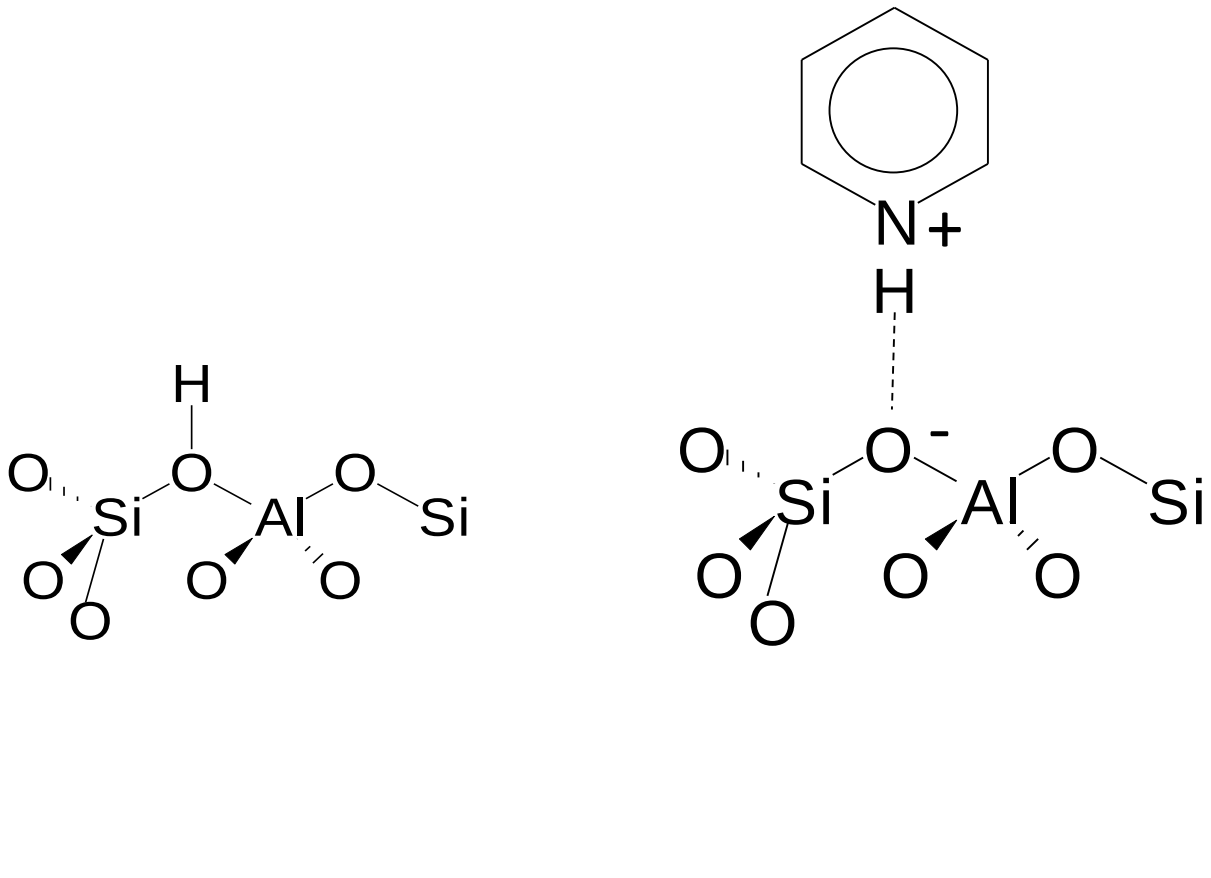

Figure 12

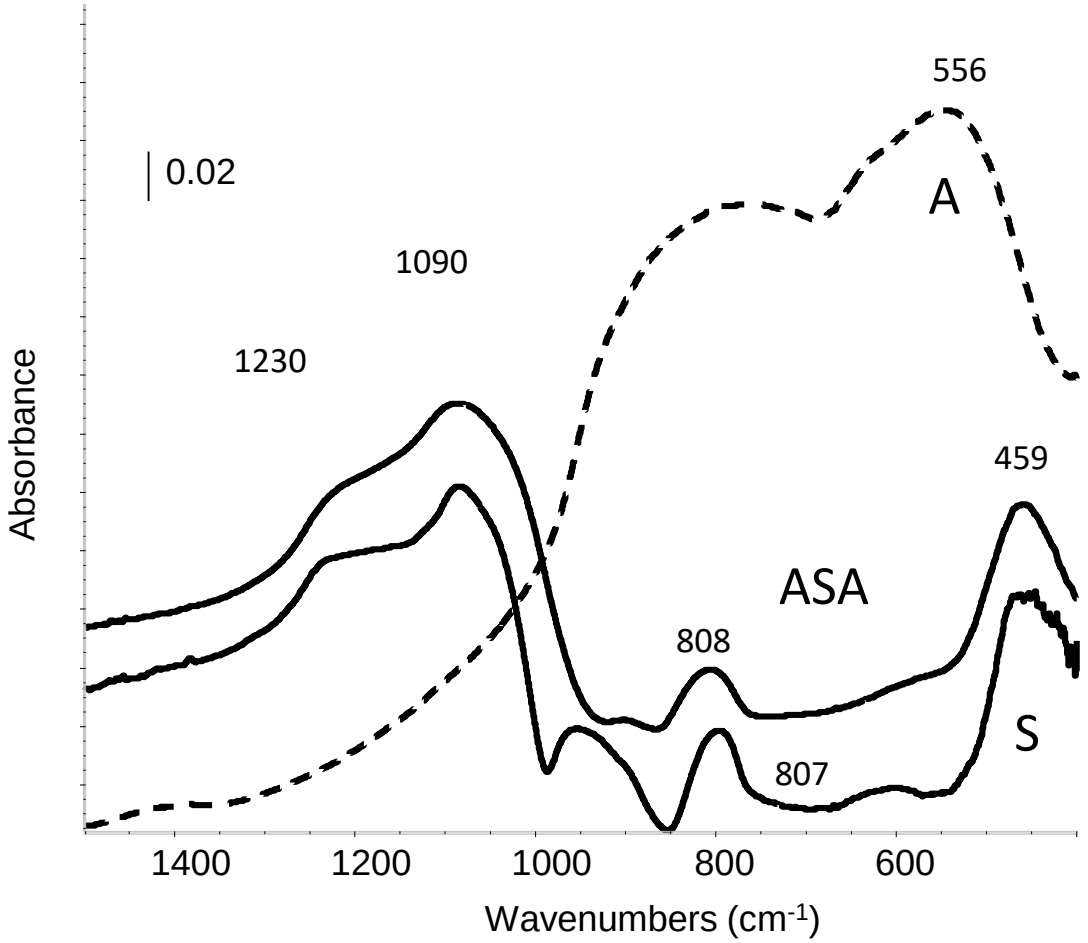
556
0.02
A
1090
1230
459
ASA
808
S
807
Absorbance
1400
1200
1000
800
600
Wavenumbers (cm-1)

Figure 13

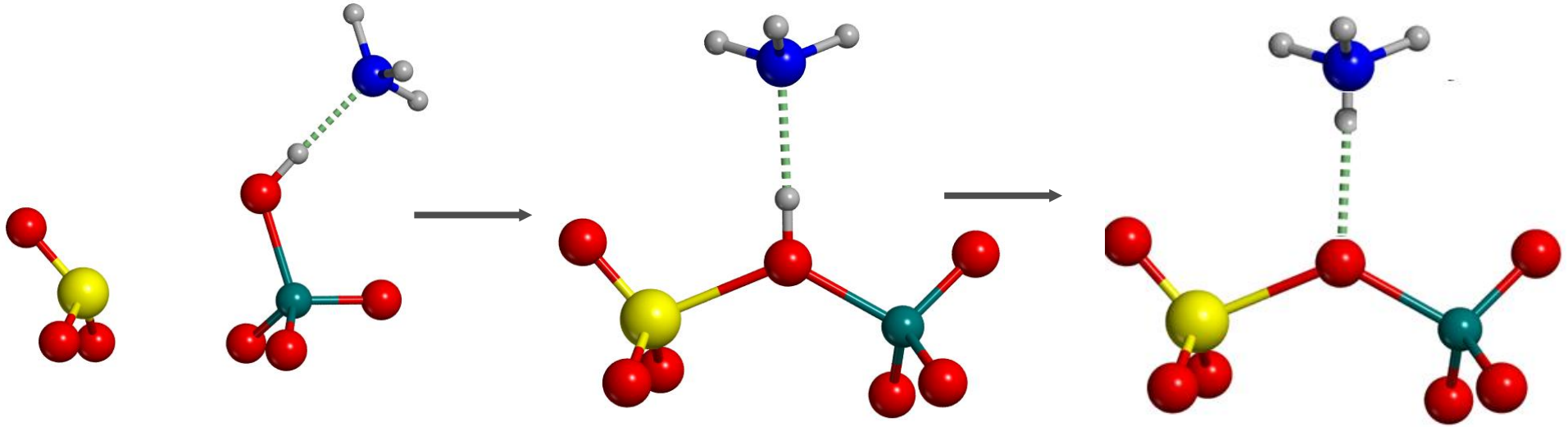

Al^{3+} interstitial site- terminal Silanol group

Figure 14